Investigation of the driving efficiency of an open-ended steel pile using prolonged blows

Christina Ioannou

Investigation of the driving efficiency of an open-ended steel pile using prolonged blows

by

Christina Ioannou

to obtain the degree of Master of Science
at the Delft University of Technology,

Student number:	5477263	
Project duration:	September , 2022 – December, 2024	
Thesis committee:	Prof. dr. M.A. Cabrera,	TU Delft, supervisor
	Prof. dr. ir. K.G.G. Gavin,	TU Delft
	Ir. Tristan Quinten,	TU Delft supervisor
	Dr. ir. Jort van Wijk	IQIP
	Dr. ir. E. Kementzetzidis	TU Delft supervisor

TU Delft

Acknowledgment

The completion of this thesis has been a transformative journey, both intellectually and personally. Throughout the process, I have gained a wealth of theoretical and technical knowledge, deepening my understanding of geotechnical engineering, physical modeling, and laboratory management. I learned not only how to navigate the complexities of research but also the importance of collaboration, responsibility, and perseverance in bringing ideas to fruition.

I would like to express my deepest gratitude to those who guided and supported me throughout this journey. First and foremost, I extend my sincere thanks to my supervisors, Dr. Miguel Cabrera and Tristan Quinten, for their invaluable guidance, insightful feedback, and continuous support throughout the research process. Their expertise and encouragement have been instrumental in shaping this work.

I am especially grateful to Kees Van Beek for his profound knowledge and experience with the centrifuge facility. His unwavering support and willingness to assist made a significant impact on the progress of this thesis. His contributions were invaluable.

A heartfelt thanks also goes to Yuen Zhang, who played an essential role in helping me conduct most of the experiments. Beyond his technical assistance, his emotional support was crucial, and I am fortunate to have gained not only a collaborator but a dear friend during this process.

I would also like to acknowledge the laboratory staff and technicians for their dedication and support in ensuring the smooth execution of the experiments. Their hard work and assistance were indispensable.

Finally, I am deeply grateful to my family, friends, and particularly my parents, for their unwavering psychological and emotional support during this challenging period. Their love, patience, and encouragement kept me going, and I am not sure I would have succeeded without them. A special thanks goes to Kostas, my person, whose presence has been a constant source of strength and comfort.

In conclusion, this thesis is the culmination of not only my individual efforts but also the contributions of many people, to whom I will always be profoundly thankful.

Abstract

This thesis investigates the key factors influencing the installation efficiency of offshore wind farm (OWF) piles, which will result to minimizing environmental impact and optimizing material usage during construction. Offshore wind energy plays a crucial role in the transition to renewable energy sources, and enhancing the installation techniques of OWFs is essential for ensuring both sustainability and economic efficiency. Issues such as sound emissions during the installation of OWFs and material efficiency in the design and construction of offshore structures are of significant importance. Reducing the emitted sound levels to mitigate the negative impact on underwater ecosystems and addressing the structural fatigue resulting from the installation process are critical challenges that need to be addressed. These improvements will lead to greater design efficiency and material economy, both of which are pivotal for the advancement of offshore wind energy. Alternative installation methods, such as methods that utilize prolonged blows, show promising potential in these areas. However, before such methods can be fully utilized in the field, they must undergo thorough testing and analysis to ensure their efficacy and safety. This thesis aims to contribute to this effort by examining the behavior of soil during pile installation using prolonged blows.

The distinguishing feature when using prolonged blows is its ability to generate a prolonged blow, which distributes the energy from the hammer to the pile and the soil in a manner distinct from conventional installation methods. Experiments are conducted at the centrifuge facility at TU Delft to explore the soil response to this innovative technique. The study focuses on three key research questions, each of which contributes to a deeper understanding of pile installation efficiency.

The first research question addresses the impact of energy on installation efficiency. In this context, the impact energy is controlled by adjusting the height from which the mass is released, allowing for a direct comparison of cases with varying energy levels. This analysis provides valuable insights into how changes in impact energy influence the pile's drivability and the overall efficiency of the installation process.

The second research question examines the effect of pile diameter on installation efficiency. By manipulating the centrifuge's acceleration level, the model pile represent prototype piles of different diameters. However, changes in acceleration levels also affect other system parameters, such as force, which must be accounted for in the analysis. This investigation aims to determine how pile diameter influences installation efficiency, including whether phenomena like soil plugging occur during the process.

The third research question explores the influence of soil saturation on pile installation. Experiments were conducted with soil saturated with a viscous fluid, and the results were compared to those from dry conditions. These comparisons shed light on the interaction between the pile and the soil, with a particular focus on the effects of larger displacement amplitudes and slower loading rates. Understanding how soil drainage conditions are affected by the slower loading rate is critical to assessing the installation's efficiency in saturated soil environments.

In conclusion, this thesis provides valuable insights into how impact energy, pile diameter, and soil saturation affect the installation efficiency of piles using prolonged blows. By addressing these key factors, this study contributes to the development of more efficient and environmentally friendly pile driving methods for offshore wind farms, ultimately supporting the broader goal of sustainable renewable energy production.

Contents

1

Literature Review

Global climate change is not a future problem. Change to Earth's climate driven by increased human emissions of heat-trapping greenhouse gases are already having widespread effects on the environment: glaciers and ice sheets are shrinking, river and lake ice breaking up earlier, plant and animal geographic ranges are shifting, and plants and trees are blooming sooner. Renewable energy sources, such as solar, wind, geothermal, hydroelectric, and biomass are considered as cleaner energy sources with highly positive effects on the climate, human health, and the economy as well. Renewable energy sources represent a vast and inexhaustible supply of energy, produce far less global warming emissions, improve public health and environmental quality, and in general contribute to a more reliable and resilient energy system(Thompson, 2016).
Ocean energy, particularly offshore wind energy (OWE), has been identified as a promising renewable energy source for reducing greenhouse gas emissions and achieving decarbonization goals. Over the past decade, electricity production from wind energy has experienced exponential growth globally. Offshore wind farms (OWFs) accounted for 10% of new wind power installations worldwide in 2019, with projections suggesting they will contribute more than 20% of total installed capacity in offshore wind electricity production by 2025. To meet these targets, the global installed capacity for offshore wind projects must increase nearly tenfold by 2030, reaching 228 GW, and is expected to further rise to 1000 GW by 2050. However, the expansion of renewable energy must occur without causing significant environmental harm or compromising ecological goals. New offshore wind projects should align with biodiversity protection and conservation objectives, such as those outlined in the "Life Below Water" Sustainable Development Goal and the Convention on Biological Diversity's post-2020 targets. (Galparsoro et al., 2022).

1.1. Wind Energy

1.1.1. What are the benefits of wind energy?

The global transition to renewable energy is crucial for halting the irreversible damage caused by climate change. As outlined in the 2015 Paris Agreement [1], achieving targeted emissions reductions requires wind energy to play a leading role, being one of the least harmful and fastest-growing renewable energy technologies. Wind energy is the world's fastest-growing energy source, with rapid development occurring not only in Europe but also globally. Wind energy is a clean, renewable resource with a minimal water footprint, contributing to its sustainability. Although the operation of wind turbines may produce some CO2 emissions, research indicates that these emissions are typically offset within the first year of operation, positioning wind energy as an effective player in carbon reduction efforts.(Summerfield-Ryan and Park, 2023 However, the wind energy industry does have undeniable environmental impacts, including noise emissions and disturbances to natural habitats. To address these concerns, measures are being implemented to mitigate such effects. It is crucial for society to ensure that, as the industry continues to develop at an accelerated pace, the environmental impacts on species and habitats are closely monitored and effectively managed.

1.1.2. How can wind energy be utilized?

One of the most effective methods for harnessing wind energy is through the use of wind turbines. These devices capture wind and convert it into electricity, transforming the kinetic energy of the wind into electrical energy. This process occurs as the wind turns the blades of the turbine, which are connected to

[1] The Paris Agreement is a legally binding international treaty on climate change.("The Paris Agreement", 2017).

a generator that facilitates the conversion of kinetic energy into electricity. A wind farm is comprised of multiple wind turbines working together to generate power. Wind energy has been increasingly utilized to address the energy crisis and promote sustainable development. Both onshore and offshore wind farms have been established for this purpose, with offshore wind power becoming increasingly favored due to its more stable wind resources and reduced environmental impact. Offshore wind energy offers several advantages over onshore alternatives, primarily because wind speeds are generally higher and more consistent in offshore locations. This results in reduced turbulence effects, which in turn can extend the operational lifespan of offshore wind turbine generators. (Desalegn et al., 2023).Moreover, since the turbines can be installed or placed far away from populated areas the dimensions of the devices can be larger. According to the research (Li et al., 2020), the maximum value of the onshore annual wind speed is smaller than the offshore annual wind speed. From the same research, it can be seen in the Figure 1.1 below how the monthly mean wind speed varies at different heights for offshore and onshore sites.

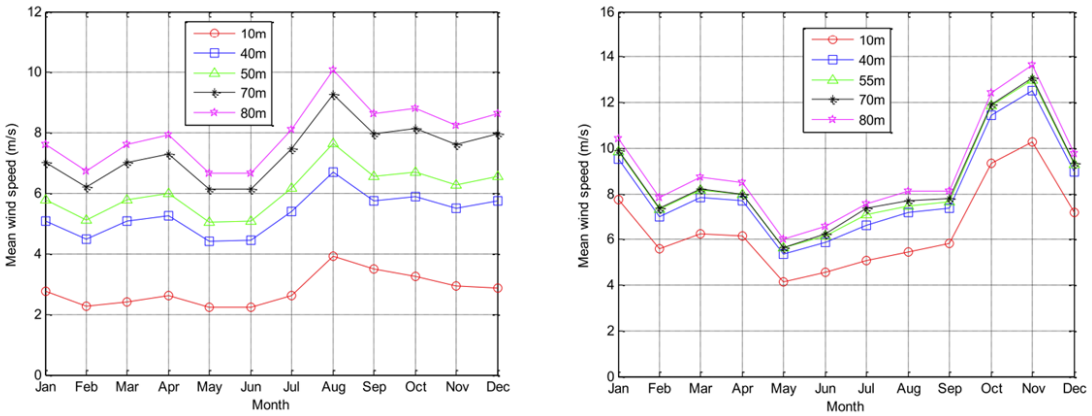

Figure 1.1: The left graph presents the onshore while the right the offshore sites.This Figure presents the monthly wind speed variations at different heights.The different coloured lines represent a different heights.(Li et al., 2020)

According to (Bilgili et al., 2011), the advantages of the offshore wind power in comparison to the onshore can be summarized as follows:

- Availability of large continuous areas, suitable for major projects
- Elimination of the issues of visual impact and noise
- Higher wind speeds, which generally increase with distance from the shore
- Less turbulence, which allows the turbines to harvest the energy more effectively and reduces the fatigue loads on the turbine
- Lower wind-shear, thus allowing the use of shorter towers

1.1.3. Offshore wind energy progress

Offshore wind energy began in shallow waters of the North Sea where the abundance of sites and higher wind resources are more favorable by comparison with Europe's land-based alternatives.
By the end of 2008, 1473 MW of wind turbines were in operation offshore, more than 99% of it in Europe, representing slightly more than 1% of the total installed wind turbine capacity. 366 MW were added offshore in 2008 (compared to 8111 MW onshore), equaling a growth rate of 30% (Bilgili et al., 2011). A significant increase to the offshore wind turbines is observed. From the Figure 1.2 below, it can be also seen that the offshore industry has a gradually increasing share of investments.

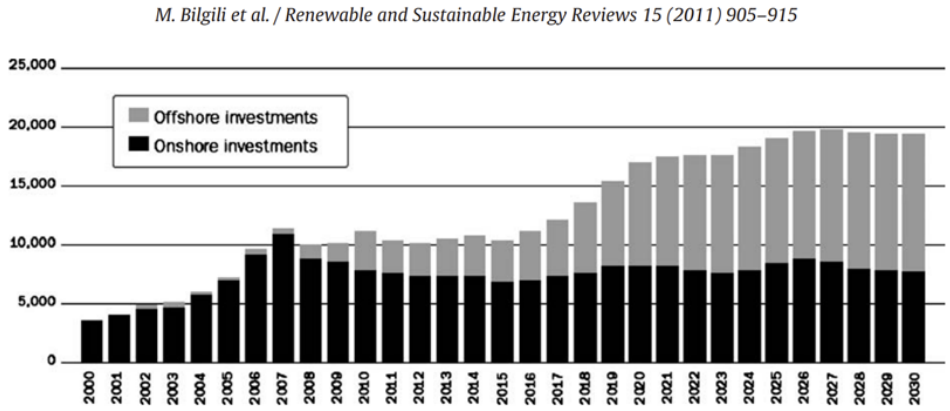

Figure 1.2: Wind energy investments in euros from 2000 to 2030 in EU.(Bilgili et al., 2011)

In addition, according to WindEurope (2023), the orders for offshore turbines in 2023 also reached a record high, averaging 14.9 MW (12.2 MW in 2022). With new, more powerful turbines about to enter the market, the average power rating of installed offshore wind turbines is expected to increase over the next few years. In the Figure 1.3 below it can be seen how the average power rating of installed turbine in Europe has increased from 2014 until 2023.

1.2. Offshore foundations

Offshore wind is a important renewable energy resource. Thus, in light of the international sustainability goals, it aims to grow offshore wind capacity further. This is driving the number of offshore wind turbines (OWTs), pushing them further offshore, into deeper waters(Gómez et al., 2022).
Different support structures exist to fix the turbine to the seabed. A few examples of these gravity structures are: tripods and monopiles, among others. However, the monopile is the most common type of offshore foundation for wind turbines (WindEurope, 2023).

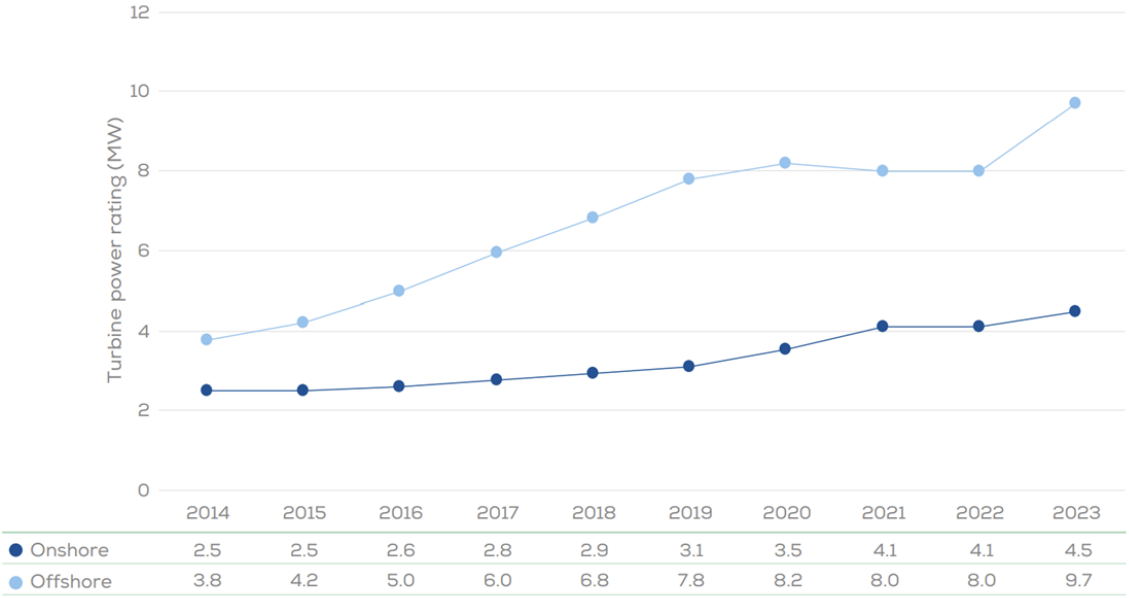

Figure 1.3: Average power rating of installed turbines in Europe, 2014-2023(WindEurope, 2023)

(a) Monopiles

(b) Tripods

Figure 1.4: Offshore foundations.(Thomsen, 2014)

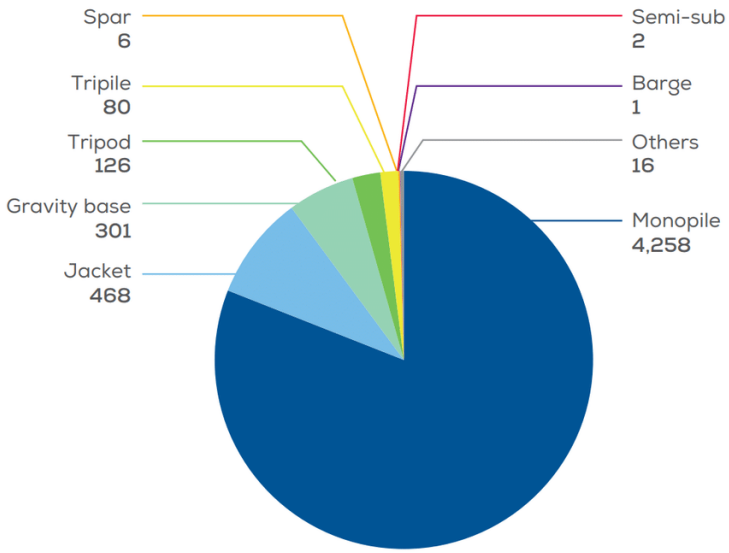

Figure 1.5: Share of monopile for substructure foundations. WindEurope, 2023

Offshore foundations are subjected to extensive loads such as ocean currents, storm wave loading, ice loads, and potential ship impact loads. Moreover, the increasing tower height and rotor blade diameters create extra loads that complicate the foundation design. The deeper waters where offshore structures are now constructed, add another parameter that makes their design more complicated. All these factors pose significant challenges in the design and construction of wind turbine support structures and foundations. The increasing demand for higher-yield wind turbines necessitates larger monopile dimensions. As monopiles grow in size, more energy is required for their installation, which in turn calls for the use of larger hammers. One significant consequence of using bigger hammers is the generation of higher noise levels during installation. The increase in noise emission is directly linked to the greater energy required to drive larger monopiles into the ground. This requires the development of alternative installation methods with a lower environmental impact to reduce the underwater noise emissions. According to Leunissen and Dawson, 2018, during the pile installation with the impact pile-driving method, noise is radiated into the water and the sediment surrounding the pile. Most of the underwater noise arises from radial expansion of the pile as it is struck by the hammer, radiating directly into the water column. Moreover, energy is transferred into the seabed, and radiates back into the water, or travels as surface waves along the water-seabed interface. Therefore, pile-driving noise does not behave strictly as a “point” source. The spectrum of a typical pile strike is broadband, with most energy below 1 kHz but with significant energy extending to > 100 kHz, especially at close range. The bigger the dimensions of the pile, the larger the hammer and the energy that is required for its installation. In addition, according to Tsouvalas, 2020, regardless of the installation method chosen, noise is generated in the seawater and elastic waves radiate into the seabed. The characteristics of the radiated wave field are highly related to the installation technique, the pile size and the local site conditions.
The monopile usually consists of a large diameter steel pipe pile that can reach up to 8-10 m in diameter with wall thicknesses up to 150 mm. Moreover, monopile with diameter of more than 12m are currently being manufactured. According to the subsurface conditions, the pile is driven into the seabed by either large impact or vibratory hammers.

1.3. Pile Installation Methods

For offshore pile installation, the most common installation technique is impact hammering.This technique is done by striking the top of the pile with the ram mass of the pile driving hammer. Impact hammering has a long track record in the offshore industry. One of the reasons is that it can work with stiff and difficult soils. During impact piling, the hammer delivers a series of short duration pulses at the pile head, forcing the it into the seabed (Tsouvalas, 2020). However, this method is associated with severe environmental challenges, particularly related to underwater noise emissions. The desire for higher yield turbines demands an increase in monopile dimensions which result in increased sound emissions during the installation procedure. Therefore, this requires the development of alternative installation methods with a lower environmental impact, particularly reduced underwater noise emissions.

To reduce underwater noise emissions a new technology is being developed. Prolonged blows technology is a new installation method which in contrast to the conventional impact hammering technique delivers a prolonged blow, and therefore distributes the blow energy over a wider range of time. That results in less noise during the installation. When the hammer strikes the pile, a stress wave travels through the pile. Since the blow duration of the hammer is very long (prolonged blows), the wave that travels through the pile is actually longer than the pile itself which results in a more gradual radial displacement of the wall pile. The working principle of the prolonged blows technology is that water will be used to generate downward pressure to install the piles.

The technique allows silent installation of large piles offshore. Installation utilizing prolonged blows is therefore expected to significantly reduce the foundation installation costs for offshore wind turbines, because less mitigative measures are required to stay within the sound emission requirements. The technology uses a large water column to drive a pile in the soil whereas conventional hammers use a steel ram. A combustion throws up this water column, which falls back onto the pile under the force of gravity, thereby delivering two blows. This cycle is repeated until the pile reaches its desired depth.Installation with prolonged blows has various advantages over conventional impact hammers. The hammer produces very low noise levels compared to conventional hammers, resulting in very significant costs reduction of the installation of foundations for offshore wind turbines, since fewer mitigate measures (for noise pollution) are required In addition, the long blow duration minimizes the fatigue during installation, even allowing the driving of large concrete piles due to the absence of detrimental tensile forces. Great scalability will allow the largest piles in the world to be driven using prolonged blows (B.V., 2024).

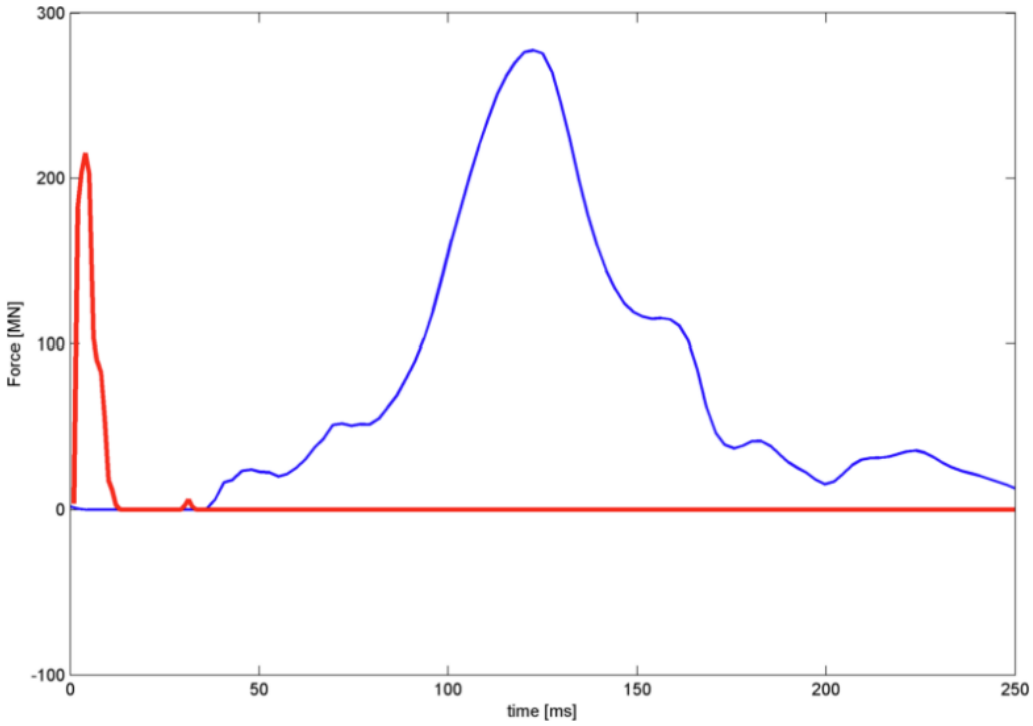

Figure 1.6: prolonged Blow (blue line) compared to a conventional hydraulic hammer blow (red line)

1.4. Underwater noise emissions

For impact piling, each strike of the hydraulic hammer generates strong impulsive sound waves in the seawater which propagate at a large distance from the construction site. The responses of marine mammals and fish to the noise range from light disturbance to strong avoidance of the construction site; in extreme cases, even permanent hearing impairment is possible. The extent of auditory damage depends upon several parameters, i.e., the principal frequency content of the radiated sound, the duration of exposure to high noise levels and the auditory characteristics of the species. Moreover, since pile driving activities extend for periods of months, the level of response may also change over time because of habituation (Tsouvalas, 2020).

1.4.1. Noise mitigation measures

Underwater noise can impact a wide variety of marine life and it has become a vital matter of international consideration. During offshore wind (OSW) farm construction, the driving of foundation piles into the sediment generates a significant amount of noise for certain foundation types. As a result, several mitigation measures have been developed to reduce noise and minimize impacts to wildlife. Quieting technology, such as bubble curtains, are effective at reducing noise at the source, which has benefits for all marine species. (of Environmental Effects Research, n.d.). These methods (e.g. bubble curtains) are costly and cannot be scaled indefinitely (as turbines continue to grow). Mitigation of sound at the source (e.g. by using a different installation technique) is therefore preferred. All in all according to (Tsouvalas, 2020), there are two strategies by which mitigation can be achieved. The first approach to reducing noise involves modifying the source mechanism itself, specifically by adopting a different pile driving technique that minimizes noise emissions at the source. This can be achieved by either adjusting the force exerted by the impact hammer or switching to alternative methods of pile driving that avoid generating high-amplitude shock waves. Examples of such methods include traditional vibratory piling, BLUE Piling, or Gentle Driving of Piles (GDP). The second approach to noise reduction is the creation of a noise mitigation barrier around the pile. These noise barriers can be classified into three main categories, based on the principle of noise reduction they employ:

- Air bubble curtains, available in various configurations,
- Casings that enclose the pile, either in the form of a depressurized double-walled cylindrical shell or lightweight inflatable fabrics, which form an air column around the pile,

- Resonator-based systems, which may include encapsulated bubbles and foam elements within a fishing net or Helmholtz-type resonators.

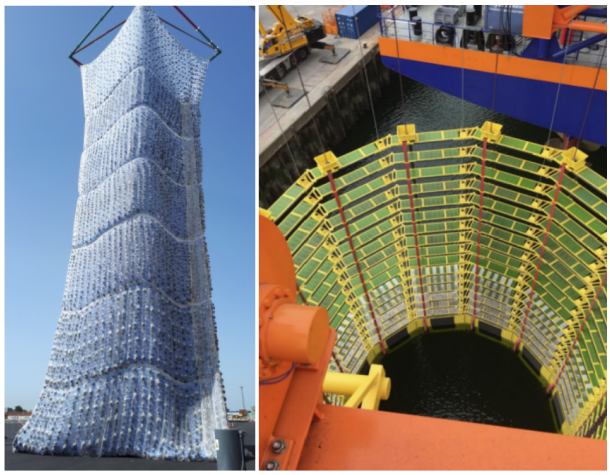

Figure 1.7: The HSD system on the left and the newly developed AdBm-NAS system showing the resonators in the array.(Tsouvalas, 2020). The casings that enclose the pile

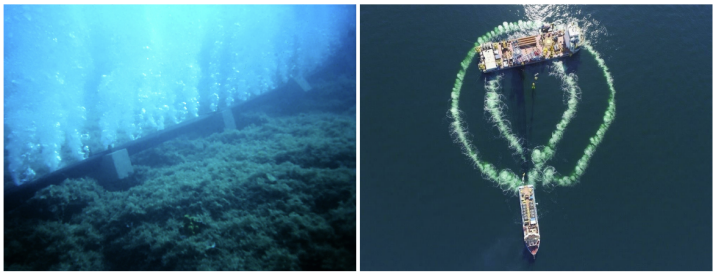

Figure 1.8: Air bubble cloud released by a perforated pile positioned on the seabed on the left. Double Big Bubble Curtain on the right(Tsouvalas, 2020). The air bubble curtains

1.5. What happens in the soil during pile installation?

1.5.1. Pore water pressure generation during pile installation

Soil is a complex material that consists of a soil skeleton with voids between individual particles. These voids are generally filled with water, gas or contaminant, but in general they form a single continuous body. In this water, body stresses can be transmitted, and the water may also flow through the pores. Therefore, the soil behavior describes the interaction of the soil particles with the respective liquid that fills the void. When soil is subjected to loading, as with all materials, stresses develop within it. However, unlike many solid materials, soil can only transfer compressive normal stresses, as it lacks the capacity to withstand tensile stresses. Additionally, the shear stresses in soil must remain small relative to the normal stresses for effective transmission. A portion of the stress is also transferred to the pore spaces, which are filled with water in saturated soils. This transferred stress within the pore spaces is referred to as pore pressure. For this research the main focus is on on open-ended, steel piles, penetrating into non-cohesive (saturated) soil, e.g. sand. Moreover, the foundation type is monopile. During pile installation, a hammer strikes the pile, generating a compression wave that travels through the pile and into the surrounding soil. As this wave propagates, some energy is dissipated, while the remaining energy is transmitted into the soil. In the soil, the energy disperses through a spherical wavefront (P waves), with vertical shear waves (S waves) radiating along a conical wavefront from the shaft due to the friction between the pile and the soil (Zeben, 2017).

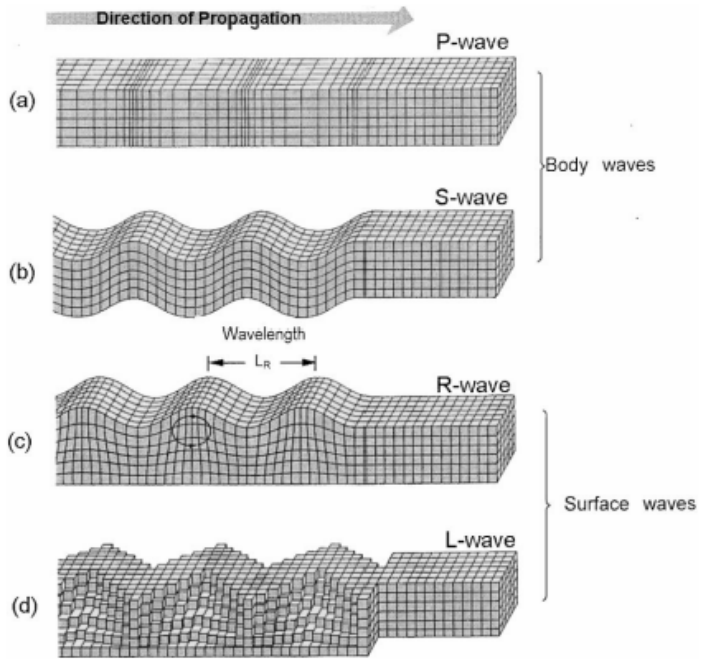

Figure 1.9: Types of seismic waves propagating in the ground: (a) compressional–dilatational waves; (b) shear waves; (c) Rayleigh waves; and (d) Love waves. Athanasopoulos et al., 2000

When soil is subjected to loading, stresses develop within the soil matrix, and a portion of these stresses can be transferred to the pore spaces, resulting in an increase in pore pressure. However, if the soil undergoes dilation under load, the pore pressure may decrease. The behavior of pore pressure generation and dissipation varies depending on the soil type and drainage conditions. In dense soils, the particles tend to roll over each other under shear stress, creating additional voids in a phenomenon known as dilatancy. Conversely, in loose soils, shearing causes particles to fill existing voids, leading to compaction. During pile installation in dense soils under undrained conditions, the material tends to dilate. However, due to large confining stresses, the volume cannot change significantly, which causes a decrease in pore pressure. This reduction in pore pressure results in an increase in effective stress, thereby enhancing the strength of the soil. After the pile driving ceases, the pore pressures will gradually equalize back to static conditions, which typically leads to a reduction in soil strength as the effective stresses decrease (Morgano, 1990). The time required for pore pressure to equalize depends on the permeability of the soil. In permeable soils, the process occurs relatively quickly, whereas in impermeable soils, it takes longer. Consequently, during dynamic loading in dense soils, the resistance to pile installation is higher, whereas during a restrike, the resistance will be lower due to the redistribution of pore pressure.

For loose materials, dynamic loading tends to cause soil densification as the particles rearrange and compact, leading to an increase in pore water pressure and a corresponding reduction in soil strength. This behavior contrasts with that of dense soils, where dynamic loading can lead to dilation and an increase in effective stress, thereby enhancing the soil's strength. During pile driving, the movement of the pile through the soil induces significant deformation in the surrounding material. With repeated impacts, cyclic loading is generated. In conventional pile driving using an impact hammer, the soil is typically in a partially undrained or even fully undrained condition, as the rapid succession of blows does not allow sufficient time for pore pressures to dissipate. However, in the case of installation with prolonged blows, it remains unclear how the longer impact affects the soil's drainage conditions and behavior during installation, as further research is needed to fully understand its effects on the surrounding soil.

1.5.2. Soil loading conditions during pile installation

When the pile is struck by the mass, two primary events occur: a compression wave propagates through the pile, and the pile exerts force on the surrounding soil, causing displacement. More specifically, if we consider an infinitesimally small soil element, the soil initially exists in a neutral stress state. As it is clear from the Figure 1.10 when the pile begins to penetrate, the stresses within the soil increase. This increase in stress results from both the direct compression exerted by the pile and the wave propagation through the material, leading to changes in the soil's mechanical behavior and stress distribution around the pile. (D. S. White et al., 2007).

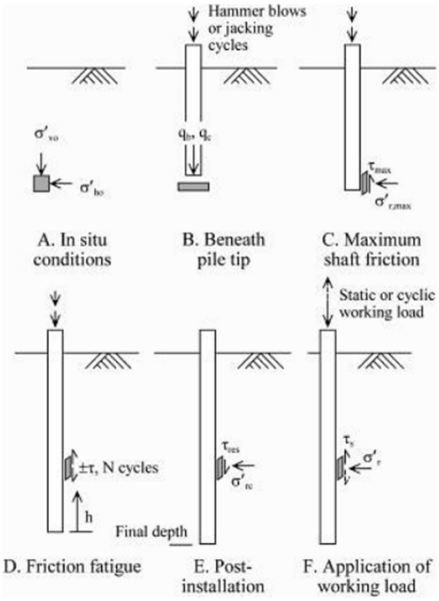

Figure 1.10: Stages in the loading history of a soil element adjacent to a displacement pile(White, 2005)

As the pile tip approaches the soil element the stresses on the element are increased and the soil is pushed laterally to finally pass the pile. As the pile tip passes the soil element, the stress level is decreased, and the element can exert an upward shear stress on the pile. At this point the maximum shear stress is exerted on the pile. As the pile penetrates deeper the soil element comes under cyclic loading from the pile driving. The repetitive loading from the pile wall causes gradual densification of the soil at the pile surface (White & Bolton, 2002). This densification causes an effect called friction fatigue which describes the decrease of horizontal stress acting on the pile wall with increased penetration (Heerema, 1980). The pile displacement and change in stresses exerted on the soil elements as the pile is driven in the soil are the main causes of pore pressure development resulting from shear forces (Zeben, 2017).

1.5.3. Cavity Expansion Analysis

Cavity expansion analysis deals with the expansion of the soil around a pile when the pile is pushed inside it, creating a cylindrical cavity. The analysis of the cavity expansion theory concentrates on quantifying the amount of pressure required to expand a cavity in a material by a specific amount. Two types of cavity expansion problems exist, the first is related to an already existing cavity, the pressure of which is in equilibrium with the stresses in the surrounding soil while the second one is related to a soil mass with no initial cavity. The soil displacing object creates a cylindrical cavity in the soil, therefore the penetration resistance is a function of limit cylindrical cavity pressure. Due to the stress increases that develop around the cavity that expands, three different zones are generated as shown in Figure 1.11. These zones are formed based on the induced strain level. The zone furthest from the pile, is know as the small-strain, linear elastic zone. Here, the soil behaves as a linear elastic material. Closer to the pile in the nonlinear elastic zone, the stress-strain range starts to increase causing the material to yield. However, the stresses are not large enough to produce failure state. In the zone closest to the pile, the plastic zone, this failure state is reached. This happens when the stresses are large enough to cause material failure. The three zones can be seen in the Figure 1.11 below.

Cavity expansion theory can be used as a tool to qualify stress changes at the pile-soil interface during loading. Moreover, the penetration resistance theory that is lined to the cavity expansion analysis can be of great use for the assessment of the density and the stress state of granular soil in situ and the soil strength. The most important findings that concern cavity expansion suggest that dilation phenomena

during the loading phase could therefore be negligible for an open-ended displacement pile with large diameter, as for example monopiles. That means that radial stress recovery caused by dilation would be less noticeable (Salgado1997).

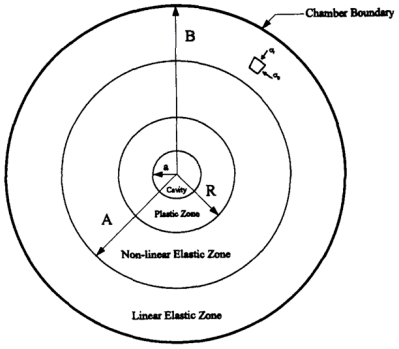

Figure 1.11: Cavity Expansion generates plastic, nonlinear elastic, and elastic zones.(Salgado1997)

It is also important to mention that two other phenomena could affect the radial stress regime around the pile. One would be the transfer of vertical shear stress into the surrounding soil mass and the second the lateral expansion of the pile shaft under the working load, also referred to as the Poisson effect.

1.5.4. Plugging

Definition When an open-ended pile is installed into the ground, the surrounding soil displaces as the pile advances, leading to soil movement around and into the pile. As part of this process, some of the displaced soil enters the pile, forming a soil column within it. Simultaneously, shear stresses develop near the pile tip during installation, which resist the intrusion of soil into the pile, potentially resulting in soil plugging. Based on these interactions, three possible outcomes can occur: Firstly, if the evolution of horizontal stresses inside and outside the pile is similar, the soil moves freely around the pile. In this case, the height of the soil column inside the pile typically matches the height of the soil outside it. This condition is referred to as the ”unplugged behavior” or ”full coring” of the pile. Secondly, if the internal horizontal stresses are significantly higher than the external stresses, soil intrusion into the pile is completely prevented. In this scenario, the pile behaves similarly to a closed-ended pile, and this is known as ”fully plugged behavior.” The third possible outcome is partial plugging. In this case, the internal stresses are higher than the external ones, restricting the free movement of the soil into the pile. However, some soil still enters the pile, but the height of the soil column inside the pile differs from the height of the surrounding soil. These different pile behaviors—unplugged, fully plugged, and partially plugged—are important considerations in understanding the mechanics of open-ended pile installation and the resulting soil-structure interaction.

Quantification There are two ways to quantify the soil plugging. Firstly, by means of the incremental filling ratio (IFR) which is the derivative of the plug length (ΔLi) in respect to the embedded pile length (ΔDp). Secondly, the plug length ratio (PLR) which is the ratio of the length of the soil column inside the pile to the pile driving length (Han et al., 2019). When the IFR equals to 1, it means that the soil moves freely inside the pile, that is referred to as fully coring of the pile. Whereas the case that IFR equals to 0 means that the soil intrusion is fully prevented and that the pile behaves as a closed-ended pile with similar geometrical characteristics. Therefore, based on these two methods, there can be understood how a pile behaves in terms of driving resistance (blow counts), load–settlement response and resistance mobilization. (Han et al., 2019).

$$\text{FFR} = \frac{\Delta h}{z} \tag{1.1}$$

$$\text{IFR} = \frac{\Delta L_i}{\Delta D_p} \times 100\% \tag{1.2}$$

According to (Han et al., 2019), the process of plug formation during the installation of an open-ended pile affects the mobilization of its base resistance as well as its shaft resistance: The formation of a soil plug during installation leads to greater soil densification, greater radial stress buildup, and consequently greater base and shaft resistance. Moreover, whether the pile is plugged or not affects its bearing capacity. In many semi-empirical methods, the axial capacity of an open-ended pile consists of skin friction and tip resistance (Henke and Grabe, 2013). As already mentioned, when an open-ended pile is fully

plugged it behaves similarly to a close-ended pile with same geometry however, the former one has a decreased base resistance since a closed-ended pile has an increased bearing capacity compared to a soil plug. In the case of full coring the base resistance is a function of the area of the steel ring at the toe of the pile (Henke and Grabe, 2013).

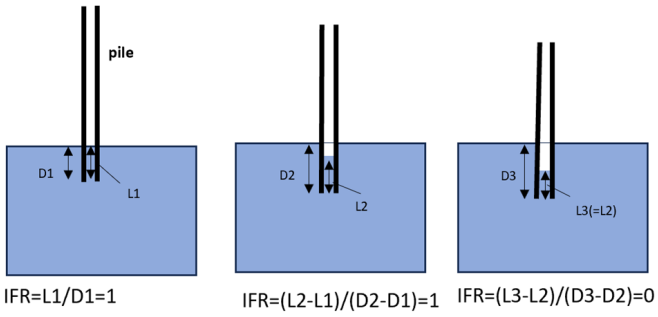

Figure 1.12: Soil plugging mode.

Another theory that analyses the plugging behaviour is called ”Active length of the soil plug” theory. According to this theory, the plug h’ lies within the embedded length of the pile as shown in the Figure 1.20 below:

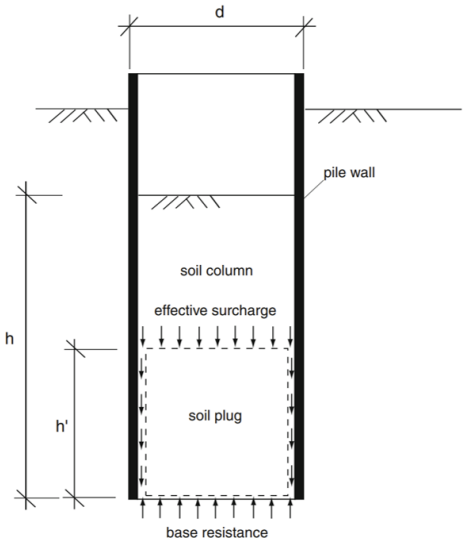

(a) Active length h’ of a soil plug.(Henke and Grabe, 2008)

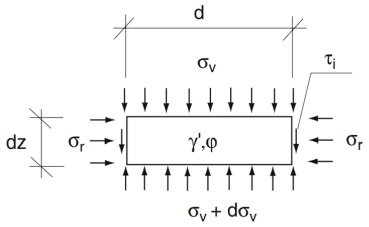

(b) Forces acting on an infinitesimal disc of the soil plug. (Henke and Grabe, 2008)

Figure 1.13: Active length of the soil plug. (Henke and Grabe, 2008)

It is generally assumed that during pile installation, a plug of soil inside the open-ended pile moves upward relative to the pile wall. The upper part of the soil column within the pile acts as a surcharge, exerting pressure on the lower layers. According to this theory, it is possible to predict the occurrence of a soil plug through a static equilibrium analysis. If the shear capacity along the length of the soil plug exceeds the mobilized base resistance, a plug will form inside the pile. Soil plugging is a phenomenon that cannot be categorically classified as either desirable or undesirable. On one hand, plugging increases the pile’s bearing capacity, which is beneficial. On the other hand, it also raises the driving resistance required during installation, which may be seen as a drawback. The overall impact of soil plugging depends on the specific environmental conditions and project requirements, and its effects can be either positive or negative depending on the context. Several factors influence the occurrence and degree of plugging, including the method of pile installation, soil density, penetration depth, and the pile’s geometry, specifically its diameter and length. While it is not yet clear which of these parameters is the most dominant, or whether a single dominant factor exists, certain trends have emerged from various studies. In general, smaller-diameter piles are more prone to plugging, as horizontal stresses and arching effects are more

likely to develop. Additionally, plugging is more likely in denser soils, where stronger intergranular forces lead to increased stress development. Finally, deeper pile penetrations tend to increase the likelihood of soil plugging. These factors must be carefully considered when assessing the impact of plugging on pile performance, as they play a significant role in determining the balance between enhanced bearing capacity and increased driving resistance.

1.5.5. How do different installation methods affect plugging effects?

According to (Henke and Grabe, 2008), the installation method plays a significant role to whether plugging effects will occur or not. The most common offshore pile installation techniques are impact driving and vibratory driving. However, since plugging behaviour has been observed to cases that the piles were jacked to the ground (Henke and Grabe, 2008), it was thought interesting to compare these three methods to understand better the plugging behaviour.

1.5.6. Pile Jacking

In this method, hydraulic rams are employed to push the piles into the ground, resulting in significantly reduced noise and vibration during installation. Given that differences in horizontal stresses inside and outside the pile can indicate the occurrence of plugging, it is essential to observe these areas separately to better understand the process. As mentioned earlier, jacking involves pushing the pile into the soil, subjecting the pile to monotonic shearing. This shearing causes the soil inside the pile to dilate, leading to a slight increase in the void ratio. As a result, high stresses develop inside the pile, with arching effects also becoming apparent. In contrast, outside the pile, there is no significant increase in stress as the pile penetrates. Therefore, the substantial difference in horizontal stresses between the inside and outside of the pile suggests that plugging is likely to occur in jacked piles, as the internal conditions promote this phenomenon more than the external environment.

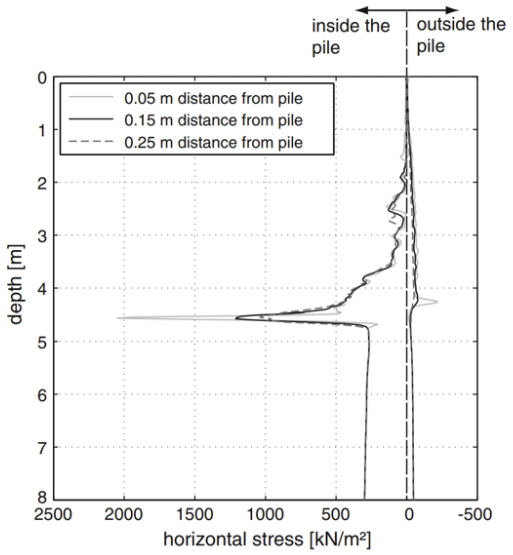

Figure 1.14: Horizontal stress distribution along several vertical paths at different distances from the pile wall- Pile jacking(Henke and Grabe, 2008)

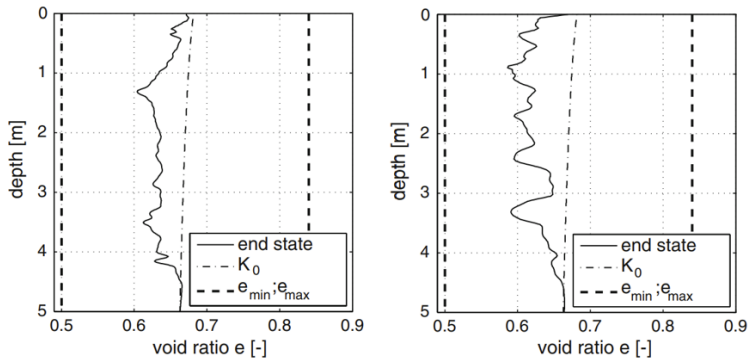

Figure 1.15: Void ratio distribution along vertical paths at a distance of 0.05m from the pile wall (left) and in the centre of the open-ended pile (right)(Henke and Grabe, 2008)

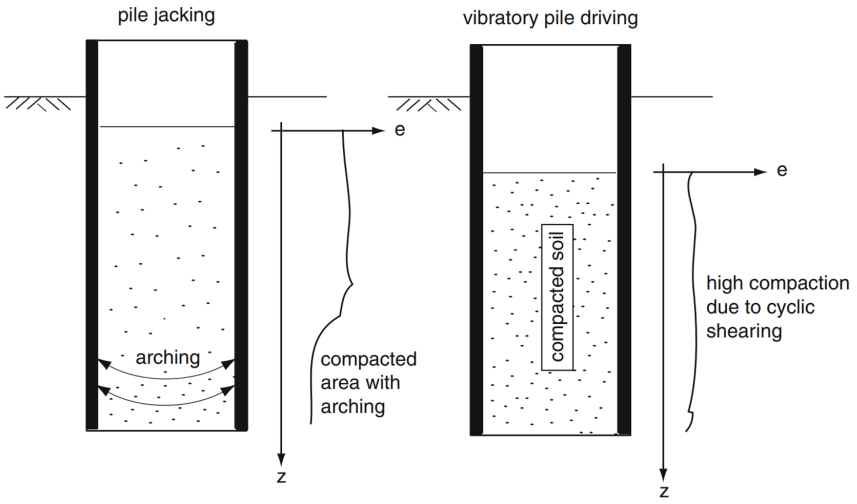

Figure 1.16: Arching mechanisms inside an open-ended pile due to pile jacking and vibratory driving(Henke and Grabe, 2008)

1.5.7. Vibratory Driving

By this method the pile is vibrated into the soil. Unlike the pile jacking, in the vibratory installation due to the continuous cyclic shearing, the voids of the soil inside the pile are highly compacted and thus the horizontal stressed are significantly less. Therefore, from various field tests it has been observed that inside a vibro-driven pile it is unlikely notice plugging effects. (Henke and Grabe, 2008). However, it should not be taken as a general conclusion that plugging does not occur in vibro-driven piles but that more influencing parameters need to be investigate as the driving input energy which is a key factor in this installation method.

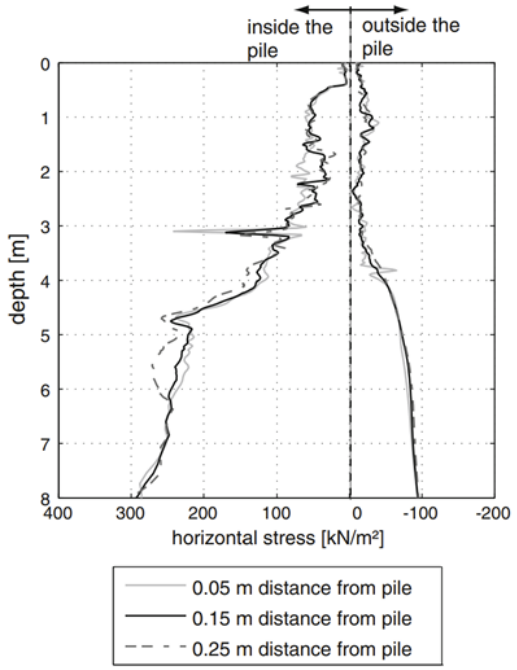

Fig. 14 Horizontal stress distribution along several vertical paths at different distances from the pile wall after about 4 m of vibratory driving into medium dense sand

Figure 1.17: Horizontal stress distribution along several vertical paths at different distances from the pile wall - Vibratory driving(Henke and Grabe, 2008)

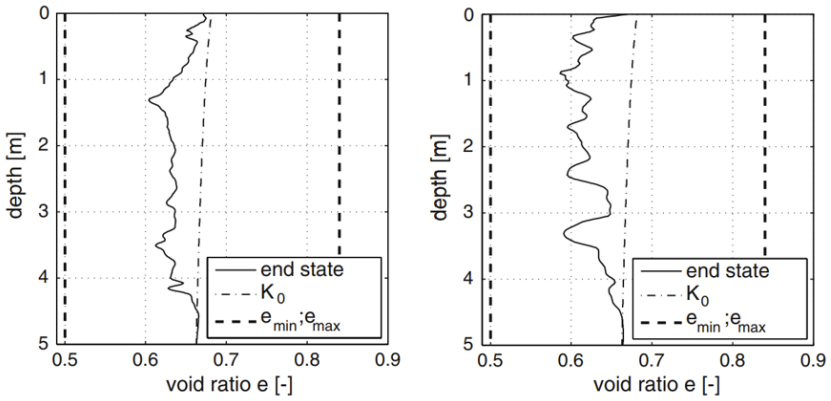

Figure 1.18: Void ratio distribution along vertical paths at a distance of 0.05m from the pile wall (left) and in the centre of the open-ended pile (right)(Henke and Grabe, 2008)

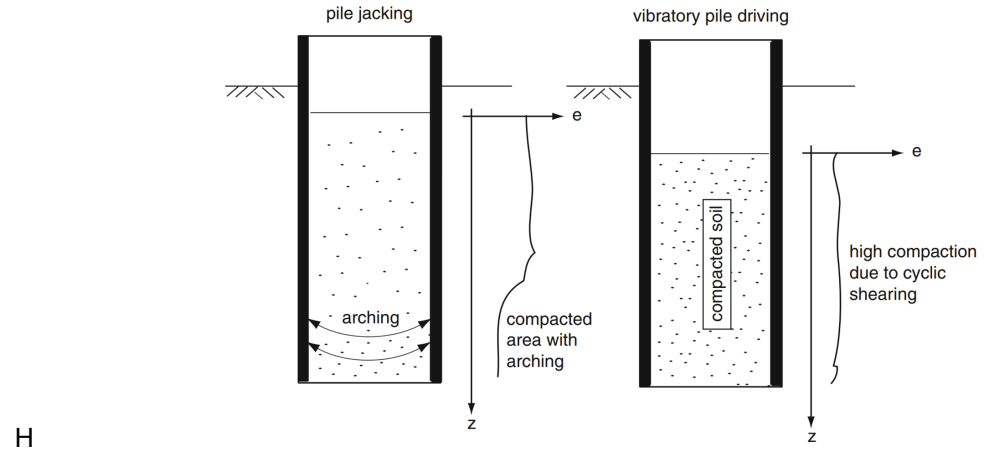

Figure 1.19: Arching mechanisms inside an open-ended pile due to pile jacking and vibratory driving(Henke and Grabe, 2008)

1.5.8. Impact Driving

Unlike vibratory pile driving, impact pile driving involves hammering the pile into the soil rather than vibrating it into place. The primary reason for this difference lies in the soil behavior at the pile-soil interface. In vibratory pile driving, cyclic vibrations tend to loosen the soil, preventing the development of arching effects and reducing the likelihood of soil plugging. This method is less prone to creating a stable plug due to the loss of confinement around the pile. (Henke and Grabe, 2008). Impact pile driving, however, is more controversial in terms of plugging potential. Some cases demonstrate the occurrence of soil plugging in impact-driven piles, while others as Henke and Grabe, 2008 argue that in impact-driven open-ended piles, the inertia of the soil body inside the pile prevents a soil plug from forming. Despite differing opinions, one clear conclusion is that for plugging to occur in impact-driven piles, certain key conditions must be met: a small pile diameter, dense soil conditions, and significant pile penetration depth. These factors increase the likelihood of arching effects developing, which in turn supports the formation of a stable soil plug.

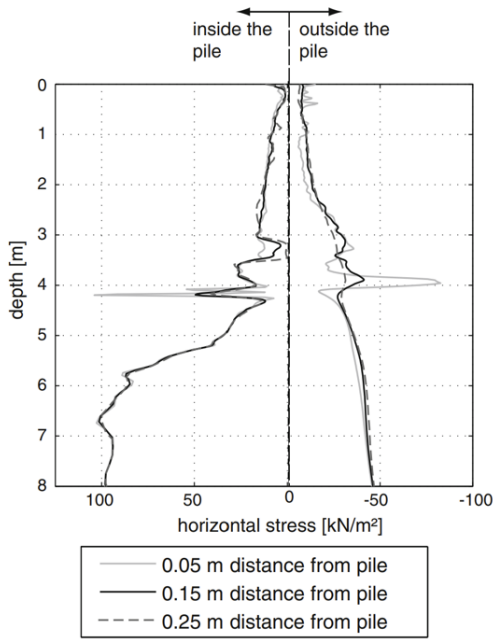

Figure 1.20: Horizontal stress distribution along several vertical paths at different distances from the pile wall - Impact Driving(Henke and Grabe, 2008)

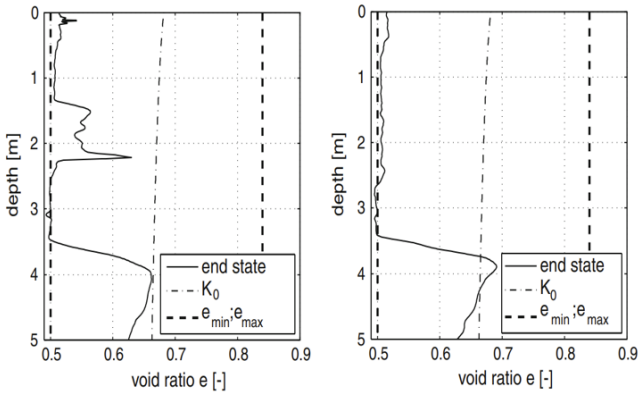

Figure 1.21: Void ratio distribution along vertical paths at a distance of 0.05m from the pile wall (left) and in the centre of the open-ended pile (right). (Henke and Grabe, 2008)

Moreover, two other parameters that affect significantly the soil plugging are the soil density and the pile geometry. Both the soil density and the installation method influence the soil plug height, with an increased tendency for plugging to occur in denser soil. Pile geometry significantly influences soil plugging. The pile diameter is the main influencing geometric factor for tubular piles. But for piles with different cross-section further geometric factors could be identified. Smaller diameter piles develop soil plug at shallower penetration depths than bigger diameter piles. The smaller the pile diameter, the higher the internal horizontal stresses at the pile toe(Henke and Grabe, 2013). Moreover, according to Puller, 2003 and Henke and Grabe, 2013, the formation of a plug is possible if one of the following criteria is fulfilled.

$$d_i < 0.02(\mathrm{Dr} - 30) = d_{i,\mathrm{lim}} \tag{1}$$

$$d_i < 0.083 d_{\mathrm{cpt}} \left(\frac{q_{\mathrm{ca}}}{p_a} \right) = d_{i,\mathrm{limt}} \tag{2}$$

In the relationship above, di,lim is the limiting diameter fro the occurrence of a soil plug, di is the internal pile diameter, Dr the specific soil compactness in (%), dcpt is the cone penetration resistance, pa the equivalent stress and qca the equivalent cone penetration resistance after Bustamante and Gianeselli (Henke and Grabe, 2013).

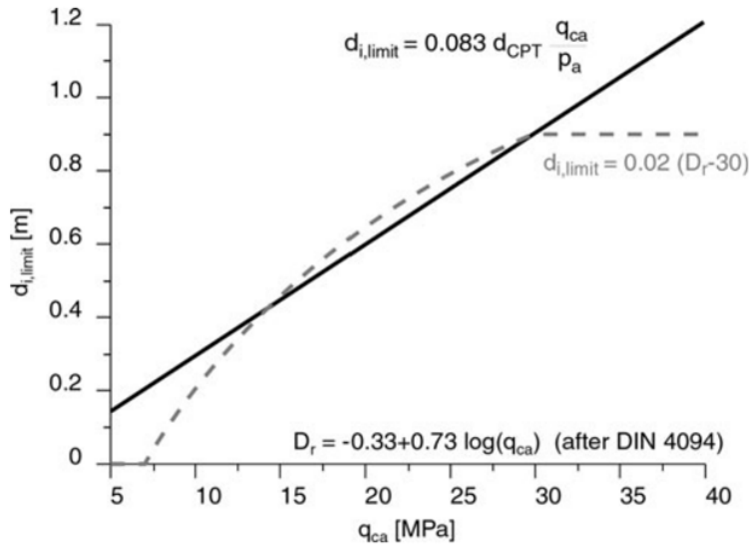

Figure 1.22: Criteria to predict plugging based on limiting pile diameter (Henke and Grabe, 2008)

1.5.9. Prolonged Blow Technology

Prolonged blow pile installation method operates by using a vast water tank, containing numerous tons of seawater, as a drop weight. This tank is lifted to a predetermined height using hydraulic cylinders and then automatically released to fall onto a pretensioned gas buffer arrangement, which serves as cushions to absorb the impact. This cushioning extends the duration of the impact by an order of magnitude compared to conventional hammers. Due to the relatively large driving energy, the increments for prolonged blow installation are fewer and of a significantly larger magnitude compared to impact driving. While not visually evident, the mode of installation shifts from stress wave-driven during impact driving to rigid body motion, primarily due to the prolonged impact duration. Therefore, the installation mode can be described as quasi-dynamic, falling between impact driving and cyclic jacking. (Quinten, T. O. (2024)) To harvest further knowledge and understanding of the soil – structure – water interaction the following setup was developed in the geotechnical centrifuge of TU Delft (Quinten, T. (2022)). The main principle followed to replicate prolonged blows in the experiment setup involves the use of a high stiffness spring to mimic its impact characteristics during centrifuge testing as well as a dedicated actuator that allows for a single blow at different accelerations utilizing a modular mass and an electromagnet. The test setup is completed by:

1. The centrifuge chamber
2. The pile-anvil system
3. A series of measurement sensors

2

Thesis Statement

2.1. Problem description

Offshore pile installation using impact driving generates underwater noise, posing environmental risks to marine life. To mitigate this, the prolonged blow technique offers a sustainable alternative, reducing noise emissions and pile fatigue by extending the duration of each blow (approximately 200 ms, compared to 8–12 ms in conventional hammers) through reduced interface stiffness. Experimental investigations, including centrifuge experiments at TU Delft using a custom prolonged blow generator, validate its potential. These studies highlight the technique's ability to minimize environmental impact and advance sustainable offshore pile installation practices.

In this study, we focus on the following research objectives:

(I) determining the effect of the impact energy on the installation efficiency of the pile;

(II) assessing the effect of pile diameter on the installation efficiency of the pile;

(III) investigating the effect of saturation with viscous fluid on the installation efficiency of the pile.

A complete overview of all experiments is provided by Table Test Matrix. It should be noted that all experiments are conducted on GEBA sand, prepared at a relative density of approximately 80%. In the following paragraphs, a research question (Q) and hypothesis (H) is presented for each research objective. In the question section, the variables which are changed between experiments are explained.

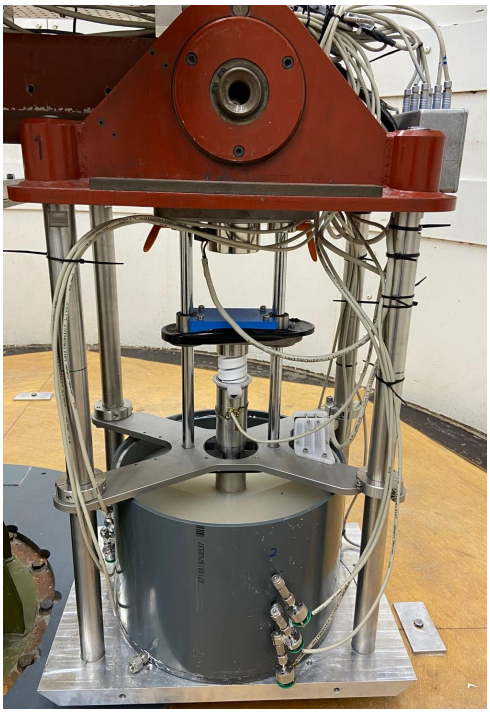

Figure 2.1: The centrifuge carrier with the dry sample

2.2. Question 1 (Q1) : What is the effect of impact energy on the installation energy

The first research question of this thesis focuses on investigating the effect of impact energy on the driveability of the pile.

The system's potential energy is determined by the mass of the ram, the height from which the mass falls, and the gravitational acceleration. By adjusting these parameters, different energy combinations and impact velocities can be achieved. To optimize the number of experiments, the driving energy is varied by altering the falling height of the mass while keeping the ram's mass constant. These experiments are conducted at different centrifuge acceleration levels. However, since changes in centrifuge acceleration affect the prototype dimensions, the results are analyzed separately for each g-level. To clearly distinguish between g-levels in the Table 3.2, a suffix in the form of "-{N}g" is added in the research question column, where {N} represents the corresponding g-level.

The experiments explore three distinct energy levels, achieved by varying the falling height of the mass while maintaining a constant mass. The selected heights are 50 mm, 40 mm, and 20 mm. Each of these energy levels is tested at three acceleration levels: 10g, 30g, and 50g.

This experimental setup enables a detailed investigation of how different energy inputs and centrifuge acceleration levels influence pile driveability during installation with prolonged blows.

2.3. Hypothesis 1 (H1): The expected influenced of impact energy on the installation efficiency

A higher falling height increases the impact energy, allowing more energy to transfer through the pile and into the soil. As the applied energy increases, it is expected that the pile installation will require fewer blows, as the penetration per blow is greater. For instance, when comparing experiments with higher and lower falling heights (e.g., 50 mm versus 20 mm), the pile is anticipated to penetrate more per blow with the greater falling height.

While soil plugging is more commonly associated with jacked piles, it can also occur in impact-driven installation techniques, particularly when the pile diameter is sufficiently small. Studies have shown that plugging effects are more influenced by the falling height of the mass than by the mass itself (Jeong et al., 2015). Thus, it is possible to observe plugging behavior in experiments with higher falling heights (50 mm). Additionally, when the acceleration level of the centrifuge decreases, the prototype pile that corresponds to the model pile will have a smaller diameter. Therefore, for lower acceleration level (10g) is it also possible that plugging behaviour will be observed.

2.4. Question 2 (Q2): What is the effect of pile diameter on the installation efficiency?

The demand for higher wind turbines is increasing, which raises the need for larger monopile dimensions. Monopile foundations are among the most popular offshore wind foundations in the market and have been used widely in offshore wind over the last few decades. The monopile is a construction consisting of a steel pipe with a diameter ranging from approximately 5-6 meters and up to 13+ metres in diameter. (CSWMonopiles, 2024). Additionally, phenomena such as soil plugging are closely related to pile geometry and are crucial during installation procedures. Therefore, how the driveability is affected by different pile diameters is an important aspect for investigation and is chosen as the second research question of this thesis.

Experiments are conducted at three different acceleration levels: 10g, 30g, and 50g. When testing in the centrifuge facility, the acceleration level plays a vital role since many values as the dimensions of the pile, or the force are affected by it. Hence it is expected that increasing the g-level in the centrifuge, the dimensions of the model pile will correspond to bigger prototype dimensions and also the force recorded during the experiments is expected to be higher.

The dimensions of the scaled model and the prototype are linked to the value of the gravitational acceleration of the centrifuge. According to Table 3.1, linear dimension scales linearly with N. Therefore, by changing the acceleration level of the centrifuge, different prototype diameters can be modelled with the same model pile.

In Table 3.1, some of the basic scaling laws are presented. Therefore, applying different n-levels to the centrifuge translates to different prototype dimensions of the pile. Additionally, other values, such as acceleration and force, are affected by the n-level of the centrifuge.

2.5. Hypothesis 2 (Q2): What is the effect of pile diameter on the installation efficiency?

Changing the acceleration magnitude for different tests results in two concurrent effects. At lower acceleration levels, the model represents smaller-diameter prototype piles, while at higher accelerations, the corresponding prototype pile has a larger diameter. Simultaneously, lower acceleration leads to reduced soil confining pressure, whereas higher acceleration results in increased confining pressure. Although the relative density of the material remains consistently around 80%, the soil's confining pressure varies with the centrifuge's acceleration level. Furthermore, the embedment ratio (L/D) of the pile remains similar across all experiments due to the adjustment of the g-level.

Smaller-diameter piles tend to develop soil plugs at shallower penetration depths compared to larger-diameter piles. The smaller the pile diameter, the higher the internal horizontal stresses at the pile toe (Henke and Grabe, 2013). Given that plugging is more prone to occur in a system with a small diameter pile being installed in stiffer soil material, it is challenging to determine which of the two described effects will dominate in each test. Additionally, plugging effects are highly influenced by the driving method and the pile geometry. At this research only the effects of pile geometry will be investigated. The driving resistance of open-ended piles is significantly affected by the plugging effect, making it important to investigate plugging behavior when a pile is installed using this technique.

Moreover, according to Puller, 2003 and Henke and Grabe, 2013, the formation of a plug is possible at least one of the criteria are met. Either equation (1), $d_i < 0.02(\text{Dr} - 30)$ or equation (2) $d_i < 0.083 d_{\text{cpt}} \left(\frac{q_{\text{ca}}}{p_a}\right)$. To satisfy those, pile diameter less than 0.9 m should be tested. Therefore, it is expected that in experiments with 10g level, plugging is possible to happen. In Table 2.1, the analogy between the prototype dimensions and the dimensions of the model are presented.

		Model Pile	Prototype		
	Units		10g	30g	50g
Outer Diameter	[m]	$42 * 10^{-3}$	0.42	1.26	2.1
Length	[m]	$175 * 10^{-3}$	1.75	2.25	8.75

Table 2.1: Model Pile and Prototype Dimensions

2.6. Question 3: What is the effect of saturation with viscous fluid on the installation efficiency?

Installation with prolonged blows is an offshore pile installation technique, meaning that it will be applied under saturated soil conditions. Thus, it is of high importance to investigate how the effective stresses and pore pressures are generated when using this technique and how they affect the driveability of the pile. The rate at which a load is applied to soil affects its drainage capacity, making it crucial to assess whether sufficient time is available for drainage. If drainage occurs, pore pressures do not influence the soil's behavior. However, under undrained or partially drained conditions, pore pressure becomes a key factor. If the soil contracts under load, pore pressure rises, reducing effective stress. Conversely, if the soil dilates, pore pressure decreases, increasing effective stress, which can negatively affect pile drivability.

Saturated experiments are prepared using a viscous fluid. When a pile is installed in saturated soil, pore pressures develop. Due to the different stress states around the pile caused by the introduction of the pore fluid, energy diffusion occurs. By measuring these pressures and observing the process of their generation and dissipation, how the energy diffuses from the pile to the soil can be deduced.

2.7. Hypothesis 3: The expected influence of saturation with viscous fluid on the installation behaviour.

The concept of prolonged blows, means that the energy is dispersed over a longer period compared to a blow from a conventional hammer, therefore it is still to be investigated how the pore pressures develop. In general, the inertial interaction between the soil and the structure occurs when forces are transmitted to the soil by the dynamic response of the structure. Installation with prolonged blows has much larger displacement amplitudes that impact hammering. The loading rate is slower, therefore soil inertia effects might be less relevant. The loading rate of the soil affects also its drainage conditions, thus is it important to investigate whether the soil will have enough time to drain or not. If time suffices , then there will be no influence. However, if the condition is undrained or partially drained, there will be an influence from the pore pressures that needs to be investigated. If the response of the soil is undrained or partially drained, two things are possible to happen. Based on the state of the soil, when force is applied to it, it might be dilated or contracted. In case of contraction, the pore pressures will be elevated and thus the effective stresses decrease. In case of dilation, there will be negative change in pore pressures that will result in higher effective stresses which is non beneficial for the pile drivability.

Due to the prolonged blows, the drivability might be negatively affected compared to a conventional impact driving method that creates a shockwave and transmits a large amount of energy instantly to the soil through the pile. On the other hand, the prolonged blows could generate effective stresses that create a beneficial stress state and facilitate installation. However, since the relative density of the sample is relatively high (around 80%), is is expected to observe dilation in this case and therefore a negative influence in the driveability of the pile.

Below the test matrix with all the experiments that were conducted is presented.

Table 2.2: Test Matrix

Date	N [g]	Ram mass [kg]	Falling height [mm]	Potential energy [J]	Test number	Relative density [%]	Research Question	Test ID
6/09/2023	50g	1.889	40	37.78	1	87.5	Q1-50g; Q2-40mm	D50g/40mm
8/6/2023	50g	1.889	40	37.78	2	81	Q1-50g; Q2-40mm	D50g/40mm
10/5/2023	50g	1.889	40	37.78	3	88.2	Q1-50g; Q2-40mm	D50g/40mm
12/9/2023	50g	1.889	20	18.89	4	75.7	Q1-50g; Q2-20mm	D50g/20mm
13/10/23	50g	1.889	20	18.89	5	82	Q1-50g; Q2-20mm	D50g/20mm
13/10/23	50g	1.889	50	56.67	6	80.7	Q1-50g; Q2-60mm	D50g/60mm
07/09/23	30g	1.889	40	22.668	7	90.8	Q1-50g; Q2-40mm	D30g/40mm
14/07/23	50g	1.889	40	37.78	8	86.5	Q1-50g; Q2-40mm	D50g/40mm
16/10/23	10g	1.889	20	3.778	9	81.8	Q1-10g; Q2-20mm	D10g/20mm
19/10/23	30g	1.889	50	28.35	10	82.3	Q1-30g; Q2-50mm	D30g/50mm
20/10/23	50g	1.889	50	47.225	11	80	Q1-50g; Q2-50mm	D50g/50mm
20/10/23	30g	1.889	20	11.335	12	80	Q1-30g; Q2-20mm	D30g/20mm
23/10/23	10g	1.889	40	7.556	13	79.3	Q1-10g; Q2-50mm	D10g/40mm
23/10/23	10g	1.889	50	9.445	14	81.1	Q1-10g; Q2-50mm	D10g/50mm
25/10/23	50g	1.889	40	37.78	15	sat	Q3	D50g/40mm
26/05/23	50g	1.889	40	37.78	16	82.4	Q1-50g; Q2-40mm	D50g/40mm
07/09/23	30g	1.889	40	22.668	17	90	Q1-50g; Q2-40mm	D30g/40mm
30/10/23	10g	1.889	20	3.778	18	79.8	Q1-10g; Q2-20mm	D10g/20mm
31/10/23	10g	1.889	40	7.556	19	84.6	Q1-10g; Q2-40mm	D10g/40mm
31/10/23	10g	1.889	50	9.445	20	81.3	Q1-10g; Q2-50mm	D10g/50mm
31/10/23	50g	1.889	40	37.78	21	sat	Q3	D50g/40mm

3

Physical Modelling

Soil is a complex material composed of small, heterogeneous particles, formed over time through various natural processes. Analyzing soil response under different loading conditions presents significant challenges due to its nonlinear bulk properties, strain amplitude and loading path dependence, and the complexities of its cyclic and dynamic behaviors. Despite these challenges, soil can be modeled as a continuum medium characterized by averaged parameters, such as strength and stiffness. Physical modeling serves as a crucial tool for understanding the interactions between soil and structures, as well as the soil's response and behavior. This approach helps to address the complexities arising from the intricate stress-strain histories of soils. There are different scales of physical modeling, each with its own advantages and disadvantages. The three primary types are small-scale models (centrifuge models), large-scale models, and full-scale models (field tests). Full-scale models are particularly realistic, as they maintain a grain size ratio that closely aligns with the prototype, thus minimizing scale effects. In contrast, small-scale tests are significantly influenced by scale effects, which can impact the validity of results. Additionally, full-scale tests accurately replicate natural conditions and processes, such as compaction, without the need for artificial soil samples. In small- and large-scale models, however, soil samples must be created to simulate real behavior, which can be time-consuming—especially for saturated samples. On the other hand, small- and large-scale models allow for easier identification of soil properties, such as relative density. In full-scale tests, site investigations are necessary to determine soil properties, which can be quite challenging. Regarding cost and test repeatability, small-scale tests are relatively inexpensive and easy to repeat, while field-scale tests are the most costly and often cannot be repeated multiple times.

3.1. Centrifuge Modelling

Physical modelling in the centrifuge is a widely used method to create similar stress conditions in the model to the prototype. The main idea is that a model which has N times smaller geometry than the prototype is tested in the centrifuge under an acceleration field with a magnitude of N times the Earth's gravity (Scofiels,1980). The centrifuge generates enhanced gravitational forces by rotating the model at high speeds. This centrifugal acceleration simulates the increased stresses that the prototype would experience under actual gravitational conditions. There have already been many studies on physical modelling with a geotechnical centrifuge as pile driving or pile installation. Some examples are the centrifuge modelling of offshore monopile foundation (Gourvenec et al., 2011) and the impact driving of monopiles in the centrifuge to study the effect on the lateral response (Maatouk et al., n.d.). Its use is broad and can be expanded on different load types, lateral or vertical, on different soil types, fine- or coarse-grained materials on different models, piles, caissons etc. Furthermore, depending on the needs of the study but on the capabilities of the facility, the gravitational acceleration of the centrifuge can vary as well.

$$N_g = \omega^2 \cdot r \tag{3.1}$$

The amplification factor with respect to the earth's gravitational acceleration, g, is often indicated as N. The g-level varies based on the distance of a reference point in the model relative to the centrifuge axis. Consequently, it is not uniform throughout the depth of the soil sample, meaning that the stress level is only scaled by N at a single level within the sample. The amplification factor above this reference point is lower than the intended stress level, while below it, the amplification factor is higher.Figure 3.1b shows the concept of under and over scaling. Moreover, in the Figure 3.1a, the distribution of the vertical stress in the model and the corresponding prototype are shown (Taylor, n.d.).

Gravity enhancement in the centrifuge affects numerous physical quantities. Therefore, it is crucial that the design of the centrifuge study considers these changes to ensure similitude between the model and the prototype. Extensive research has addressed this issue, (Granier et al.2007), culminating in a ”scaling law catalogue.” It is important to note that the replication of prototype stress conditions in the model—and consequently its mechanical behavior—is only achievable when the same type of soil is utilized. The key scaling parameters relevant to this study are presented in the table below. The influence of enhanced gravity is specific to each physical quantity and varies based on its dimensions, as defined by the International System of Units (SI).

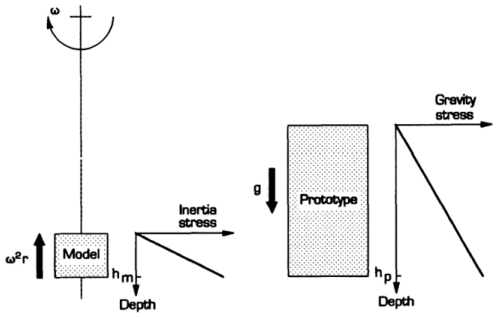

(a) Inertial stresses in a centrifuge model induced by rotation about a fixed axis correspond to gravitational stresses in the corresponding prototype (Taylor, n.d.)

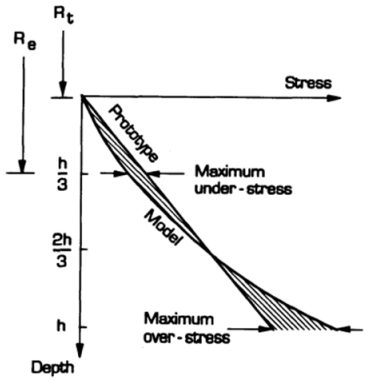

(b) Comparison of stress variation with depth in a centrifuge model and its corresponding prototype Taylor)

Figure 3.1: Scale Effects(Taylor, n.d.)

Table 3.1: Scaling Parameters

Term	Prototype	Model	SI Dimension
Acceleration	1	N	$[L/T^2]$
Velocity	1	1	[L/T]
Area	1	$1/N^2$	$[L^2]$
Volume	1	N^3	$[L^3]$
Density	1	1	$[M/L^3]$
Unite Weight	1	N	$[M^2/T^2\ L^3]$
Mass	1	$1/N^3$	[M]
Force	1	$1/N^2$	$[ML/T^2]$
Stress	1	1	$[L/M\ T^2]$
Strain	1	1	[-]
Dynamic Time	1	1/N	[T]
Seepage Time	1	$1/N^2$	[T]
Frequency	1	N	[1/T]
Energy	1	$1/N^3$	$[ML^2/T^2]$
Impulse	1	$1/N^3$	[ML/T]

3.2. TU Delft Centrifuge

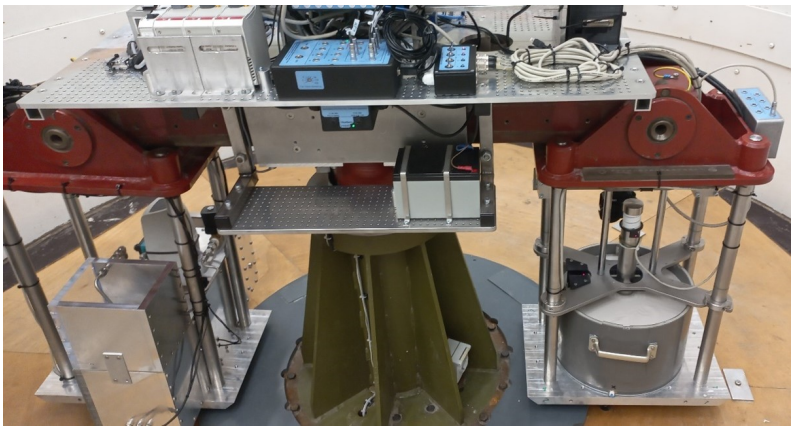

Figure 3.2: Centrifuge

The centrifuge facility that was used for the experiments that were conducted for this research is at Geo-Engineering lab of the Civil Engineering and Geosciences that is part of the Delft University of Technology, Figure 3.2. The centrifuge, originally designed by Allersma in 1990, underwent significant renovations in 2009 by Dijkstra to enhance its functionality (Quinten,2019). This advanced centrifuge features a nominal radius of 1.3 meters and is capable of achieving a maximum acceleration of 300 g, with a top rotation velocity of 450 RPM. The dimensions of the carriage are 0.38 m in length, 0.32 m in width, and 0.56 m in height. It is designed to accommodate a maximum payload of 30 kg at an acceleration of 300 g, equating to a total capacity of 9000 kg.F. These specifications make the centrifuge a powerful tool for simulating increased gravitational forces in various experimental applications.

3.2.1. Experimental set up

The set of the experiments consists of a soil sample, an actuator and the centrifuge facility.
To simulate a BLUE-blow, the anvil is fitted with a stiff linear spring. For installation a dedicated actuator is development and verified by means of numerical simulation. (Quinten, 2022) The soil sample is placed on the bottom plate of the actuator as be seen also in the Figure 3.3 below:

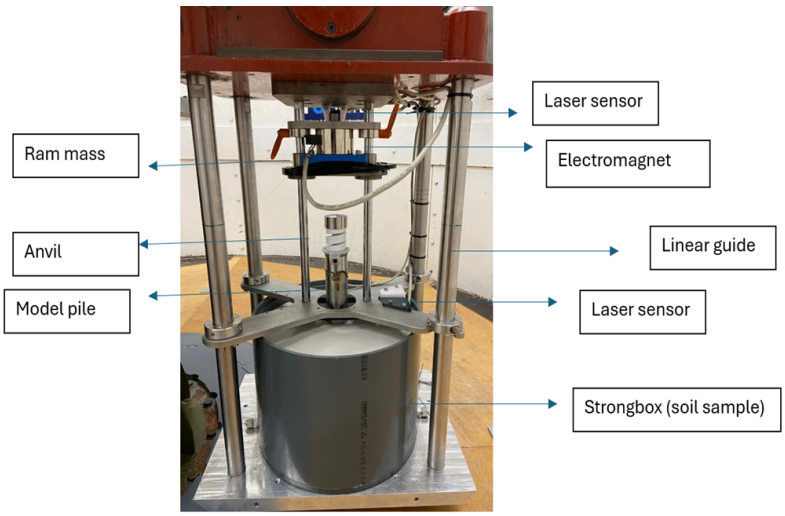

Figure 3.3: Centrifuge-carrier with strongbox and pile

3.2.2. Sensors

In the dry tests, data collection is facilitated through the use of two laser sensors and strain gauges. The laser sensors monitor the movement of both the pile and the ram mass, while the readings from the strain gauges are converted into force signals, utilizing the known material properties of the pile. To quantify the pile driving energy, the strain experienced by the pile is recorded and transformed into a force signal. Given the established material properties, such as the modulus of elasticity (E), the strain readings are effectively converted. The strain gauges are arranged in a full Wheatstone bridge configuration, consisting of four strain gauges positioned axially on the exterior of the pile, evenly spaced at 90° intervals. This setup ensures accurate and reliable measurements of the forces involved during the pile driving process. In the saturated experiments, the strongbox was modified to enhance its functionality, now incorporating four plate filters at the bottom Figure 3.4 and nine pore pressure sensors Figure 3.5, Figure 3.6 strategically positioned at three different vertical levels and radial distances from the center of the sample. The sensors are located at distances corresponding to one, two, and three diameters from the center of the pile, labeled as 1D_out, 2D_out, and 3D_out, where D_out represents the outer pile diameter of 42 mm. The radial distances of the sensors are set at 0.5D_out, 1D_out, and 1.5D_out. This configuration allows for comprehensive monitoring of pore pressure variations throughout the soil sample during the experiments, facilitating a detailed analysis of the saturated conditions and their effects on pile driving performance.

Figure 3.4: four filters at the bottom of the strongbox

Figure 3.5

Figure 3.6

Figure 3.7: pore fluid pressure sensors

3.2.3. Data Acquisition System

The data acquisition system consists of both low-frequency (MP3) and high-frequency components. The high-frequency system is crucial for precise load measurements, as it captures data at a rapid rate, ensuring accuracy. While the high-frequency system provides more comprehensive displacement measurements, the low-frequency system can also record displacements, and pore fluid pressures though with less detail. This dual system approach allows for a robust analysis of both load and displacement during the experiments.

3.2.4. Cyclic loading

Louwerse, F. (2023) investigated the effects of cyclic loading on soil-pile interfaces, focusing on cyclic amplitude, cyclic rate, and the number of cycles, using both element-scale Direct Shear Tests (DST) and lab-scale pressure chamber experiments with an instrumented model pile. Key findings from the cyclic shear tests include that the initial cycles significantly reduce shear and vertical stresses, and this reduction is amplified with increasing cyclic amplitude and cycle number, indicating contractive behavior through normal displacement. Dilation observed in monotonic tests was absent in cyclic shear tests, and stiffer conditions reduced shear stress but limited normal displacement. The interface friction angle between steel and Geba sand was measured at 23.15°.

The pressure chamber experiments of Louwerse, F. (2023), revealed that soil densification occurs along the pile shaft due to particle rearrangement and breakage during penetration, leading to higher pressures along the shaft compared to the pile tip. Larger displacement amplitudes (e.g., installation with prolonged blows) generated higher lateral pressures than smaller amplitudes. While friction fatigue could not be conclusively assessed due to sensor limitations, strain gauge data from the installation with the prolonged blows showed the greatest force development, suggesting a correlation between penetration depth and shaft friction. Further improvements in instrumented pile sensors are needed to better evaluate friction fatigue.

Experiments in dry conditions using the DST and pressure chamber highlight the need for further testing under saturated conditions to better simulate offshore monopile environments. Improvements are necessary, including addressing sensor failures, adding reliable pore pressure sensors, and recalculating load capacities. The pressure chamber development has made progress, but issues like faulty sensors, sealing problems, and challenges in instrumenting the model pile persist. Replacing the top ring and optimizing the setup could enhance experimental success. Expanding the setup to study particle breakage and interface phenomena would provide deeper insights into soil-structure interactions during pile driving.

4

Sample Preparation

This chapter provides a detailed description of the sample preparation procedures for both dry and saturated conditions, highlighting the similarities and differences between the two approaches. Both types of samples were prepared using GEBA Sand, a fine sand with the characteristics listed in Table 4.1. In both cases, the target relative density was approximately 80%. For the dry samples, particular care was taken to achieve this relative density through controlled compaction methods. In contrast, the preparation of saturated samples involved using a viscous fluid to ensure proper saturation. The following sections will elaborate on the specific techniques used for each case. A table outlining the geotechnical properties of GEBA Sand is provided below to further clarify its characteristics.

Table 4.1: Geotechnical properties of Geba sand according to (Wang et al., 2020)

geotechnical Properties	Geba Sand
D50 [mm]	0.117
Specific gravity, Gs [-]	2.65
Minimum void ratio [-]	0.64
Maximum void ratio [-]	0.72
Residual friction angle [degree]	36.0

4.1. Dry Samples

At first the samples were being prepared with the dry pluviation technique. Dry pluviation is a technique applied for preparation of sandy soil samples for physical modeling.(Cheshomi et al., 2021). This technique is significantly influenced by the height from which the sand is poured into the strongbox, therefore, it is crucial to maintain a constant height throughout the procedure.
The soil particles are rained in the mold after passing through the mesh with certain opening sizes. Soil was rained into the strongbox from a specific height creating uniform thin soil layers inside the strongbox. After each layer was made, the sample was hit with a hammer perimetrically and uniformly to densify. However, it was observed that this technique results in a sample that is denser on the outside, while the degree of compaction decreases towards the center. Therefore, even though the sample had a total relative density of around 80%, the sample was locally looser or denser which was affecting the results of the pile installation. Thus, the shock wave technique was employed, by which the strongbox was placed on a device that generates a shock wave to the sample by manually lifting it up and then letting it drop (instead of using the hammer for the compaction).
The procedure followed was similar to the procedure followed for the dry pluviation method since the soil was drained into the strongbox from a specific height. This sample was gradually built up by thin soil layers. To achieve a relative density of 80% in the specific strongbox, a soil mass of around 19 kg should be added to the strongbox. Every 3 kg that were added, the sample was subjected to a shock wave to densify. That way a more uniform densification was applied.

4.2. Saturated Samples

Two saturated samples were also made and tested in the centrifuge under 50 g acceleration. This paragraph outlines the procedure for saturating the samples. For the saturated experiments, the same strongbox is utilized, albeit with some modifications. Specifically, it is equipped with four plate filters at the bottom and nine pore pressure sensors. These two additions can be seen in Figure 5.1 , Figure 5.1 and Figure 5.1 below. Viscous fluid is introduced into the strongbox through a tube connected to a valve located at the bottom. An internal network of small channels directs the fluid flow toward four porous stones embedded in the filter plate, ensuring an even distribution of viscous fluid into the sample. The pore pressure sensors are strategically positioned at three different vertical levels and three radial distances from the center of the sample. These radial distances correspond to one diameter, two diameters, and three diameters from the center, labeled as 1Dout, 2Dout, and 3Dout, respectively. Here, Dout represents the outer pile diameter, which is 42 mm. The sensors are also placed at radial distances of 0.5Dout, 1Dout, and 1.5Dout. This configuration allows for comprehensive monitoring of pore pressure variations throughout the sample during the experiments.

The system that was used to saturate the sample consists of two parts. A vacuum chamber and a container filled with viscous fluid that was placed above the vacuum chamber as can be seen also in the Figure 4.1a below. The reason for that is to achieve a height difference between the container of the viscus fluid and the vacuum chamber, in which the strongbox will be placed, to achieve a hydraulic head difference. The vacuum chamber and the container were connected to a tube that had a reduction valve to help to create pressure difference between the two. Moreover, these two were connected to another tube so that the viscus fluid could flow from the container to the vacuum chamber and lastly to the bottom of the strongbox with another tube that was connected between the vacuum chamber and the bottom of the strongbox. Therefore, it is evident that the flow of the viscous fluid occurred from the bottom upwards until the sample was fully saturated. To facilitate this upward flow, a pressure difference had to be maintained between the container and the vacuum chamber. The steel tube connecting the vacuum chamber and the container included a third branch, which was utilized to connect the container to a tank of viscous fluid for filling purposes. Below a figure of the chamber is presented to make the visualisation easier.

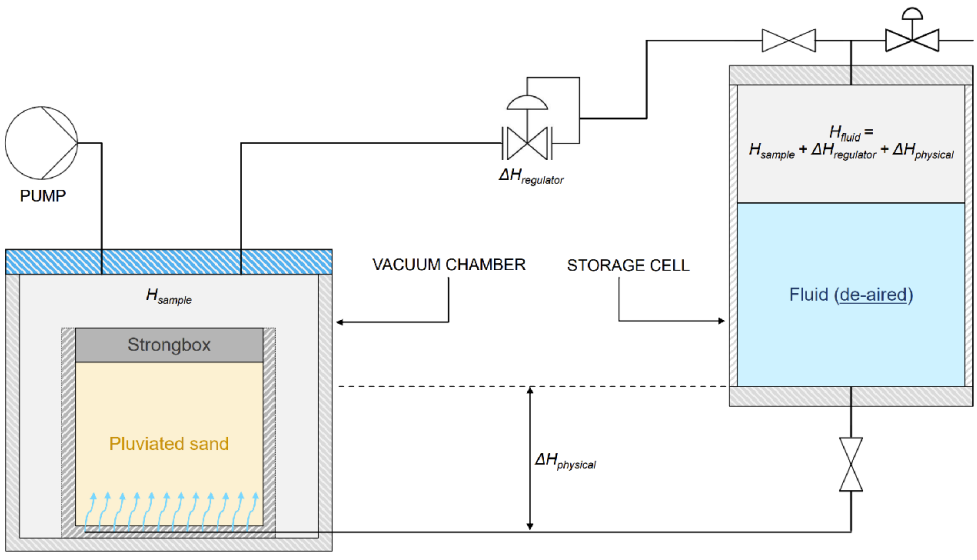

Figure 4.2: The vacuum chamber and the container with the viscous fluid

(a) The vacuum chamber and the container with the viscous fluid

Figure 4.1: On the top is the strongbox with the pore fluid sensors and below is the hardware by which the sample was saturated.

It is important to note that the branch between the container and the chamber could be sealed using an additional valve. Furthermore, the tube equipped with a reduction valve between the container and the chamber could also be blocked. This configuration ensures precise control over the fluid flow during the saturation process. In summary, the strongbox was positioned inside the vacuum chamber and connected via a tube through which the viscous fluid flowed. By creating a pressure difference, the viscous fluid was gradually drawn from the bottom of the strongbox to the top. This saturation process was deemed complete when the soil surface was covered by a thin layer of viscous fluid, as illustrated in the accompanying picture. Prior to placing the strongbox in the vacuum chamber, a dry sample was prepared. The sand was carefully poured into the strongbox, and the shock wave technique was employed to densify the dry sample. This procedure is described in detail in the preceding paragraph of the 4.1.

4.2.1. Lessons learned from the procedure of the saturation

First saturated sample The first attempt to saturate the sample is now described, along with some problematic aspects and the ideas implemented in the subsequent attempt. Initially, the pressure difference between the vacuum chamber and the storage cell is set to 15 kPa. Consequently, the pressure in the viscous fluid container remains at approximately -80 kPa, while the vacuum chamber is maintained at around 95 kPa. The flow is slow but steady during the first hour; however, after a while, uplift is observed. This issue may stem from the high pressure difference or the slow absorption of the viscous fluid by the soil sample. Due to the high viscosity of the fluid, the permeability of the soil is reduced, leading to a diminished flow through the pores. This reduction increases the likelihood of fluid being trapped beneath the sample, ultimately resulting in floating.

Based on these observations, it was decided to close the valve between the storage cell and the strongbox, effectively inhibiting flow between the two. This adjustment allowed the viscous fluid already present in the strongbox to be absorbed by the soil. Additionally, heaving occurs due to gravity as the soil becomes saturated; as the soil absorbs the viscous fluid, the weight of the saturated material may lead to uplift, exacerbating the issue of heaving.

As anticipated, the soil surface began to decrease, indicating that the soil was gradually absorbing the fluid. The valve was then reopened, but the pressure difference between the storage cell and the vacuum chamber was reduced, with the new pressure in the vacuum chamber set to 10 kPa. Unfortunately, heaving was observed again. Consequently, the previous procedure was repeated: the valve was closed, allowing the sample to soak.

Meanwhile, the pressure in the vacuum chamber could be maintained automatically, necessitating a reapplication of the vacuum to decrease the pressure. An interesting observation was made: the moment the vacuum was activated and pressure began to decrease, the soil surface rose rapidly. This observation supports the assumption that the high-pressure difference was causing the sample to heave, as the viscous fluid did not have sufficient time to be properly absorbed, resulting in a layer that pushed the entire soil body upward.

Moreover, when the pressure difference increases, the soil surface becomes wet more quickly in certain areas, likely due to suction effects. While some fluid is drawn from the soil, a larger portion remains trapped, requiring additional time for absorption. Thus, the wet surface expands more rapidly, and the soil surface heaves faster as the pressure difference rises. Additionally, small cracks begin to form at the sides, extending toward the center of the sample.

Figure 4.3: Procedure of sample saturation

This procedure was followed until the sample was fully saturated, which lasted around two days Therefore, one more problem was the time that the sample needed to be properly saturated.
One more remark is that in case the dry sample is not completely uniformly densified, and some parts are denser than other the pores in these ares will be smaller so the capillary rise will be higher, that is probably why the sample starts to get wet from the sides towards the middle.Another contributing factor could be the slightly higher permeability along the smooth walls of the strongbox.
This increased permeability may facilitate fluid movement more readily along the sides than through the soil matrix, further exacerbating the heaving observed during the saturation process. As already described to properly densify the dry sample apart from the shock wave technique it was also hammered. Due to this hammering, the outer part of the sample was likely denser that the inner parts.

Second saturated sample For the second saturated sample, some modifications were made in order to resolve some of the issues presented in 4.2.1. Firstly, a plate was placed on top of the sample to obstruct the lift-up from happening, as can be seen in the Figure 4.4a below. For the case of -up-heave we are using a surcharge so there is more downward pressure on the sample. When the heave was obstructed, the pressure difference could be increase which would lead to increase flow and therefore less time for the sample to be fully saturated. Thus, some of the problems were successfully solved.
In this procedure a dry sample was first made and then the viscus fluid was gradually flowing from the bottom of the sample to the top until the sample was fully saturated.

(a) Plate onto the sample to decrease heaving

(b) Saturated sample

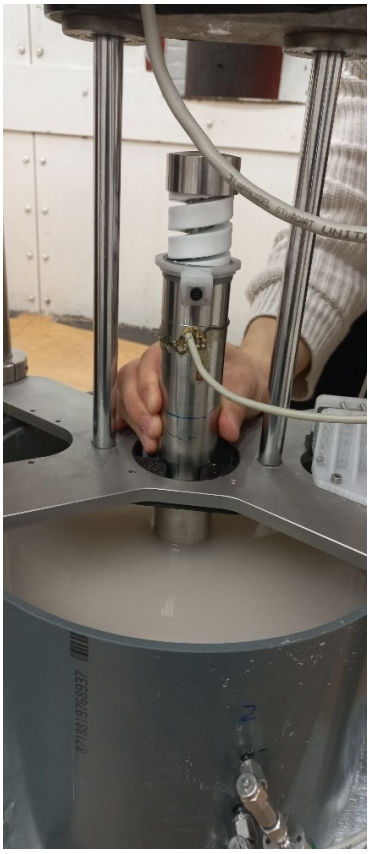

(c) Saturated sample

5

Results

5.1. Introduction

In this chapter, the results that were obtained during the experiments that are included in the in the Test Matrix Table in section 3 are presented. The main goal of this research is to answer the three research questions that were described above and are summarized once more below:
1) What is the effect of impact energy on the installation efficiency
2) What is the effect of pile diameter on the installation efficiency?
3) What is the effect of saturation with viscous fluid on the installation efficiency?

5.2. Test Procedure

As already mentioned, the process of an experiment consists on the preparation of the soil sample and the implementation of the test in the centrifuge facility. The latter refers to the procedure of the pile installation into the soil when using prolonged blows.
At first the pile with the anvil and the mass on top is left to settle by its own weight at 1g. Then, the centrifuge starts to spin until the desired g-level is reached. The g-level varies from experiment to experiment. The g-levels that were tested were 10,20,30,50.
After the pile settles at its own weight, the mass is lifted at a desired height. The height of the falling mass again varies from experiment to experiment. Since the potential energy of the system is a function of the falling height, three different falling heights were chosen and therefore three different potential energies were tested. As result, there are conducted experiments with high (50mm), low(20mm) and middle (40mm) falling height, resulting to high, low, middle potential energy respectively. When the mass is set to the correct height, the centrifuge starts to spin until the desired g-level is reached. At the point that the acceleration has reached the desired value, the mass is released and the pile is stroked. After the first stroke, the mass is lifted up again. This procedure continues until the pile is fully installed into the soil. One important comment is that since the energy was the same throughout an experiment, the falling height was the same for each blow counting the distance from the top of the anvil. Only one experiment has been conducted for increasing energy for each blow and therefore no reliable conclusions can be driven out of this experiment.
The sensors that were used consist of two displacement sensors, one showing the displacement of the top of the pile and the other showing the displacement of the mass. Moreover, on the top of the pile strain gauges were placed to measure the force transmitted to the pile from the stroke. The strain gauges were placed in a full-bridge configuration and were translating Voltage into KN.
It is also worth mentioning that, since the fall of the mass onto the pile and the transmission of the stress wave throughout the pile are procedures that happen very quickly, they need a high frequency acquisition system to capture everything completely and smoothly. Since the frequency is very high, the amount of the data collected at this period of time is huge. Therefore, it was useful to apply a technique called 'triggering technique'. Since the only data that were of use were the ones during the strike and a small period of time before and after it, a trigger was applied to activate the acquisition system just before the fall of the mass. To activate the system there should be an increase in voltage above a specific threshold. When this threshold was exceeded the triggering was activated and the system started to record data. That helped to limit the data up to a smaller period of time, just before the strike and just after the strike. Due to the large number of experiments conducted, including some repetitions, only a selected subset is used to draw the final conclusions in this thesis. The selection process is outlined in the section 6.3. After selecting the relevant experiments, the raw data is assessed to ensure the reliability of the mea-

surements and their alignment with general expectations. The assessment process and its outcomes are detailed in Section 6.3.
For this thesis, a systematic strategy was adopted to address the research questions. First, the research questions were clearly defined, forming the foundation for planning the experimental program. Based on these questions, a series of experiments were scheduled to collect the necessary data. The raw data obtained from the experiments included mass displacement, pile displacements, and strain gauge readings, which were subsequently converted into force signals for further analysis.
The initial step involved correlating these basic data sets with the blow number and penetration depth. This phase aimed to establish a preliminary understanding of the relationships between key variables, such as the pile penetration or mass displacement relative to the number of blows, and the force relative to penetration depth. These correlations provided insights into the fundamental mechanics of the system during the installation process.
The second step delved deeper into the analysis by calculating the work produced during each blow and the cumulative work. The cumulative work calculation illustrated how the energy imparted during successive blows accumulated over the installation process. An essential factor considered in this analysis was the resistance, which is primarily governed by the depth of penetration.
To address the first and second research questions, where the key variables include the falling height of the mass and the acceleration level, this methodology was applied to progress from raw data to a detailed analysis of the installation process with the prolonged blow technique.
For the second research question, the plugging effects were also a significant focus. These effects were quantified using the incremental filling ratio, calculated based on the pile penetration and the amount of soil inside the pile. This analysis provided a clearer understanding of how soil behavior influences the installation dynamics, particularly in scenarios involving prolonged blow techniques.

5.3. Overview of results

5.3.1. Selection of experiments for further analysis

The graphs bellow present the cumulative increment of the penetration divided by the diameter of the pile ($\Delta z/D$) against the number of the blows, to prove the similar results between the tests that are performed under the same condition. To answer the research questions some of the experiments that share the same conditions are selected.
Therefore, a sensitivity comparison is performed which proves that between these experiments the deviations are minor. The two sensors of the setup record the displacement of the mass and the displacement of the pile. There are also strain gauges, so the values of the force are also recorded. However, since the type of the soil is the same and the relative density is kept almost same throughout the experiments, the penetration is very much affected by the force between the experiments with identical conditions, as for example mass, falling height and gravitational acceleration. In addition, the driving resistance of the pile is often expressed by the number of blows that are required for the pile to be installed.
Therefore, it is thought sufficient to prove the similarity of the results by plotting the values of the cumulative increment of the penetration divided by the diameter of the pile ($\Delta z/D$) against the number of the blows. For the experiments with gravitational acceleration 30g and falling height 20 and 50, only one experiment was conducted for each, and therefore they are not represented in the graphs below since the sensitivity comparison is not applicable. In total, 21 experiments were conducted can be also seen in Table 3.2. The goal is to have at least 2 tests per different conditions to get reliable results. For the conditions of gravity acceleration 50 and falling height 40 more tests were performed because 2 were done at the beginning of the testing schedule for familiarization with the laboratory equipment. In addition, in one of the five experiments, the sensors were not working so no results were obtained.

5.3.2. Experiment at 10g

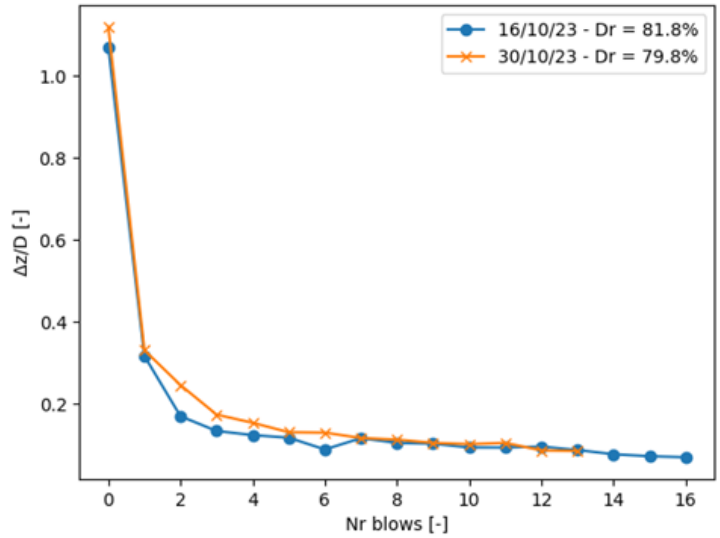

Figure 5.1: Experiments at 10g at 20mm falling height

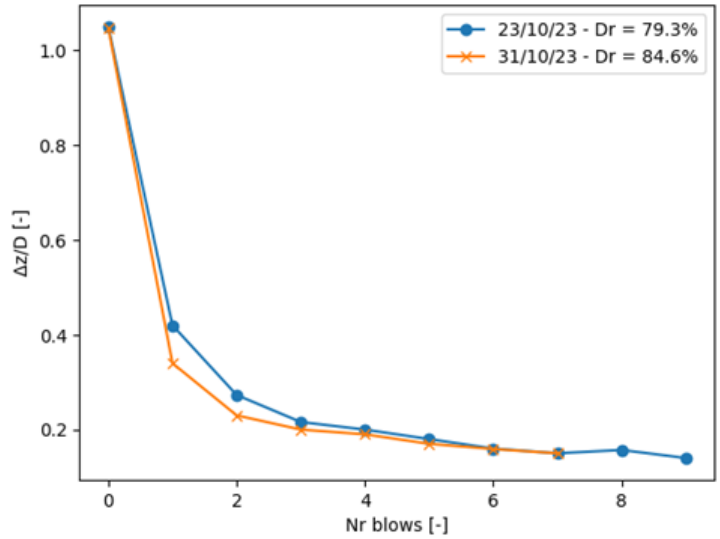

Figure 5.2: Experiments at 10g at 40mm falling height

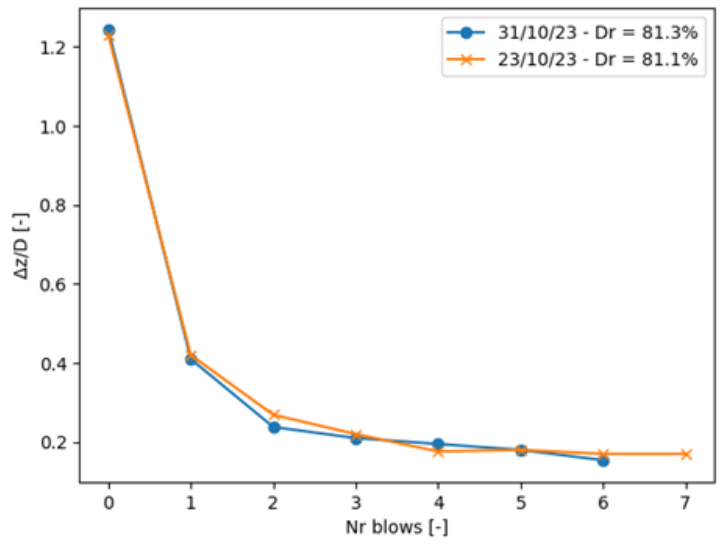

Figure 5.3: Experiments at 10g at 50mm falling height

From the set of experiments at gravitational acceleration 10 and falling height 20mm, since the relative density of both is almost the same and both the lines are almost on top of each other, the graph with the blue line (16/10/23) is chosen since more blows were operated. For the set of experiments at gravitation acceleration 10 and falling height 40mm there is a small deviation at the relative density of the samples, however, is it less than 5%. The chosen test is the blue line (23/10/23) since the relative density is closer to the desired values of 80% and the number of blows is bigger. For the set of experiments a gravitation acceleration 10 and falling height 50, the results are almost identical. The relative density is almost the same. The chosen test is the orange line (23/12/23) since the number of blows is bigger. For the set of tests with gravitational acceleration 30 and falling height 40mm, both relative densities of the two different samples are similar. The chosen line is the orange (27/07/23) since the number of blows is bigger.

5.3.3. Experiments at 30g

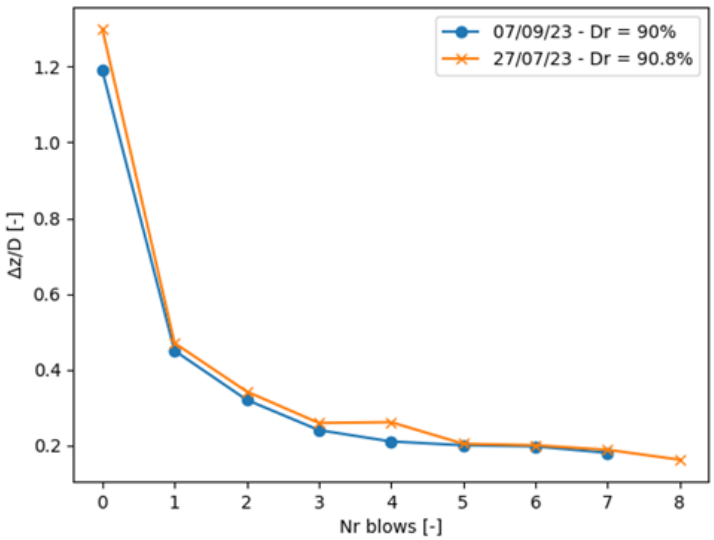

Figure 5.4: Experiments at 30g at 40mm falling height

For the set of tests conducted with a gravitational acceleration of 30g and a falling height of 40mm, the relative densities of the two different samples are similar. The data from the test on 27/07/23 (represented by the orange line) was chosen because it includes a greater number of blows. For the experiments at 30g with falling heights of 20mm and 50mm, only one test was performed for each condition, and thus, they are not included here.

5.3.4. Experiments at 50g

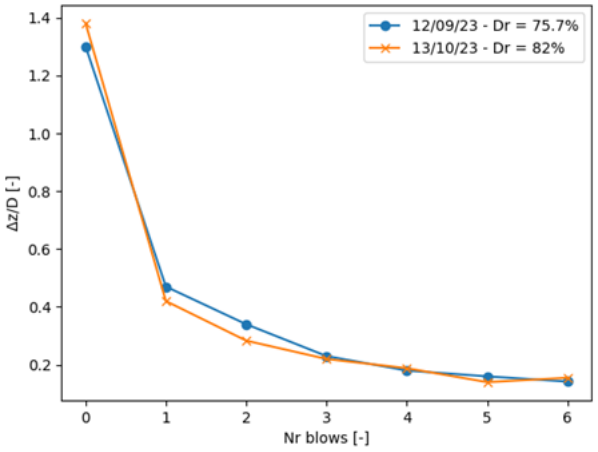

Figure 5.5: Experiments at 50g at 20mm falling height

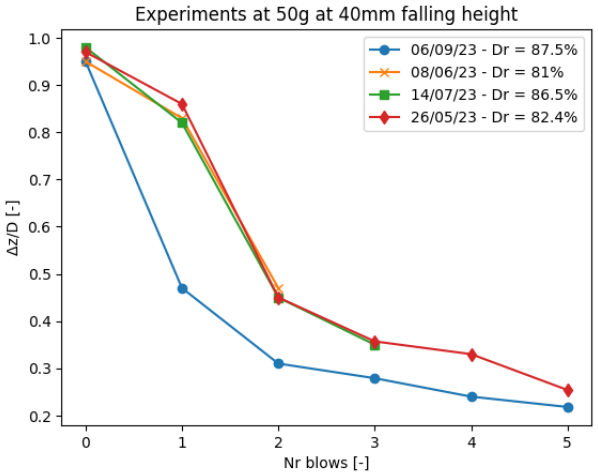

Figure 5.6: Experiments at 50g at 40mm falling height

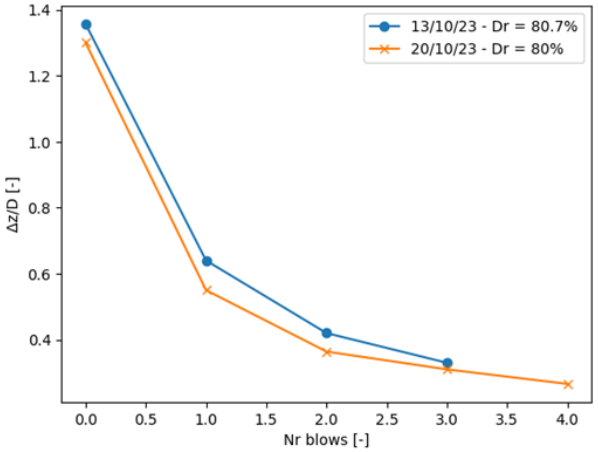

Figure 5.7: Experiments at 50g at 50mm falling height

For the set of tests conducted at a gravitational acceleration of 50g and a falling height of 20mm, the number of blows was the same between the two experiments. However, there was a slight deviation in relative densities, and thus the orange line (13/10/23) was selected, as its relative density is closer to the target value of 80%, and the data appears smoother.
In the tests at 50g with a falling height of 40mm, five experiments were performed, of which four yielded reliable results. Unfortunately, the test represented by the orange line (08/06/23) had to be stopped prematurely due to equipment malfunction. Similarly, the green line (14/07/23) corresponds to a test that was also terminated early. The tests chosen to address the research questions are those represented by the blue line (06/09/23) and the red line (26/05/23). It's noteworthy that the differences in penetration between these two tests are clearly caused by variations in relative density. Interestingly, in a similar set of tests conducted at 10g with a 20mm falling height, despite a comparable deviation in relative densities, the differences in penetration were less pronounced. This is because gravitational forces between the soil grains increase with higher gravitational acceleration.
For the tests conducted at 50g and a 50mm falling height, the lines are closely aligned, and the relative densities of the samples are very similar. The orange line (20/10/23) was chosen as it represents the test with the most blows. From the above graphs it can be seen that results are very close so there is no need for providing special reasoning regarding which graphs per set will be chosen to answer the research questions. It is evident that as the falling height increases while maintaining the same g-level, there is a noticeable reduction in the number of blows, which begins to provide valuable insight into addressing research question 1. Moreover, the consistency of self-weight penetration across all experiments conducted at the same g-level is an important observation. This consistency not only reinforces the reliability of the experimental results but also suggests that the sample preparation method and experimental conditions were consistently maintained throughout the testing process.

5.4. Assessment of raw experimental data

Before attempting to formulate answers to these questions, it is essential to fully understand and comprehend the obtained data. Therefore, the following section presents and explains the raw experimental data in detail. For the dry tests, the data is captured by two laser sensors and strain gauges. The two laser sensors record the movement of the pile and the ram mass, and the reading of strain gauges can be converted to force signal since the material properties are known. To measure the pile driving energy the strain of the pile is recorded and converted to force signal. The material properties of the pile, as the modulus of elasticity E, are known, the strain readings can be converted into a force signal. The strains are placed according to a full Wheatstone bridge. They consist of four I strain gauges that are placed axially on the outside of the pile, evenly spaced at 90°intervals. Therefore, from the dry experiments there are three outputs to be understood and processed. The displacements of the pile when the mass falls on it, the displacement of the mass as it is released during the spin, the force by which the mass hits the pile.

5.4.1. Pile Displacement

The movement of the pile is monitored using a laser positioned at the top of the actuator. A small plastic plate, which was 3D printed, was affixed to the top of the pile, allowing the laser to reflect and measure the corresponding displacement. The configuration was set such that, as the pile moved downward, the recorded displacement was positive.In Figure 5.8 below illustrates a series of blows from an experiment conducted at 30g acceleration, focusing on a high-energy scenario. The plots represent the penetration of the pile as the mass strikes it, continuing until the pile reaches full installation at a depth of approximately three times its outer diameter.

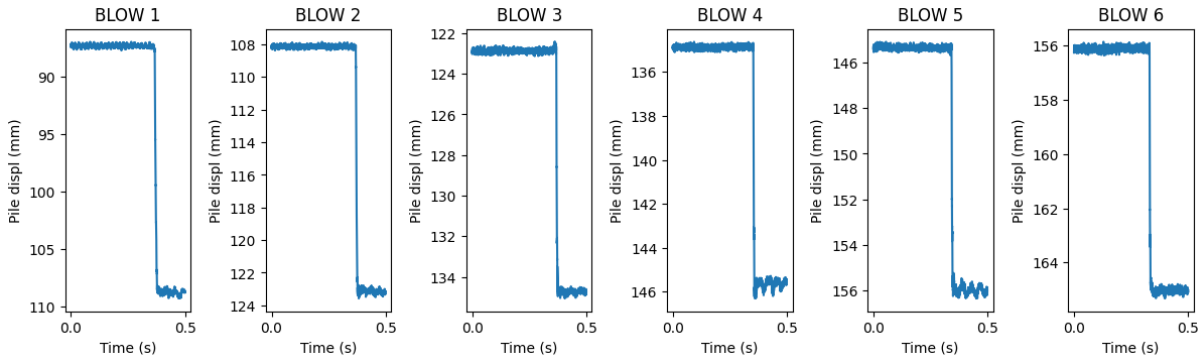

Figure 5.8: Pile displacement (mm) vs Time (s) for 30g at 50mm falling height

5.4.2. Mass Displacement

Following the same reasoning with the pile displacement, the movement of the mass is also presented below for the same experiment. A plastic plate was placed on the side of the mass to reflect again the signal of the corresponding laser. However laser was placed at the bottom of the actuator this time, therefore since the mass was also moving downwards towards the pile the values of the mass displacement are negative. The plate was also 3D printed.

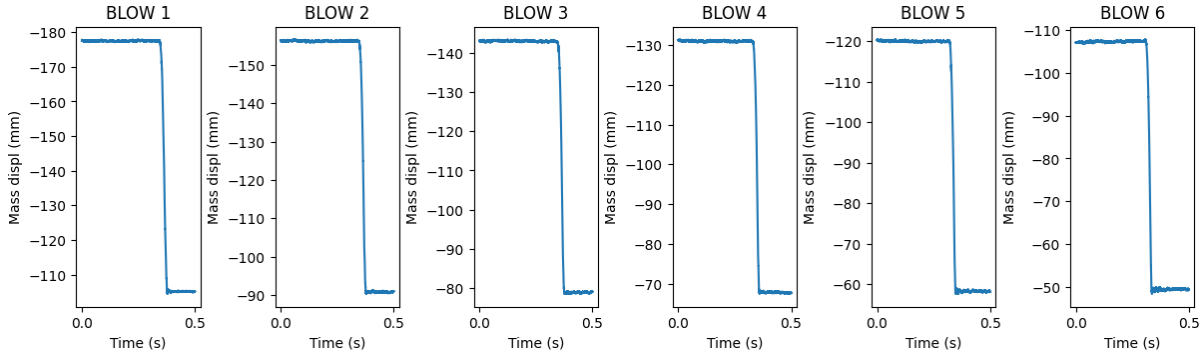

Figure 5.9: Mass displacement (mm) vs Time (s) for 30g at 50mm falling height

5.4.3. Load Cell

The strain gauges on the top of the pile measure the force that is transmitted to the pile when the mass strikes the pile. The configuration of the gauge is full-bridge, and has four active strain gauges. The advantage of the full bridge configuration is that it is available in three different types, two that are sensitive to bending strain and one that measures axial strain. Moreover all three minimize the effects of temperature. The set of graphs below present the signal in KN per second for all the blows of this experiment. Since the mass falls onto the pile, the pile is compressed and therefore the values of the force are negative.

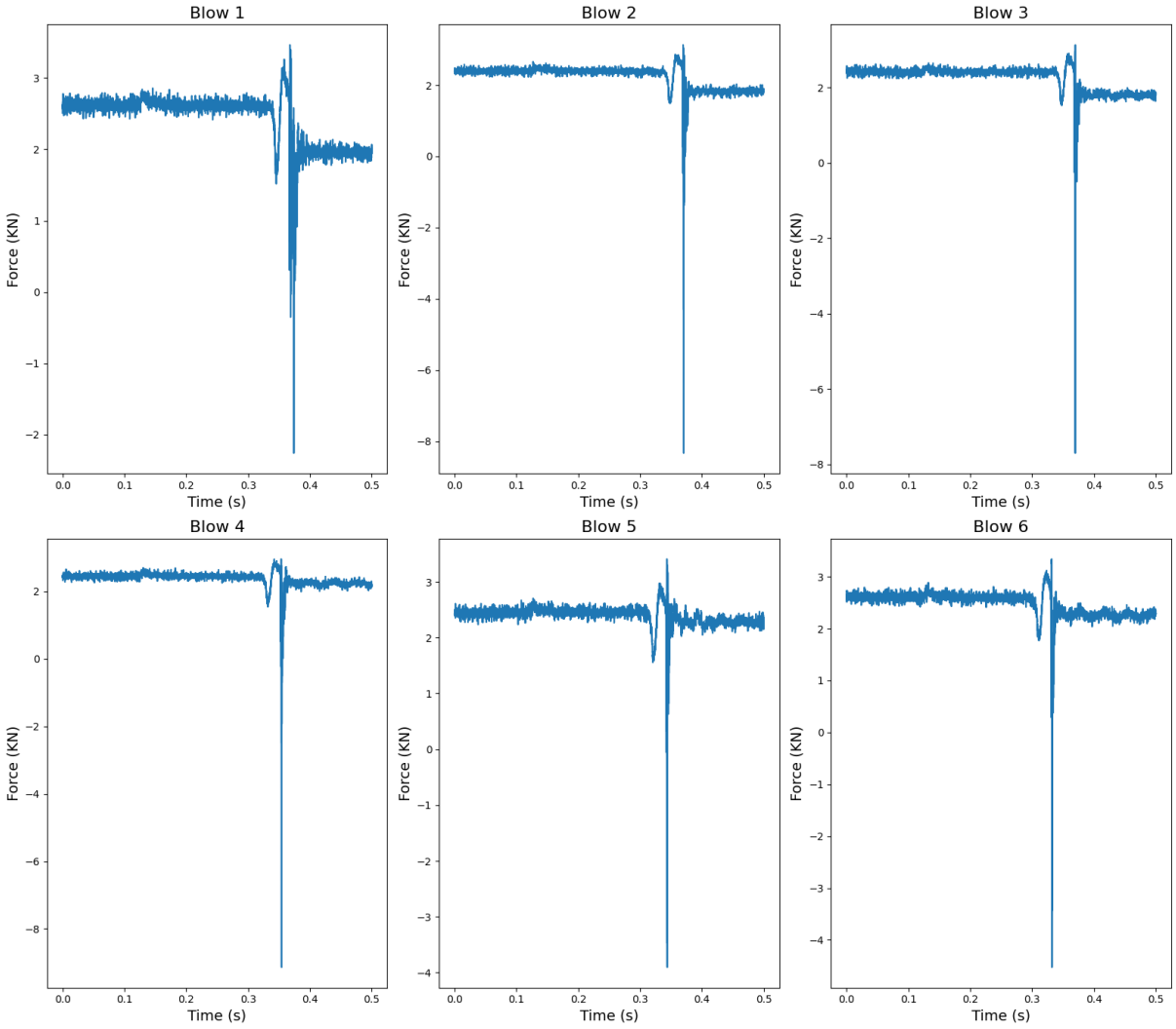

Figure 5.10: Force (KN) vs Time (s)

As shown in Figure 5.11, the force, the displacement and the and the mass of the system, will be plotted for the experiment that was conducted under gravitational acceleration 50 when the mass is released from 50mm. The pink line is the force over time, the blue line is the pile displacement over timer and the green line is the mass displacement over time. As it can be also seen from the Figure 5.11, below at time 0s all three lines are zero. When the mass (green line) is released, the force (pink line) starts to increase and then decrease creating an 'S' shape. This shape is caused due to electromagnetic reaction of the magnet and the mass when it is released. As can be seen in the graph, this 'S' shape is created before the mass hits the pile, therefore is not caused due to the movement of the pile but due to the reaction of the magnet. After the mass hits the pile, the pile also starts to move (blue line). After the pile is hit by the mass, it penetrates to the soil. When the mass falls develops velocity and therefore force. This is the measured force that is indirectly captured from the strain gauges. In addition, this force is transmitted to the pile during the collision and makes it penetrate the soil. Some of the energy from the force is lost during the impact and some is lost as the energy wave travels through the pile. The remaining energy is what makes the pile penetrate.

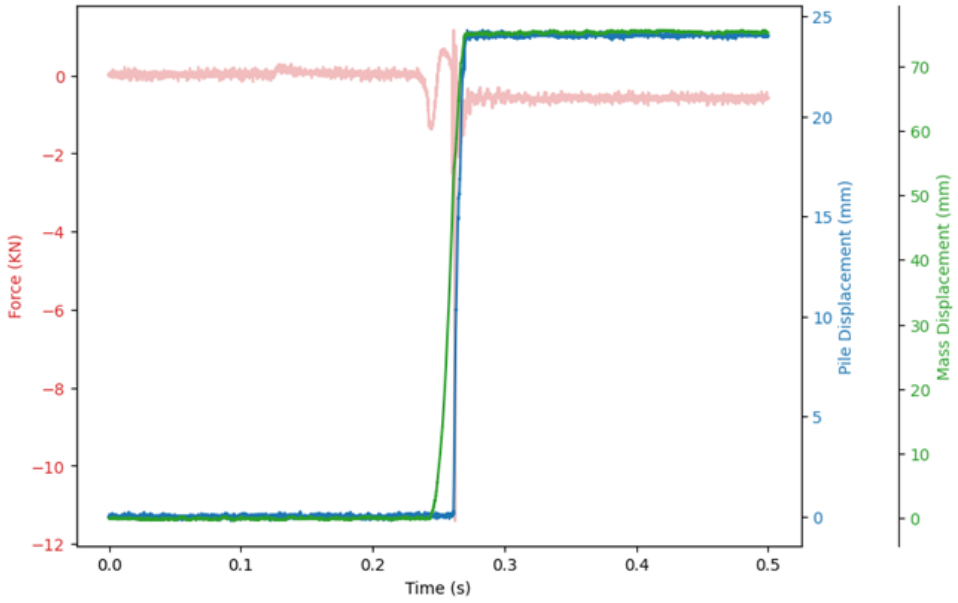

Figure 5.11: Force over Displacement over Time for the first blow of test at 50g at 50mm. D50g50mm

The moment of the impact is the most important part of the graph above, since before that moment the system is inactive and after that the system reaches a plateau as the system does not receive extra energy and is at equilibrium. Therefore, the Figure 5.12, below is zoomed at the moment of the impact until the pile stops its penetration.

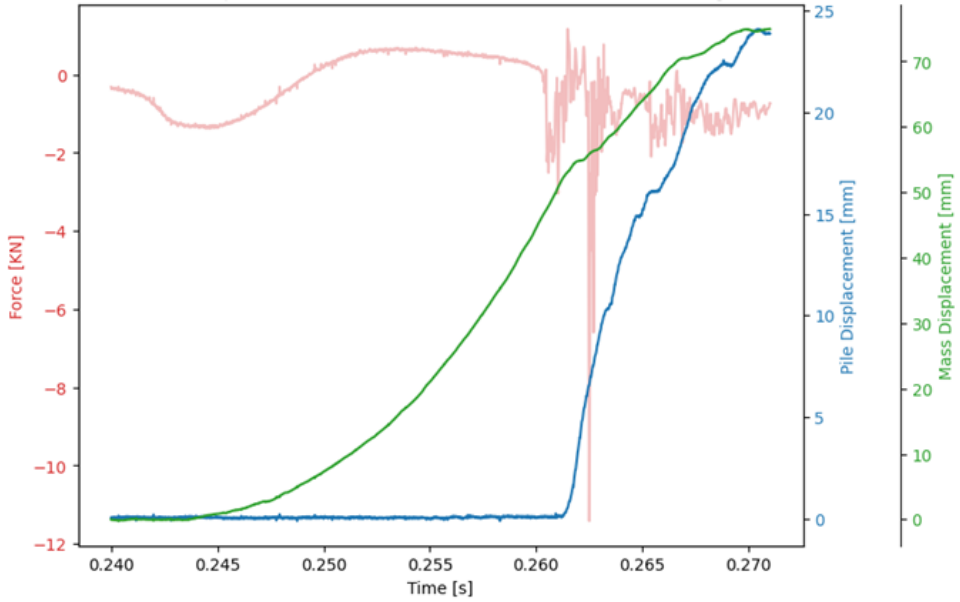

Figure 5.12: Force over Displacement over Time for the first blow of test at 50g at 50mm-zoomed

The two Figures presented above,Figure 5.11, Figure 5.12, provide insight into the data recorded by the sensors and the operation of the system. The green line represents the displacement of the mass, the blue line indicates the displacement of the pile, and the pink line reflects the force signal. The mass is released when the centrifuge reaches the required acceleration, marking the point at which the green line begins to rise. Subsequently, the pink line exhibits an 'S' shape, which is attributed to the electromagnetic reaction of the magnet that holds the mass. As the mass has not yet made contact with the pile, the pile has not begun to move, resulting in the strain gauges being unable to capture any strains from the pile. Therefore, it is reasonable to conclude that the gauges are recording signals generated by the electromagnetic reaction of the magnet. The moment the blue line begins to rise indicates when the mass strikes the pile, initiating the pile's penetration into the soil. During this penetration phase, the strain gauges capture the strains within the pile, which are then translated into a force signal. Once the pile ceases to move, both the green and blue lines reach a plateau, while the pink line gradually stabilizes. Below Figure 5.14 shows the force over time for experiments with different g levels (10g, 40g, 50g) when the mass falls from the same falling height, for the first blow of each experiment, are presented. The starting and the ending points in the graphs are chosen based on the pile displacement. The moment that the pile starts to move is selected as the starting point and the moment that the pile stops is selected as the ending point. The impact duration is calculated based on the difference of the moment that pile starts to move and the moment that the pile stops. It is evident that as the gravitational acceleration increases, the impact duration decreases. Moreover, as the gravitational acceleration increases the value of the force increases as well. Both the force and impact duration are affected by the acceleration level. The impact duration is anticipated to be shorter for experiments conducted at higher falling heights, which correspond to greater energy levels, compared to those at lower falling heights under the same acceleration.

$$S_y = 0.5gt^2 \tag{5.1}$$

$$U_y = gt \tag{5.2}$$

In the relationships above, g stands for the gravitational acceleration, t stands for the time, uy stands for the velocity and sy stands for the displacement. Time is also influenced by the acceleration level of the centrifuge. When a body is allowed to free fall under 1g conditions, its motion is governed solely by gravitational acceleration. Consequently, when the same body is released to free fall under conditions of higher g levels, the time required to cover the same distance is reduced. Regarding force, since the linear dimension is influenced by the g-level, as discussed in the section on scaling parameters, it will also be affected by the gravitational acceleration. Consequently, a higher g-level results in a greater force.

The Figure 5.13 below illustrates the velocity over time from an experiment conducted at a gravitational acceleration of 50g with a falling height of 50mm. The blue line represents the velocity of the ram mass, while the orange line depicts the velocity of the pile. Initially, it is evident that the pile begins to move as the ram mass reaches its maximum velocity. An intriguing observation is that, after the pile starts to move, the motion of the mass is not continuous. The mass appears to pause, then impacts the pile, followed by another halt while the pile continues to penetrate the soil. This cycle repeats until the energy supplied to the system is fully utilized. Consequently, the intermittent motion of the mass introduces additional energy into the system, which must be considered when calculating energy expenditure and other factors influenced by this energy.

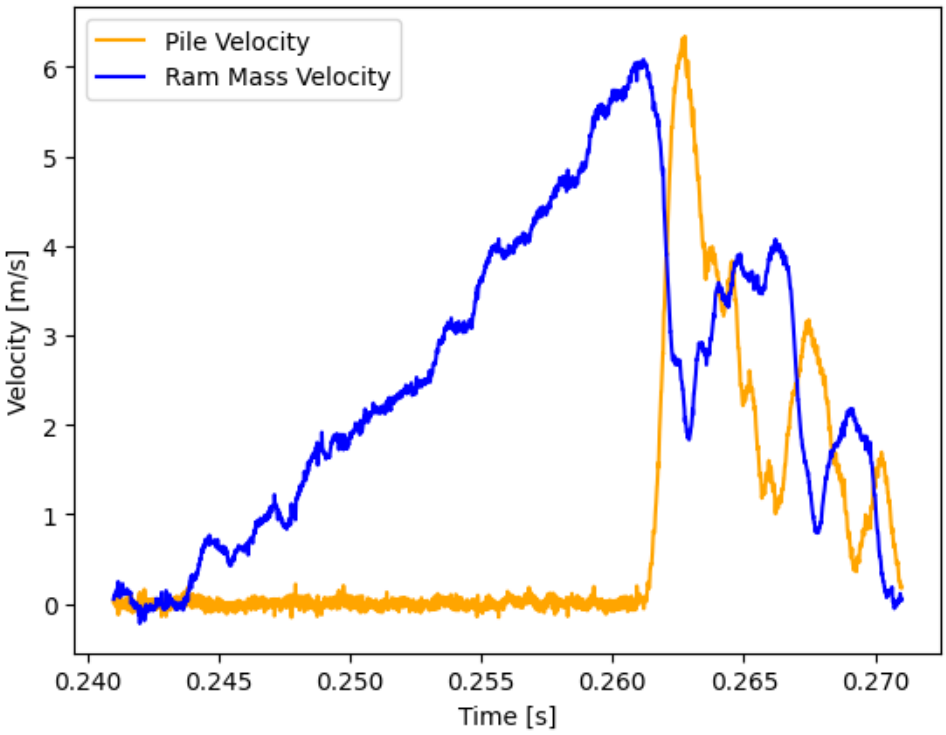

Figure 5.13: Velocity against Time at 50g at 50mm

The Figure 5.14 below also helps to understand the data and more specifically how the readings of the strain gauges are converted to force signal. In also provides information about the differences in the force values that are caused due to different acceleration when every other parameter is kept the same.

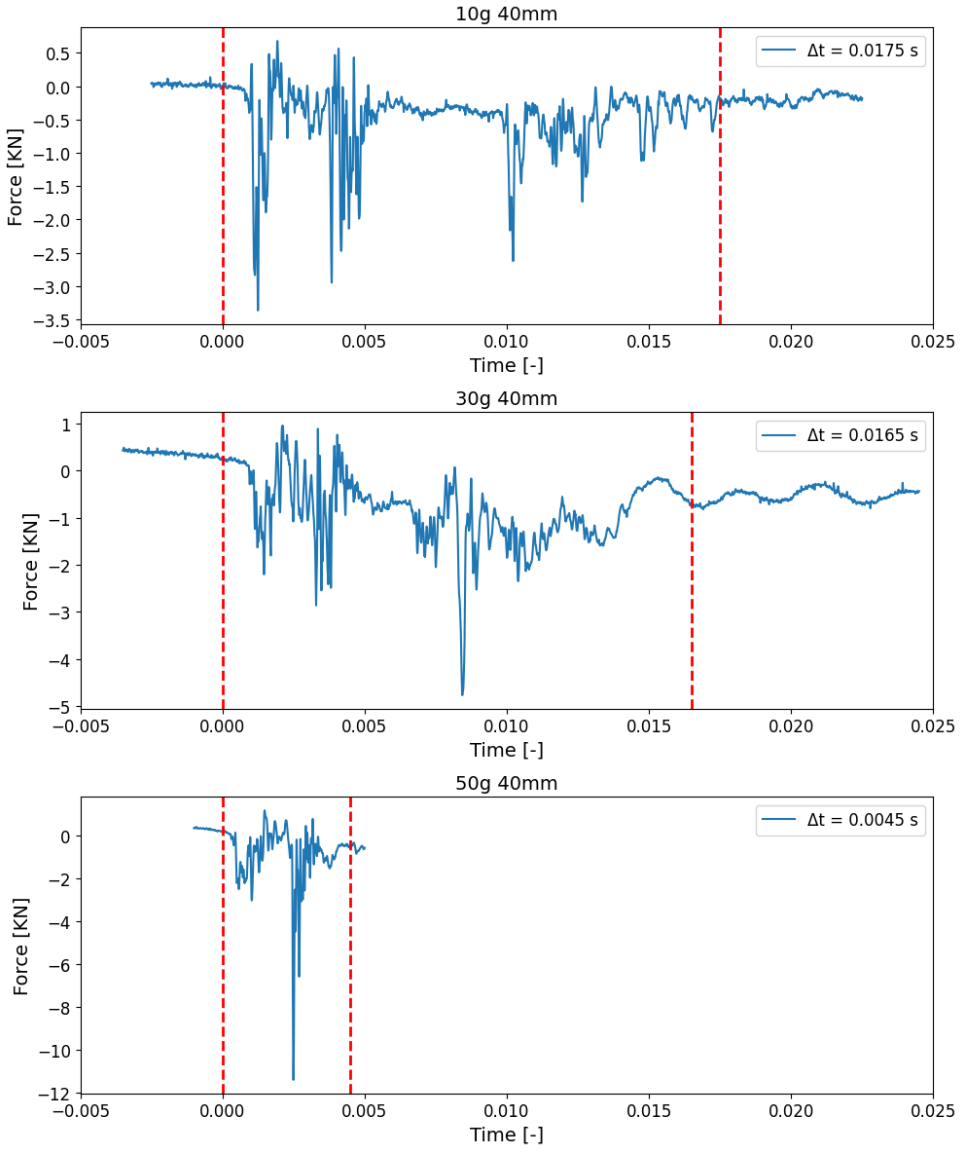

Figure 5.14: Force over Time for the first blow at experiments with 40mm falling height for various g levels

In Figure 5.15, all the blows for one experiment at 50g are presented.

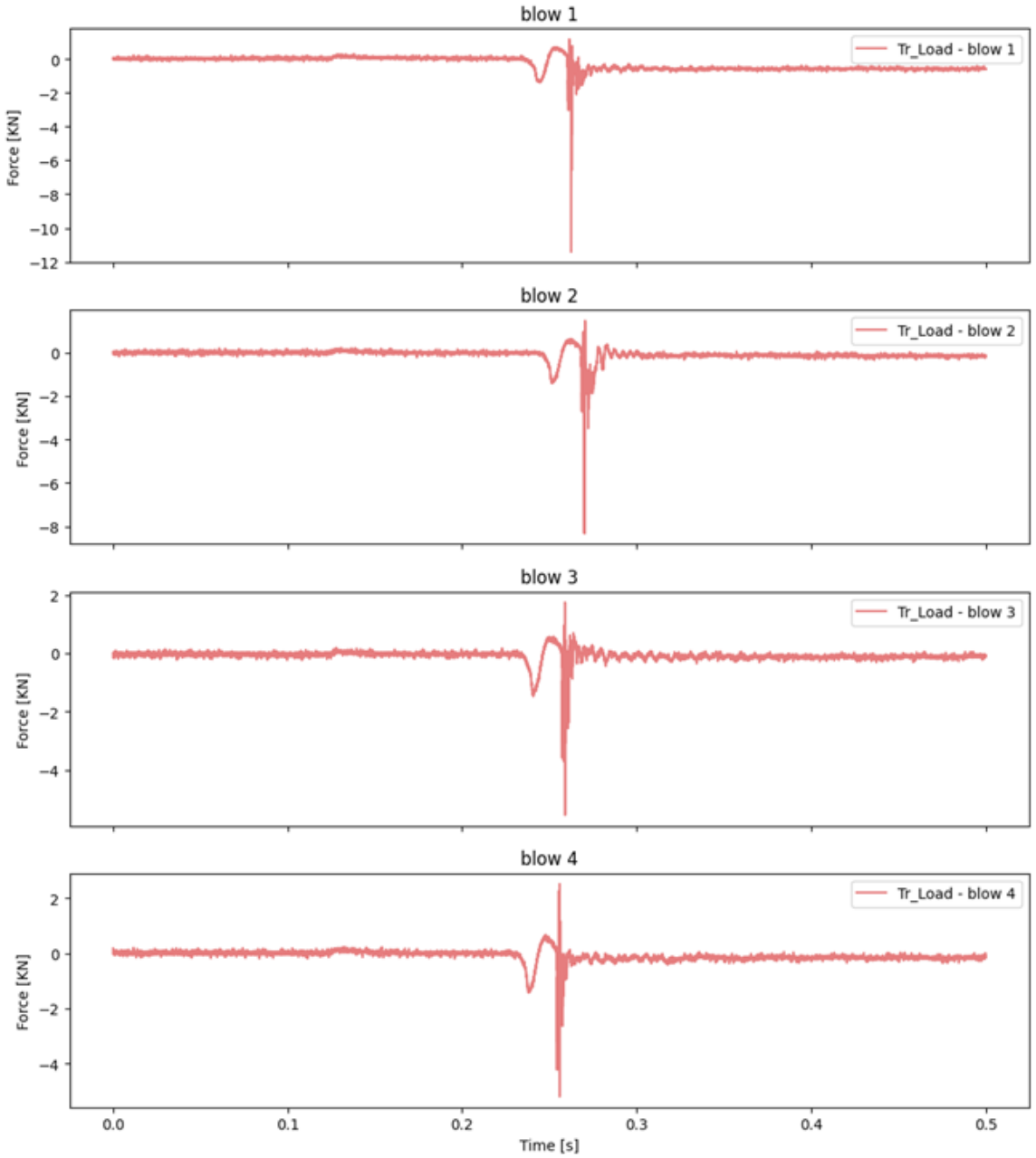

Figure 5.15: Force over Time for all the blows at an experiment at 50g at 50mm falling height

The Figure 5.15 primarily offer insights into the functioning of the system and the type of data obtained. They illustrate how these data points are interrelated and how they can be interpreted to address the research questions posed in this study.

5.5. The effect of impact energy on the installation efficiency - Research Question 1

5.5.1. Introduction

To begin addressing the first research question, which investigates the effect of impact energy on installation efficiency, we will compare and discuss a set of results obtained from tests conducted at the same g-level but with different falling heights, thereby varying the energy levels. Consequently, the only parameter that will change is the impact energy of the test, allowing us to explore its influence on installation efficiency.
To address this research question, we will first present graphs illustrating pile penetration over time for two different experiments. Additionally, we will include plots depicting the work and cumulative work against resistance. Lastly, we will present graphs comparing the work/potential energy of the system against penetration.

5.5.2. Energy Transmission in Pile Installation

In this research, a critical focus is placed on understanding and analyzing the mechanism of energy transmission during pile installation. The motivation for developing a new installation technology using **prolonged blows** stems from the desire to alter the way energy is transmitted to the soil. This alteration is expected to address issues such as noise emissions and structural fatigue, both of which are influenced by how energy propagates from the hammer to the pile and subsequently to the surrounding soil.

The primary goal is to study the behavior of energy in this context and to compare the conventional installation method with the new method employing prolonged blows. By gaining insights into the energy dynamics, the research aims to evaluate the effectiveness and efficiency of the new technology.

5.5.3. Measuring and Calculating Energy Transmission

To quantify energy transmission, this research utilizes two approaches:

1. **Experimental Measurements** through sensors and strain gauges.
2. **Theoretical Calculations** based on the principle of energy conservation.

Both methods provide complementary perspectives on the energy dynamics and are compared to validate and substantiate the findings.

5.5.4. Theoretical Method: Energy Conservation Principle

The theoretical approach to energy calculation is grounded in the **principle of energy conservation**, which states that energy cannot be created or destroyed, only transformed. The key formulas employed in this research are as follows:

Impact Force
Force (F) is derived from Newton's second law:

$$F = m \cdot a$$

where:

- m is the mass of the hammer,
- a is the acceleration.

Acceleration (a) can be expressed as:

$$a = \frac{v}{t}$$

where:

- v is the velocity of the hammer at the moment of impact,
- t is the duration of the impact (time interval from when the mass strikes the pile to when the pile stops moving).

Substituting a into the equation for force:

$$F = \frac{m \cdot v}{t}$$

Velocity of the ram mass
The velocity of the ram mass (v) just before impact can be theoretically calculated using the formula for free-fall motion:

$$v = \sqrt{2 \cdot g \cdot h}$$

where:

- g is the acceleration due to gravity,
- h is the height from which the mass is released.

Energy Calculation
The kinetic energy (E_k) of the hammer at the moment of impact is:

$$E_k = \frac{1}{2}mv^2$$

Assuming no significant energy losses, this kinetic energy is transferred to the pile and surrounding soil. The work done by the pile during penetration (W_{pile}) can then be calculated based on the force and displacement:

$$W_{\text{pile}} = \int_{x_0}^{x_f} F(x)\, dx$$

Comparison with Experimental Data

- The theoretical velocity (v) calculated from $v = \sqrt{2gh}$ is compared with the experimental velocity derived from sensor data. The experimental velocity is obtained as the derivative of displacement with respect to time:

$$v_{\text{exp}} = \frac{dx}{dt}$$

- Similarly, the force calculated from theoretical equations is compared to the force directly measured by the strain gauges.

5.5.5. Experimental Method: Sensor Measurements

Sensors and strain gauges provide direct measurements of force (F) and displacement (x). From these measurements:

- Work (W) is calculated for each time increment (Δt) as:

$$W_i = F_i \cdot \Delta x_i$$

- The total work is the sum of all incremental work values:

$$W_{\text{total}} = \sum_{i=1}^{n} F_i \cdot \Delta x_i$$

Alternatively, in continuous form:

$$W_{\text{total}} = \int_{x_0}^{x_f} F(x)\, dx$$

5.5.6. Key Comparisons

The results from the theoretical calculations based on the principle of energy conservation are compared to the experimental data obtained from sensors. This includes:

1. **Impact Force:** Comparison of calculated and measured force values.
2. **Velocity:** Comparison of theoretically derived hammer velocity ($v = \sqrt{2gh}$) with the velocity obtained from sensor data ($v = \frac{dx}{dt}$).
3. **Energy Utilization:** Analysis of the work done by the pile (W_{pile}) relative to the mass's initial kinetic energy of the mass (E_k).

5.5.7. Conclusion

By combining theoretical and experimental approaches, this research provides a robust framework for understanding energy transmission during pile installation. The insights gained will facilitate a substantial comparison between conventional installation methods and the novel technique of prolonged blows, paving the way for improved energy efficiency and reduced environmental impact.

5.5.8. Estimation of Work During Pile Penetration

To quantify the work produced during the penetration of the pile, the following methodology is applied. The raw experimental data include time-series measurements of force (obtained from strain gauges) and displacement. Work (W) is, in general, defined as the product of force (F) and the corresponding displacement (Δx) achieved by that force. Thus, for each time increment Δt, the instantaneous work can be approximated as:

$$W_i = F_i \cdot \Delta x_i$$

where F_i is the force recorded at the i-th time increment, and Δx_i is the displacement during that time increment. Summing these discrete work values over the duration of the pile movement provides the total work done:

$$W_{\text{total}} = \sum_{i=1}^{n} W_i = \sum_{i=1}^{n} F_i \cdot \Delta x_i$$

Here, n represents the total number of time increments from the moment the mass strikes the pile to the point where the pile ceases to move. In a continuous framework, the work can be expressed as the integral of force with respect to displacement:

$$W_{\text{total}} = \int_{x_0}^{x_f} F(x)\, dx$$

where x_0 is the initial position of the pile, and x_f is its final position after penetration.

5.5.9. Definition of Piling Energy

The **piling energy** is defined as the fraction of the input energy utilized for pile penetration. Initially, the system possesses potential energy ($E_{\text{potential}}$), given by:

$$E_{\text{potential}} = m \cdot g \cdot h$$

where:

- m is the mass of the falling object,
- g is the acceleration due to gravity, and
- h is the height from which the mass is released.

Assuming no energy losses due to factors such as air resistance or friction, this potential energy is fully converted into kinetic energy (E_{kinetic}) at the moment of impact:

$$E_{\text{kinetic}} = \frac{1}{2} m v^2$$

where v is the velocity of the mass at impact. However, in practice, not all the energy is transmitted to the pile for penetration due to system inefficiencies, such as energy losses through vibration, heat, or deformation of the pile and surrounding soil.

To estimate the energy utilized specifically for pile penetration, the ratio of the work done by the pile to the initial potential energy is calculated:

$$\text{Piling Energy Ratio} = \frac{W_{\text{total}}}{E_{\text{potential}}}$$

This ratio serves as an indicator of the efficiency of energy transfer during pile installation. In essence:

- $E_{\text{potential}}$ represents the energy offered to the system.
- W_{total} represents the work effectively used for pile penetration.

The underlying assumption in this calculation is that all available energy (potential and converted kinetic) contributes to pile penetration, with minimal losses. The closer the piling energy ratio is to 1, the more efficient the energy transfer for penetration.

5.5.10. Significance of the Piling Energy Ratio

The piling energy ratio provides critical insights into the dynamics of the installation process, including energy transfer efficiency and the mechanical interaction between the pile and the soil. This parameter is pivotal for optimizing pile driving methods and improving energy utilization during installation.

5.5.11. Observations at 50g centrifuge acceleration

Firstly, Figure 5.16 illustrates the pile penetration over time for two different falling heights, which correspond to two distinct energy levels. From the figures, it is evident that as the falling height increases, fewer blows are required for the pile to achieve full penetration, specifically reaching a depth of approximately three times the outer diameter of the pile. This observation supports Hypothesis 1, indicating that as the g-level increases, the penetration per blow also increases, resulting in a reduced total number of blows needed.

Furthermore, this graph not only provides insight into answering the first research question but also aids in understanding the data. The actuator allows for a single blow each time; therefore, when the mass is released onto the pile, the pile penetrates during the spinning phase. Following this, the centrifuge must stop, the mass must be repositioned, and once the centrifuge reaches the desired acceleration level, the mass is released to strike the pile. This procedure continues until the pile reaches the desired depth. Understanding the differences in penetration as the falling height increases is crucial, as a greater falling height leads to higher impact energy. Additionally, pile driving resistance is often expressed in terms of the number of blows. Thus, Figure 5.16 depicting penetration at each blow over time serve as a foundational step in observing the effects of impact energy on driving efficiency.

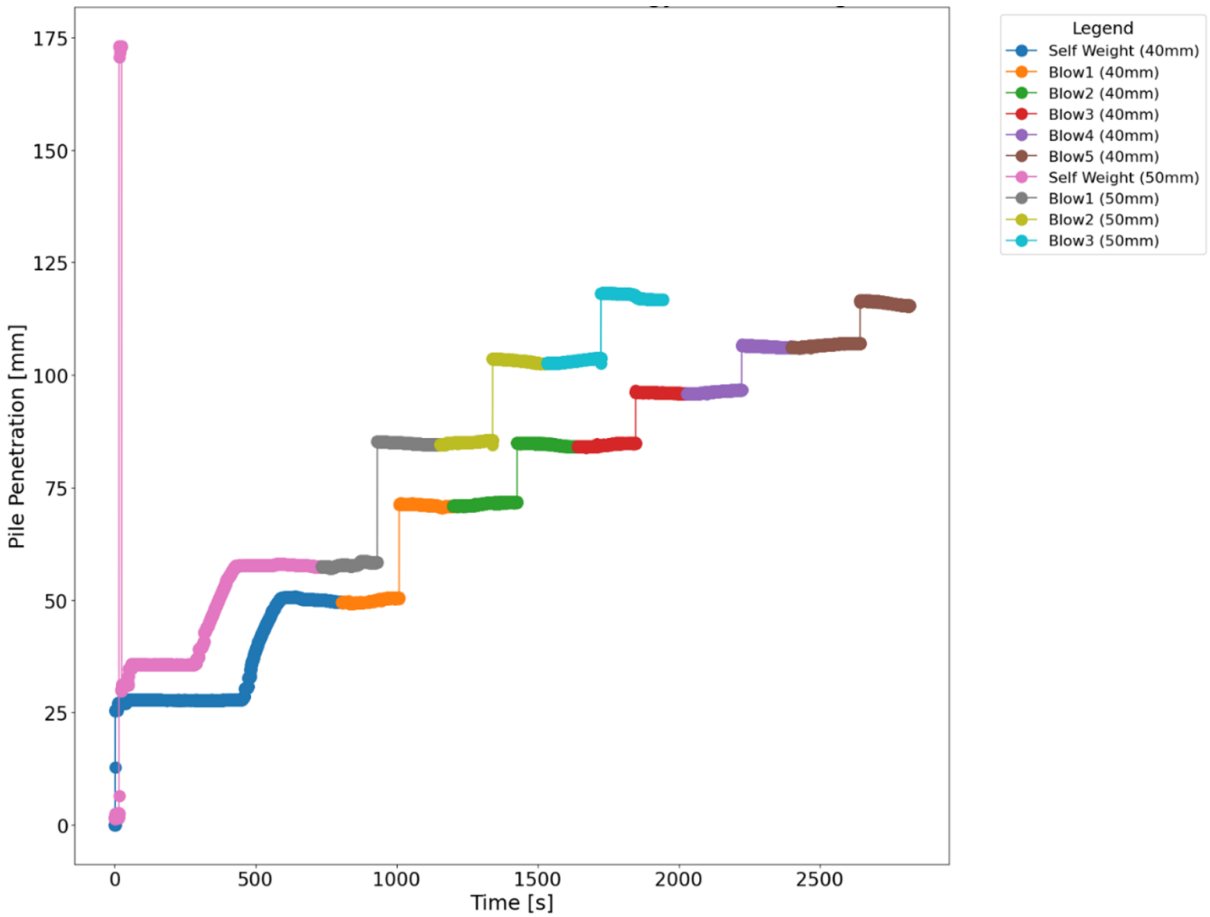

Figure 5.16: Penetration over Time for different energy levels at 50g

The Figure 5.17 presents the cumulative work of the force against the resistance of the pile (ultimate pile capacity). The analytical calculations of the work and the capacity are included in the Appendix.
The resistance encountered during pile installation is closely related to the depth of penetration. This relationship exists because resistance is influenced by various factors, including soil characteristics (e.g., cohesion, friction angle, and particle size), the unit weight of the soil, the geometry of the pile, and the depth at which the pile is driven. Among these factors, only the depth changes dynamically during the installation process, making it the primary variable controlling resistance. As the depth increases, the pile interacts with a greater volume of soil, which typically results in higher resistance values due to increased overburden pressure and soil confinement. Higher resistance values signify that the pile has achieved deeper penetration, which is crucial for ensuring the structural stability and load-bearing capacity of the foundation. In essence, while resistance depends on several parameters, depth is the dominant factor that dictates its variation during installation. As the pile penetrates deeper the penetration per blow decreases which is reasonable.
The force also varies as the pile penetrates deeper into the soil. This variation occurs because the force signal is derived from strain readings that are converted. The strain is influenced by the mass upon impact with the pile, generating a force wave; however, during penetration, the reaction of the soil further affects the strain within the pile. Although the changes in force are minor, the overall effect is dominated by the changes in penetration per blow.
Resistance is a function of soil depth and consequently increases with greater depths, resulting in a decreasing trend in the force signal. When comparing two falling heights—one at 20mm and the other at 50mm—it is evident that for the same resistance values, the cumulative work done in the experiment with the greater falling height is significantly higher. This observation is reasonable and supports Hypothesis 1, as well as previous findings, indicating that when the falling height and, therefore, the impact energy are greater, the penetration per blow also increases. A similar graph but for 30g is presented at Figure 5.20. Again, it is evident when the falling height and, therefore, the impact energy are greater, the penetration per blow also increases.

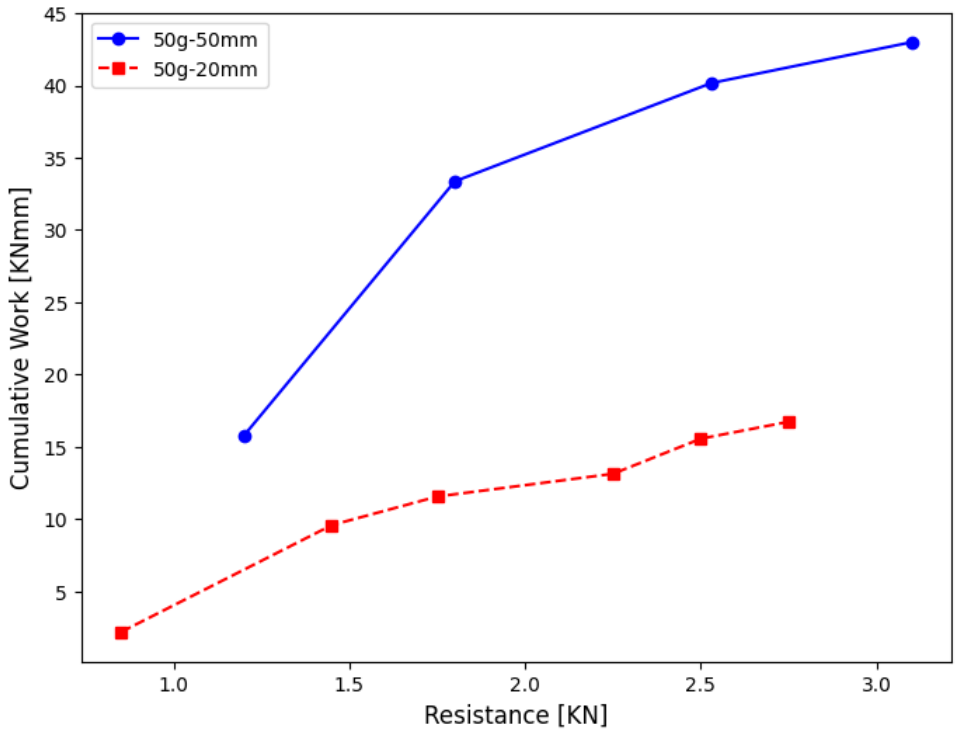

Figure 5.17: Cumulative Work against resistance for 50g at 2 different falling heights

The next Figure 5.18 serves as a logical continuation of the Figure 5.17 ,Figure 5.20 and provides valuable information pertinent to the first research question. The earlier Figure 5.17 illustrated the relationship between work and pile resistance, demonstrating that an increase in falling height correlates with higher energy, resulting in greater penetration per blow and increased work. The resistance of the pile is significantly influenced by its characteristics, which remain constant across the experiments, as well as by the soil characteristics, which are also uniform, and the soil depth, which increases with each blow. Consequently, it can be concluded that for the same soil horizon, the work generated in the experiment conducted with a falling height of 40mm exceeds that produced in the experiment with a falling height of 20mm. In the Figure 5.18, the vertical axis represents work normalized by potential energy, calculated as follows:

$$\text{Potential Energy [J]} = \text{mass [kg]} \times g\ [\text{m/s}^2] \times h\ [10^{-3}\ \text{m}] \tag{5.3}$$

The mass is initially positioned at a specific height, and before it is released, it possesses potential energy. This potential energy is determined by the height of the mass above its point of impact and is governed by the formula:

$$PE = mgh$$

where m is the mass, g is the acceleration due to gravity, and h is the height. When the mass is released, it accelerates toward the pile due to gravity, and its potential energy is progressively converted into kinetic energy. The kinetic energy of the mass just before impact can be expressed as:

$$KE = \frac{1}{2}mv^2$$

where v is the velocity of the mass at the moment of impact. The conversion from potential to kinetic energy is dictated by the conservation of mechanical energy in an ideal system. For the purposes of this thesis, a simplification is applied: it is assumed that no energy is lost during the fall due to air resistance, friction, or other dissipative forces. This assumption allows for the complete conversion of potential energy into kinetic energy, simplifying the energy calculations. While this idealization is useful for theoretical modeling, it is important to note that in real-world scenarios, a small amount of energy loss may occur during the fall. However, this simplification ensures that the focus remains on analyzing the energy interactions during the subsequent phases of impact and penetration.
The potential energy reflects the energy provided to the system when the mass is released to free fall onto the pile. Thus, the ratio of work to potential energy indicates the proportion of the offered energy that is effectively converted into piling energy, serving as a measure of the efficiency of the installation procedure. The horizontal axis represents the cumulative increment of penetration divided by the radius of the pile.

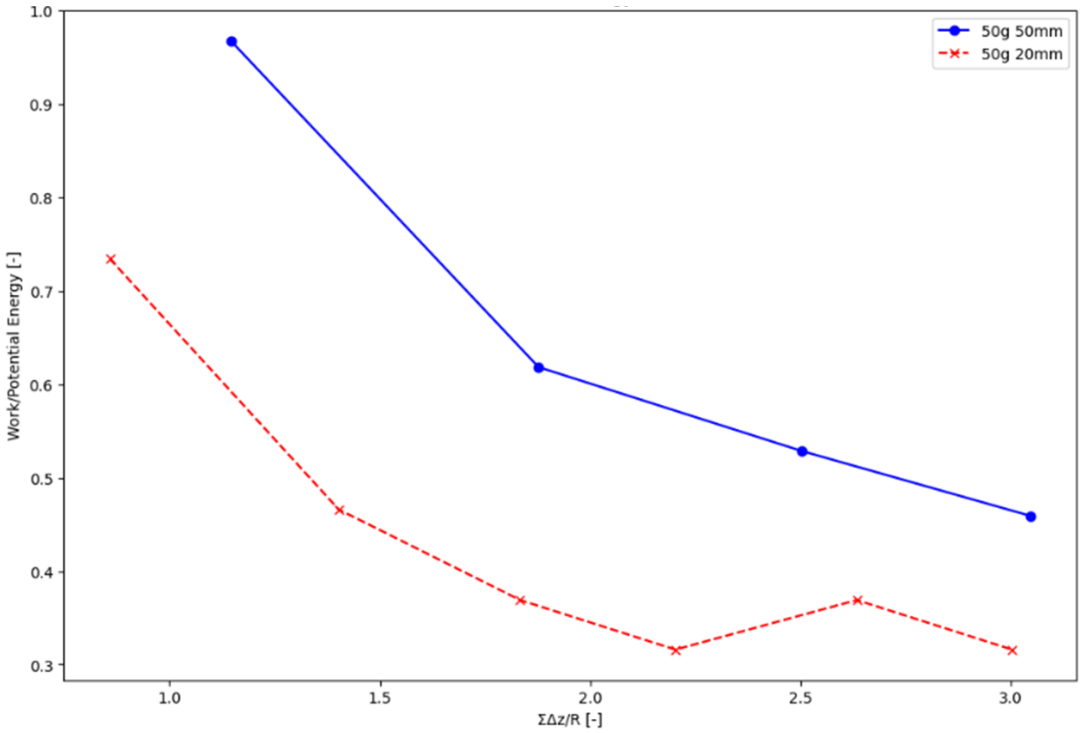

Figure 5.18: Work over potential energy against against penetration at 50g

5.5.12. Observations at 30g centrifuge acceleration

The Figure 5.19 presents the pile penetration over time for two different falling heights, which correspond to varying energy levels at a gravitational acceleration of 30g. The figures clearly demonstrate that as the falling height increases, fewer blows are necessary for the pile to achieve full penetration, specifically reaching a depth of approximately three times the pile's outer diameter. This finding reinforces Hypothesis 1, suggesting that an increase in g-level results in greater penetration per blow, thereby reducing the total number of blows required. Notably, this observation is consistent with the respective Figure 5.16 presented for 50g.
Moreover, this graph not only contributes to addressing the first research question but also enhances our understanding of the data. The actuator facilitates a single blow at a time; thus, when the mass is released onto the pile, penetration occurs during the spinning phase. Subsequently, the centrifuge must halt, the mass must be repositioned, and upon reaching the desired acceleration level, the mass is released to impact the pile. This process continues until the pile reaches the intended depth.
Recognizing the variations in penetration as the falling height increases is essential, as a higher falling height translates to increased impact energy. Furthermore, pile driving resistance is typically quantified by the number of blows. Therefore, Figure 5.19, which illustrates penetration for each blow over time, serves as a critical initial step in examining the influence of impact energy on driving efficiency.

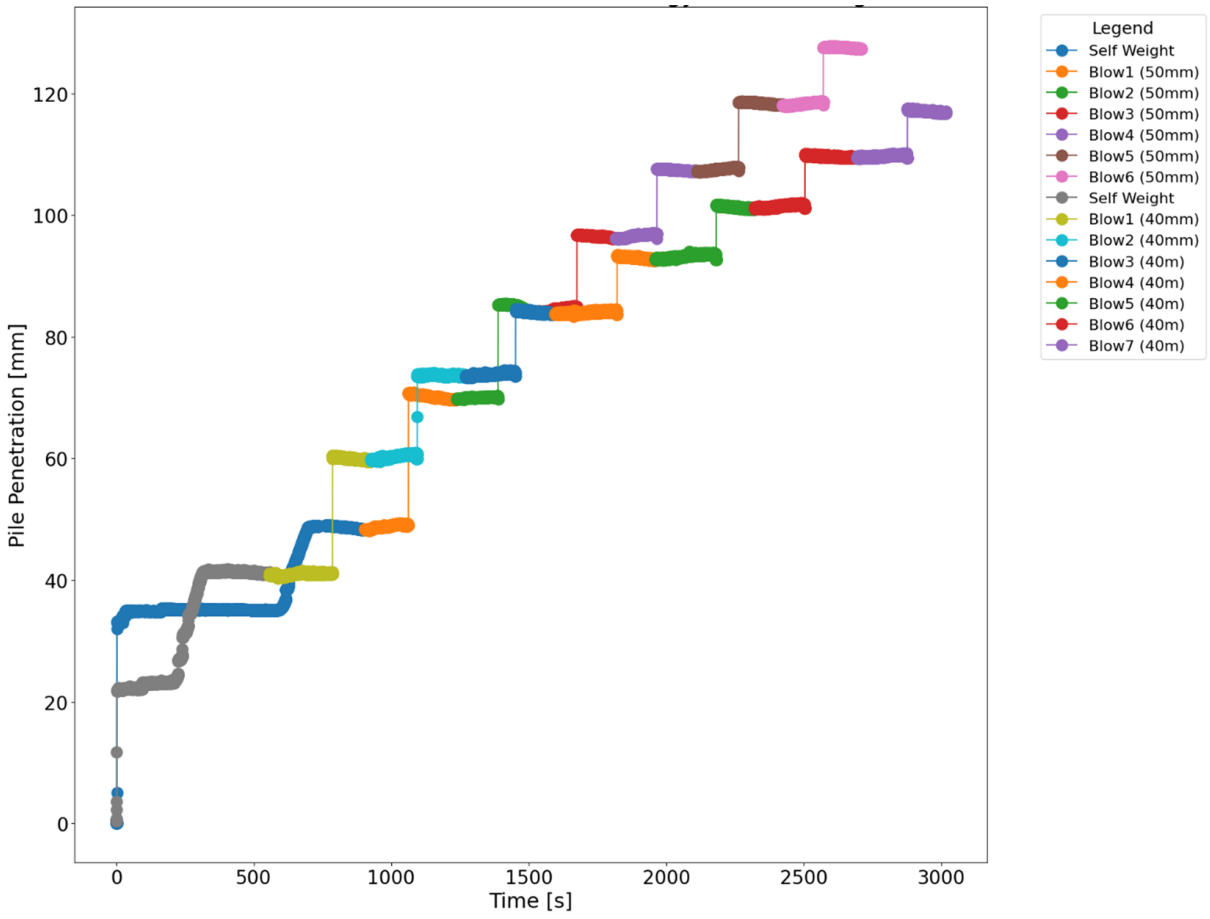

Figure 5.19: Penetration against Time for different energy levels at 30g

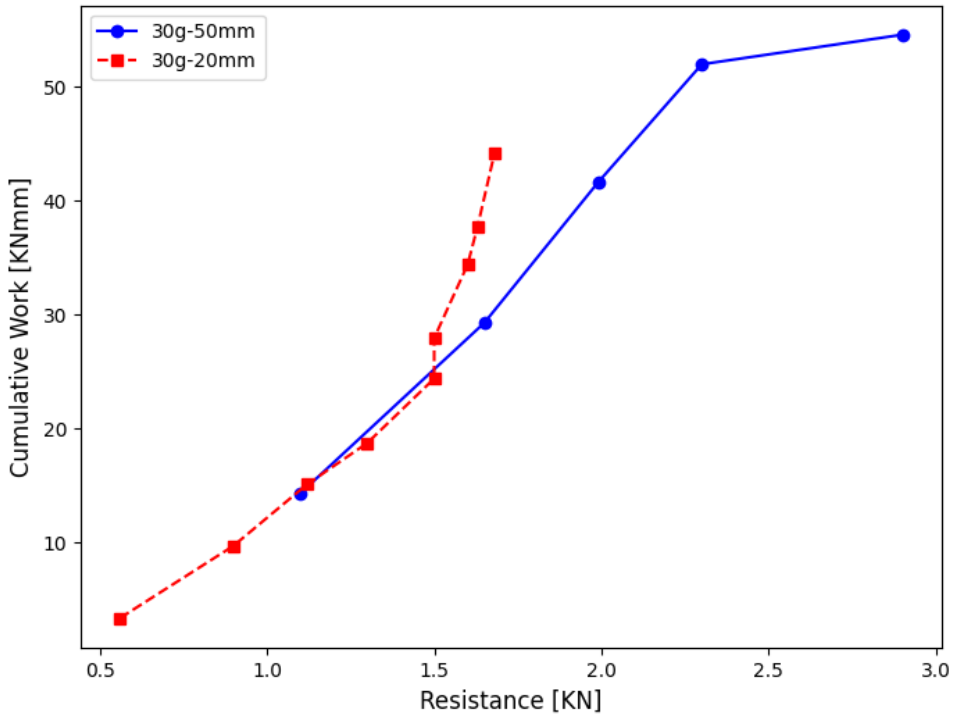

Figure 5.20: Cumulative Work against resistance for 30g

The Figure 5.20 above presents intriguing information regarding the impact of different falling heights tested at the same acceleration level of 30g. The initial observation is the comparison of this graph with the one previously presented for 50g (igure 5.17). In the 50g case, there was a significant difference in the cumulative work from the outset of penetration. However, in this instance, both lines begin at nearly the same level. As the pile penetrates further, the lines begin to diverge.
This indicates that for the 30g cases, both falling heights generate similar work up to a certain depth. Beyond this depth, the tests conducted with the greater falling height demonstrate increased efficiency. Specifically, achieving the same amount of resistance requires less work, meaning that less energy is needed for penetration in the case of the larger falling height. This finding highlights the importance of falling height in optimizing pile installation efficiency under different acceleration conditions.

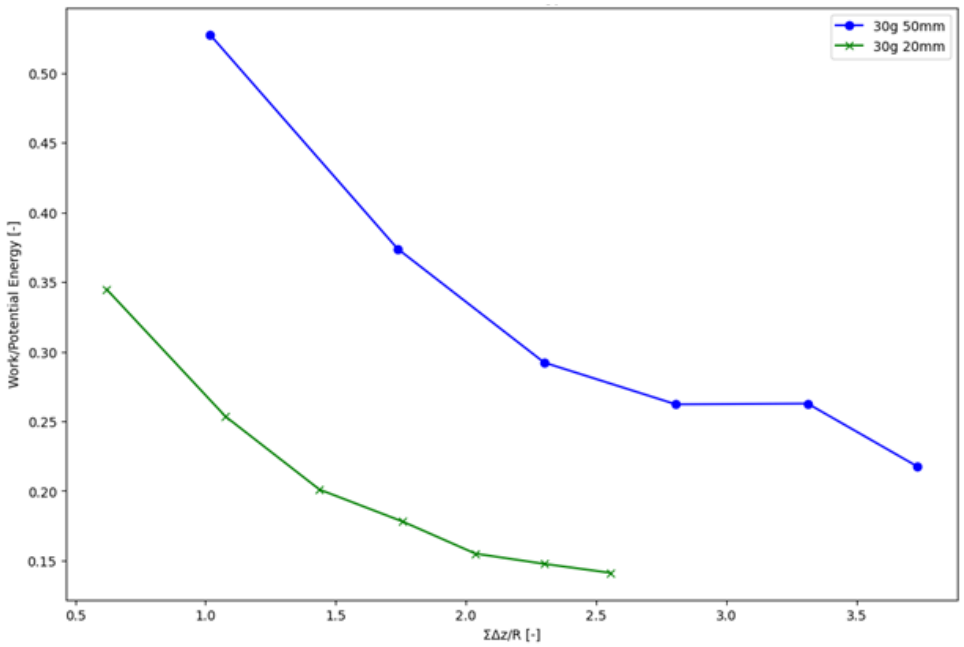

Figure 5.21: Work over potential Energy against penetration

From this Figure 5.21 it is obvious that the trend of the line is descending which is reasonable since

the penetration per blow decreases as the pile reaches deeper depths. Moreover, the Figure 5.19 and Figure 5.21 confirm hypothesis 1. In addition, another observation is that for ΣΔ/R = 3, the ratio of work/potential energy for the experiment with 50mm is 0.5 whereas for the experiment with 20mm is 0.3. That means that when the falling height is bigger and thus the energy is higher, the energy that corresponds to the installation is higher and therefore the losses are less comparing to an experiment with lower falling height. Both cases have losses, however the piling energy (part of the energy from the offered energy that is spend to the pile driving) for the experiment that the falling height is 50mm is significantly higher that the piling energy for the experiment that the falling height is 20mm. During the installation process, energy losses are inevitable due to the principles of physics governing energy transfer. Initially, potential energy from the elevated mass is converted into kinetic energy as the mass falls. Ideally, this conversion should be efficient, with minimal energy lost to factors such as air resistance or friction in the guide mechanism. When the mass strikes the pile, kinetic energy is transferred into the pile as impact energy, but not all of this energy becomes useful for pile driving. Some energy dissipates as heat, vibration, or noise during the impact, resulting in losses. Additionally, when the pile penetrates the soil, energy is absorbed by soil resistance, leading to further losses. Factors such as soil compaction, particle rearrangement, and friction at the pile-soil interface contribute to these energy expenditures. The primary objective is to optimize energy utilization at each stage: ensuring maximum conversion of potential energy to kinetic energy and maximizing the conversion of kinetic energy to effective piling energy. This means designing the system to minimize energy dissipation during impact and soil penetration, enabling the pile to absorb and use as much energy as possible to achieve the desired depth efficiently. Below a sankey graph is presented:

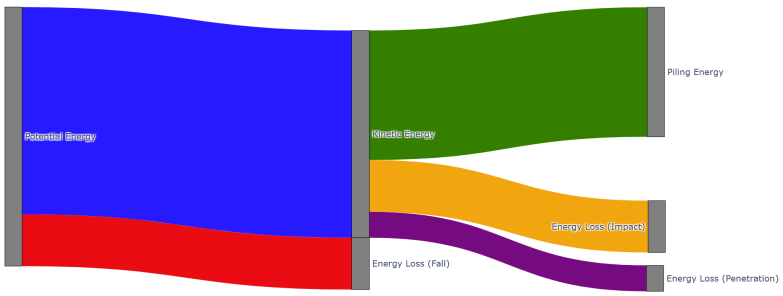

Figure 5.22: Sankey Graph: Energy loss during installation

5.5.13. Observations at 10g centrifuge acceleration

The graph for the 10g experiments with a 50mm falling height appears unusual. This issue arises because the energy transfer at the 10g acceleration level is slower, causing each blow to be irregular. Additionally, the incremental difference in penetration between consecutive blows is very small and sometimes even negative, as the penetration after the n+1 blow can exceed that of the nth blow. As a result, it is difficult to observe a clear trend, especially when compared to the more consistent results obtained at the 50g and 30g acceleration levels. Unfortunately, due to the irregular nature of the data, no reliable conclusions can be drawn from the 10g experiments at this falling height. Furthermore, the 10g experiments at a 20mm falling height yield even worse results, as the amount of energy involved is even smaller. However, an important observation can still be made from these tests. When comparing the 50g-50mm and 30g-50mm experiments to the 10g-50mm experiments, it is evident that the relationship between acceleration and energy transfer is not linear. Specifically, when analyzing the data from tests where the mass falls from a 50mm height, the 10g results show much lower increments in penetration, even though the falling height is the same. This observation suggests that the level of acceleration (g) has a more significant influence on energy transfer than the falling height itself.

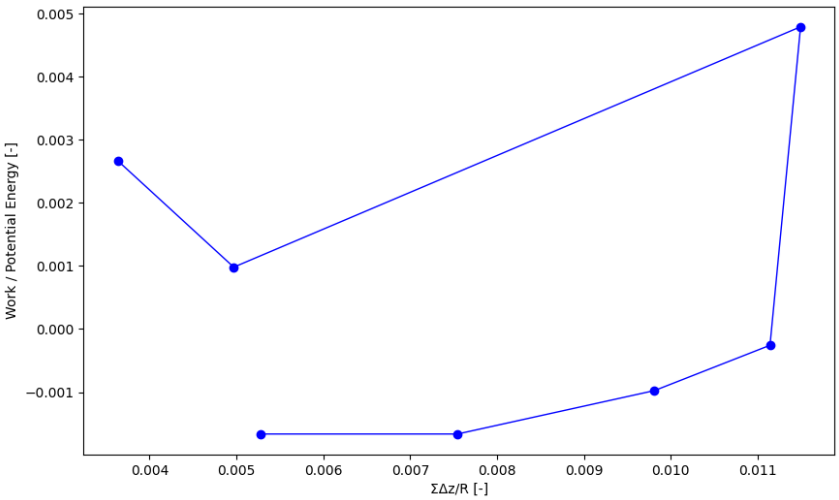

Figure 5.23: Work / Potential [-] Energy vs ΣΔz/R [-]

This implies that the acceleration (g-level) is a dominant factor in determining the amount of energy imparted during each blow, as opposed to the height from which the mass falls. The non-linear relationship between the acceleration level and the resulting energy transfer warrants further investigation and analysis to understand its impact more fully.

5.5.14. Overall Conclusion for Research Question 1

Overall, the graphs above clearly indicate that when the impact energy is higher, fewer blows are required to reach the desired depth, resulting in greater penetration per blow. This leads to decreasing values of cumulative work as the pile reaches deeper depths. The comparison of cumulative work against resistance reveals distinct differences between the 30g and 50g experiments. In the 50g cases, there is a significant disparity in the work generated during penetration for different impact energies. Notably, the experiments conducted at lower impact energy for the 50g configuration prove to be more efficient, as they require less work to achieve the same level of resistance, meaning less energy is needed.

While the 50mm falling height at 50g converts more energy into piling energy (due to the greater energy input), this does not necessarily mean that this piling energy is fully utilized. As shown in the cumulative work versus resistance graph, despite the 50mm falling height generating more piling energy, the experiments with a falling height of 20mm ultimately require less energy to reach the same penetration depth, indicating a higher efficiency for the lower falling height.

Reducing the falling height leads to a decrease in the total offered energy, resulting in a lower maximum achievable piling energy, which is a fundamental physical constraint. Consequently, the penetration per blow decreases due to this reduced energy input. However, this reduction does not affect the overall efficiency. Efficiency is defined strictly as the portion of energy that is actually utilized, remaining independent of the total energy offered or the penetration per blow. It focuses solely on the quality of energy transfer rather than the absolute amount of energy or the resultant displacement.

In the case of the 30g experiments, the efficiency results differ. It is evident that to achieve the same amount of resistance, the same amount of work is generated up to a certain depth. Beyond this depth, the experiment with a 50mm falling height appears more efficient, as it produces less work to reach a higher level of resistance, thus requiring less energy. This deviation after a specific depth could be attributed to the generation of stresses within the pile (plug formation).

From the analysis, it can be inferred that in the 50g scenario, a smaller falling height (20mm instead of 50mm) could be more efficient, whereas in the 30g scenario, a larger falling height (50mm instead of 20mm) may yield better efficiency. Variations in falling height lead to differences in energy levels, and differences in g-level also result in varying energy levels. However, the reasons behind these differences need to be thoroughly investigated to identify the dominant factors.

In the next section (addressing the second research question), the effects of varying g-levels will be further explored. It is evident that a balance must be established between falling height (energy) and g-level (energy, pile dimensions, and intergranular forces). To better understand how to achieve this balance, comparisons will now be made between different g-levels while maintaining the same falling height.

5.6. The effect of pile diameter on the installation efficiency - Research Question 2

5.6.1. Introduction

In transitioning to the second research question, the focus shifts to investigating the impact of pile diameter on driving efficiency. By leveraging the advantages of scaling laws, experiments are conducted at various acceleration levels, allowing the model pile to be tested under different conditions while ensuring that its dimensions correspond to those of the prototype pile. This section presents figures illustrating the work and cumulative work against resistance for different acceleration levels, all while maintaining the same height from which the mass is released. As the height remains constant and the gravitational acceleration varies, the prototype dimensions of the pile differ across the various scenarios. Initially, the plugging effects observed in the experiments at different gravitational levels will be discussed. Subsequently, figures depicting the work relative to potential energy against penetration will be presented. Lastly, graphs illustrating the force versus pile displacement as a function of time will also be included. These latter graphs will provide valuable insights into the impact duration as the acceleration level changes.

5.6.2. Plugging effects

The plugging effects observed during the experiments will be examined. As anticipated and stated in Hypothesis 2, no significant plugging was observed in the majority of the experiments. Below, a representative example is presented in Figure 5.24. These experiments were conducted at an acceleration of 50g, with the mass released from a height of 20mm. In the accompanying graph, the green dots represent the measured values of plugging after each blow, while the blue line serves as the best fit for these measured points. The red line illustrates the theoretical scenario of complete coring, indicating that no plugging occurred. As indicated by the graph, the trendline of the measured points aligns precisely with the theoretical fully coring line. This theoretical state is calculated based on the penetration of the pile, and since the pile is open-ended, the length of soil inside the pile is equal to the length of soil outside the pile.

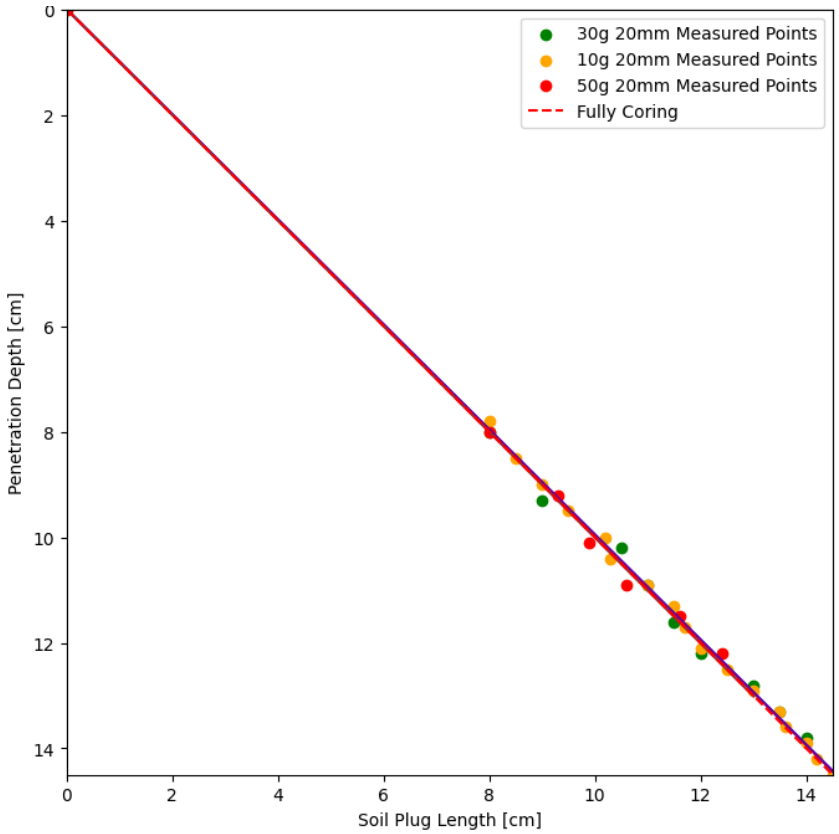

Figure 5.24: Soil Plug length against Penetration Depth for Different g-levels

The most accurate method for determining the presence of plugging behavior is to calculate the stresses both inside and outside the pile. It is assumed that a soil plug within the pile moves upward relative to the pile wall during installation. Measurement data indicate that the plug length, denoted as

$$h'$$

, typically ranges from 10% to 20% of the embedded length of the pile. Notably, not the entire soil column moves upward. The upper portion of the soil column acts as a surcharge. Using this theoretical framework, it is possible to predict the occurrence of a plug through static equilibrium analysis. If the shear capacity along the length of the soil plug exceeds the mobilized base resistance, a plug forms within the pile (Henke and Grabe, 2013). However, in this research, stress measurements inside and outside the pile are not conducted; instead, conclusions are drawn based on the observed differences in soil column lengths both inside and outside the pile. For future research it is recommended to to calculate stresses both inside and outside the pile to determine if plugging takes place.
It is important to note that various parameters can influence soil plugging, with pile diameter being one significant factor. Based on the characteristics of the model pile tested, the specific soil conditions, and the depths examined, this research concludes that no soil plugging behavior was observed. This finding reinforces the understanding of plugging dynamics in relation to pile design and installation methods, highlighting the need for further investigation into how different parameters may impact soil behavior during piling operations.
Even though no plugging was visible, it is still necessary to investigate how the g-level, particularly the pile diameter, affects drivability efficiency. Therefore, comparisons are made between experiments conducted at different g-levels while maintaining a constant falling height. This approach allows for a clearer understanding of the relationship between g-level and drivability efficiency, providing insights into the effects of pile diameter on the overall performance of the installation process.
The differences in cumulative work against the resistance across various g-levels are presented below. This analysis aims to determine whether differences exist between the experiments when the falling height of the mass remains constant, but the g-level varies, and, if so, to explore the underlying reasons for these differences.

5.6.3. Observations for a falling height of 40mm at various centrifuge g-levels

Firstly, the Figure 5.25 below illustrates the relationship between the cumulative work against the resistance of the pile, which represents the ultimate pile capacity. This graph is similar to the Figure 5.17 and Figure 5.18 presented in the discussion of the first research question. However, it now compares experiments conducted under different gravitational accelerations. In the previous graph, experiments were plotted at the same gravitational level with varying falling heights, whereas in this case, the falling height remains constant while only the gravitational level changes.

As depicted in the Figure 5.26, the trend of the lines closely resembles that of the earlier Figure 5.17 and Figure 5.21.However, in this case, the two experiments initially align in terms of work produced as the pile penetrates. However, after a certain depth, the two lines begin to diverge. The experiment conducted at 50g with a 50mm falling height appears to be more efficient, as it requires less work to reach the same level of resistance as the experiment conducted at 30g with a 50mm falling height, meaning it utilizes less energy overall. This observation underscores the importance of both g-level and falling height in influencing the efficiency of the pile installation process.

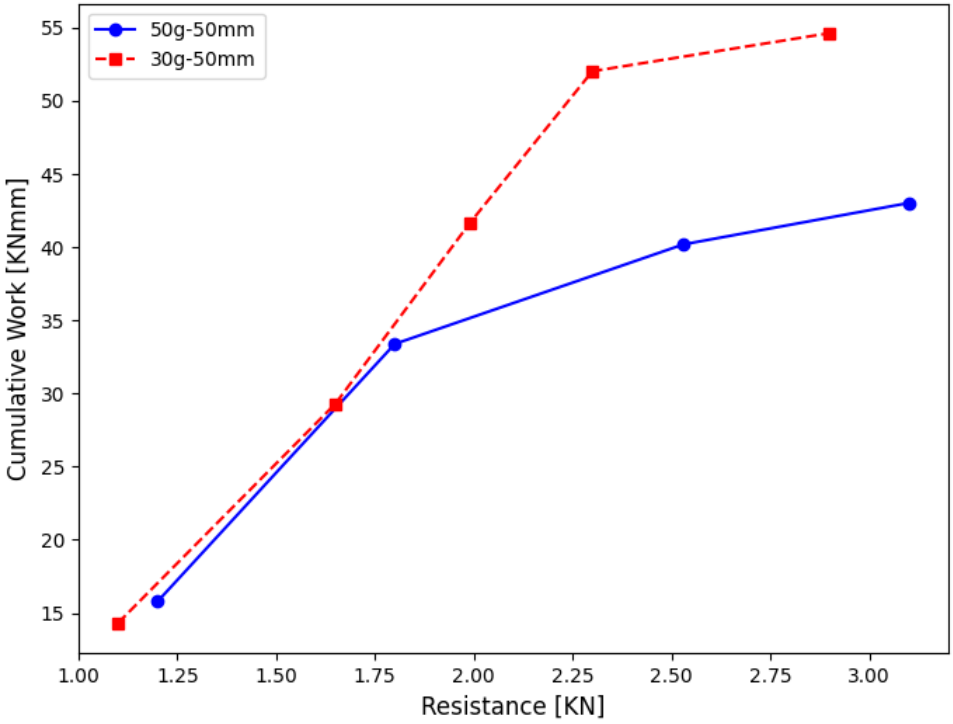

Figure 5.25: Cumulative Work against Resistance Different g-levels for falling height 50mm

The Figure 5.25 clearly illustrates that the cumulative work for both the 50g and 30g cases is remarkably similar when the falling height of the mass is 50mm. This finding is noteworthy, particularly in light of the differences observed at varying falling heights when the gravitational level remains constant (5.17). For instance, when resistance increases from 2 kN to 3 kN, the work required for the pile to penetrate in the 50mm and 50g scenario is significantly greater than that for the 50g at 20mm. From this perspective, the 50g at 20mm demonstrates greater efficiency, as it requires less energy to achieve a comparable level of resistance(5.17). A similar trend is evident in the case of 30g at different falling heights(5.20). Specifically, when comparing cumulative work between the 20mm and 50mm scenarios for 50g, it is apparent that the cumulative work remains relatively consistent for both. However, as resistance rises from 2.5 kN to 3 kN, a decreasing trend is observed in the cumulative work for the 50mm-50g scenario compared to the 30g-50mm case. This suggests that the 50mm-50g configuration may require less energy to penetrate deeper, thus indicating greater efficiency. Furthermore, when analyzing the falling height of 20mm, a comparison between the 50g and 30g (5.25) cases reveals that, as the pile penetrates deeper, the 50g configuration produces less cumulative work. This reduction in work implies lower energy requirements, reinforcing the notion that this combination is the more efficient option.

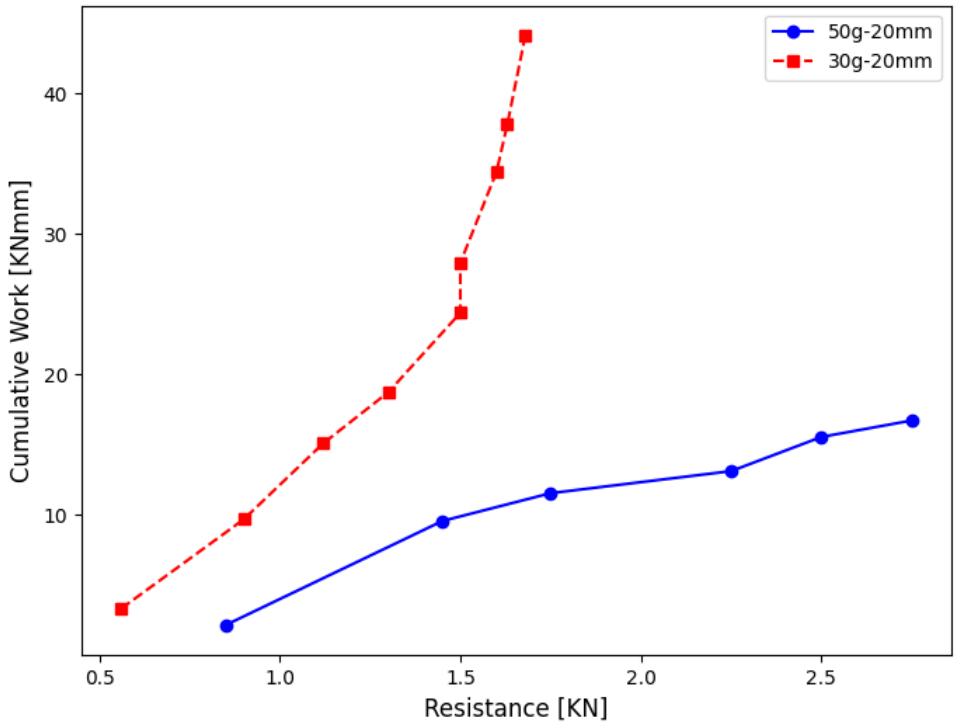

Figure 5.26: Cumulative Work against Resistance Different for falling height 20mm for various g-levels

The graph 5.27 presented below, where the y-axis represents the ratio of work to the potential energy of the system. This allows us to visualize the portion of the offered energy that is converted into piling energy across the different experiments.

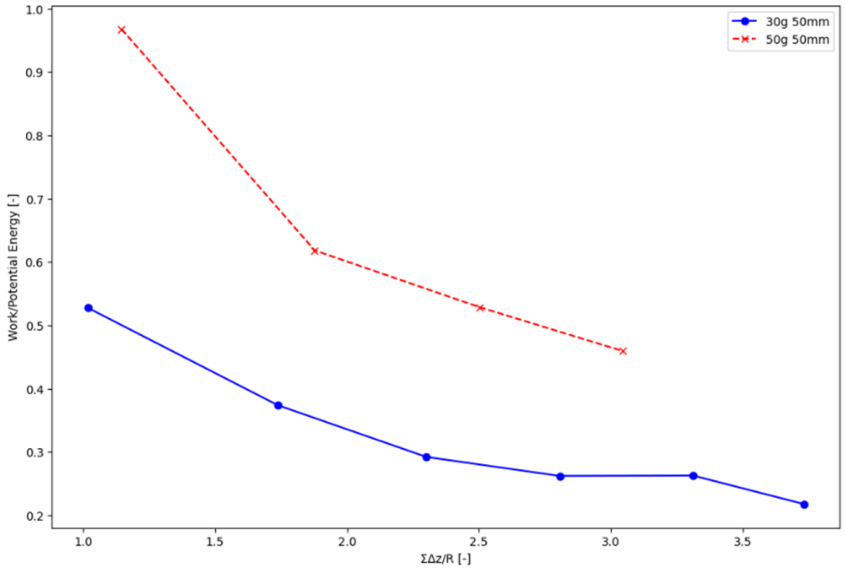

Figure 5.27: Work over Potential Energy against Penetration Different g-levels

Similarly to the previous Figure 5.18, it is evident that the experiment conducted at 50g converts a greater amount of energy into piling energy compared to the experiment at 30g. While both Figure 5.21 exhibit similar trends, the slopes differ due to the variations in offered energy associated with different gravitational levels, as well as the changes in force as the pile penetrates deeper. This indicates that for experiments conducted at higher g-levels, with all other parameters held constant, a larger proportion of the offered energy is converted into pile-driving energy. Moreover, since these experiments correspond to prototype piles with larger diameters, it can be concluded that piles with greater diameters not only yield higher work values but also convert a larger fraction of the offered energy into piling energy. This finding supports the second hypothesis. An additional Figure 5.28 of interest is presented below, which illustrates the force against pile displacement over time. One notable observation from this graph is the

difference in blow duration between the two experiments: one conducted under 10g acceleration and the other under 50g acceleration. Both experiments share the same falling height and correspond to the first blow of each respective experiment. Another significant observation is the time required for the pile to penetrate deeper. The colored time bar indicates that the experiment conducted at 50g penetrates more rapidly. Additionally, the pile displacement at 50g is greater than that at 10g for the first blow, as previously noted in Hypothesis 2. These observations are also supported by Figure 5.14, which illustrates the blow duration across different g-levels.

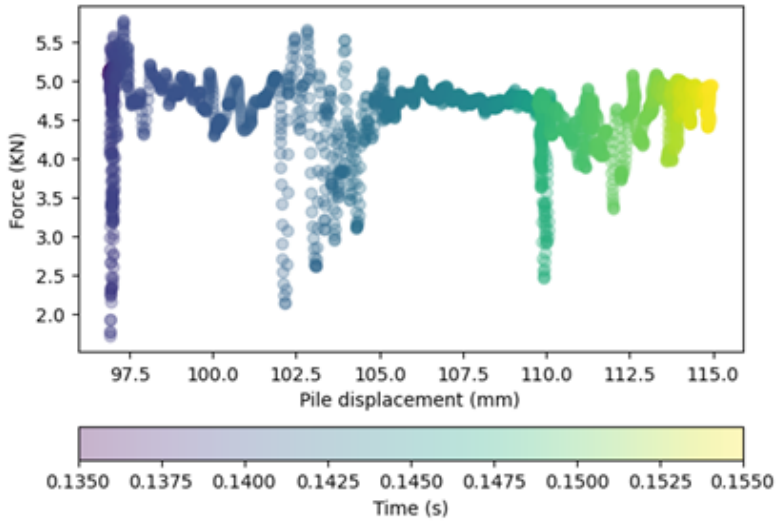

Figure 5.28: Force against Pile Displacement as functions of Time- Blow 1 for 10g at 50mm

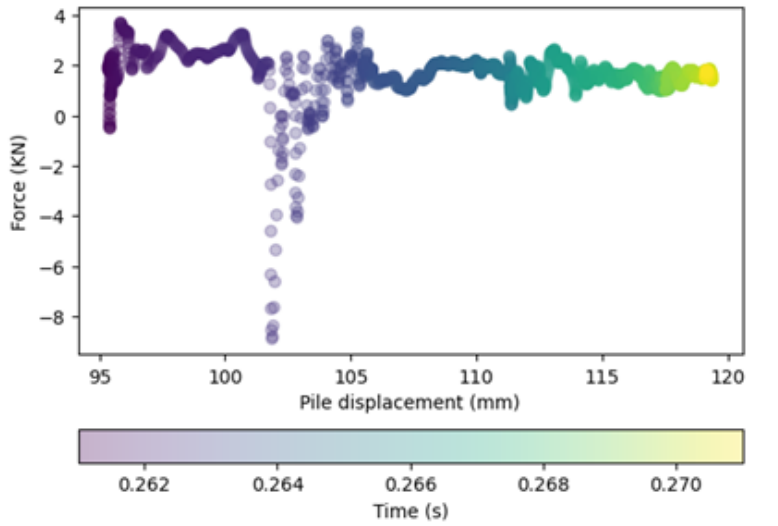

Figure 5.29: Force against Pile Displacement as functions of Time- Blow 1 for 50g at 50mm

5.6.4. Overall Conclusion for Research Question 2

Comparisons were made between the tests conducted at different acceleration levels, ensuring that all other parameters remained unchanged. Additionally, the study examined whether plugging effects developed during the pile driving process. As anticipated, no plugging effects were observed up to the target depth of approximately three times the pile diameter for the dimensions tested.

Another aspect examined was impact duration. As anticipated, the impact duration for experiments conducted at lower g-levels was longer due to the time-dependent nature of free fall. Specifically, blow duration decreases as g-level increases, but this relationship is nonlinear. Additionally, the velocity of impacts rises with increasing g-levels.

A significant observation is that when the g-level is increased while the mass is released from the same falling height, a larger proportion of the offered energy is converted into piling energy. Moreover, it is important to note that when comparing the cumulative work at a 50mm falling height, the two lines align up to a specific depth. However, when comparing the experiments at a 20mm falling height (for both 50g and 30g), the lines deviate from the beginning. Therefore, for all the cases examined thus far, it is evident that as the offered energy increases, so does the piling energy. However, this generalization cannot be applied universally to the work produced and cumulative work across different g-levels and energy levels as can be seen in 5.25 and 5.26

When comparing different g-levels (30g and 50g) at a higher falling height (50mm), the results remain similar up to a certain depth. Beyond this depth, further research is needed to identify the reasons for the observed deviation in the lines. One possible explanation could be the formation of soil plugs and the generation of stress within the pile, as smaller diameter piles (in the case of 30g) are more susceptible to plugging effects. Conversely, when comparing experiments across different g-levels (30g and 50g) at a lower falling height (20mm), it is evident that the lines deviate from the beginning, indicating that the 50g experiments are more efficient, as they require less energy to achieve the same penetration.

As mentioned in the first research question section, establishing a balance between falling height and g-levels is essential to determine which scenario is the most efficient.

The findings imply that under prototype conditions, piles with larger diameters are more efficient than those with smaller diameters when a suitable amount of energy is applied. This is reflected in the percentage of the offered energy that is converted to piling energy and the minimum energy required to achieve a specific penetration depth. This can be seen in 5.26, 5.25, 5.27, 5.27. However, further investigation is necessary to ascertain whether the piling energy is fully utilized. Analyzing the saturated samples, along with examining the generation and dissipation of pore pressures, will provide greater insight into the extent to which the piling energy is effectively employed. Overall, these results underscore the critical relationship between pile diameter and installation efficiency in the context of varying acceleration levels.

5.7. The effect of saturation with viscous fluid on the installation efficiency

5.7.1. Introduction

The third and final research question is addressed in the following section, focusing on experiments conducted with saturated samples. Two saturated samples were prepared using a viscous fluid for saturation, and corresponding experiments were carried out. The strongbox used for these saturated experiments differs from that of the dry sample tests, as it is equipped with nine pore fluid pressure sensors to capture detailed measurements.

To accommodate the saturated conditions, the strongbox was modified by incorporating four plate filters at the base, in addition to the nine pore pressure sensors. These sensors are strategically positioned at three distinct vertical levels: 1Dout, 2Dout, and 3Dout, where Dout represents the outer diameter of the pile, which measures 42mm. Furthermore, the sensors are placed at varying radial distances from the center of the sample, specifically at 0.5Dout, 1Dout, and 1.5Dout. These modifications allow for comprehensive monitoring of pore pressure changes throughout the experiment, providing valuable insights into the effects of saturation on the pile installation process.

Due to practical challenges encountered during the execution of the saturated experiments, only limited data and insights could be gathered.

In the first experiment, several issues arose, leading to incomplete data collection. Some of the pressure sensors malfunctioned, and the high-frequency data acquisition system failed to operate properly, resulting in no data capture. The low-frequency system managed to record data during the initial spin, where the pile settled under its own weight, but during the first blow, an early detachment between the mass and the magnet occurred, causing the mass to fall prematurely before the centrifuge reached 50g acceleration. While the second blow proceeded without issues, and data was collected successfully, the premature mass drop in the first blow prevented the creation of a cumulative penetration graph. Additionally, due to the malfunction of the high-frequency data acquisition system, no force signal graph could be generated.

5.7.2. Low frequency measurements

The data acquisition system is comprised of both low-frequency and high-frequency components. For accurate load measurements, the high-frequency system is essential, as the measurements occur at a rapid rate. While displacements are more complete when captured by the high-frequency system, they can also be recorded, albeit less thoroughly, by the low-frequency system. In this case, most of the issues arose with the high-frequency system. Therefore, all available data obtained from the low-frequency system will be presented.

The Figure 5.33 below displays the normalized pile penetration against the number of blows for both saturated experiments. The two lines are close, though not entirely coincident, which may be attributed to slight variations in the homogeneity of the sample saturation. Nevertheless, both experiments required a similar number of blows for the pile to penetrate to roughly the same soil depth, and the incremental penetration per blow (Δz\Delta zΔz) was very similar. These results indicate that, despite the data limitations, the experiments were successful, and the available findings are reliable.

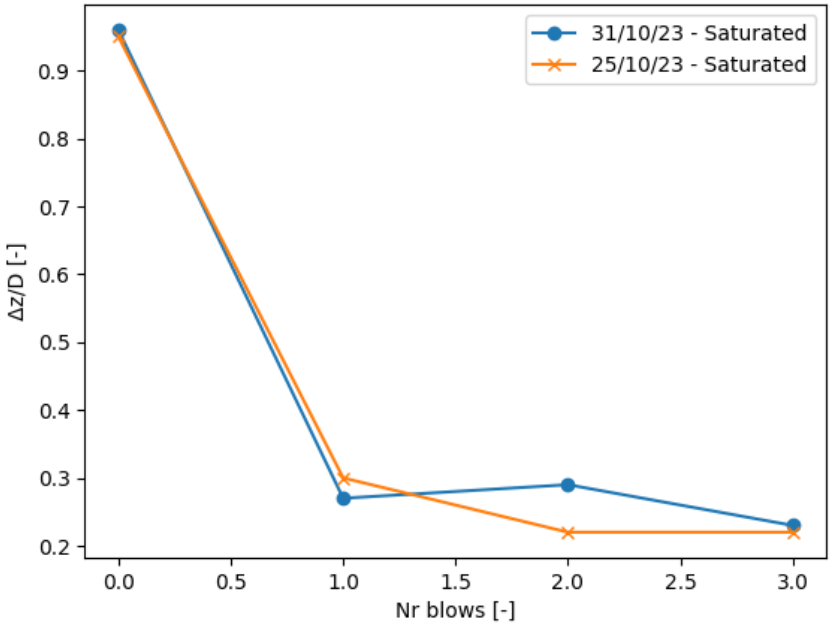

Figure 5.30: penetration against Nr of blows for saturated sample at 50g for 40mm falling height

Both of these experiments were conducted at 50g with the mass released from a height of 40mm. To provide a comparative analysis, the corresponding Figure 5.31 for the dry sample is also presented alongside the results from the saturated experiments.

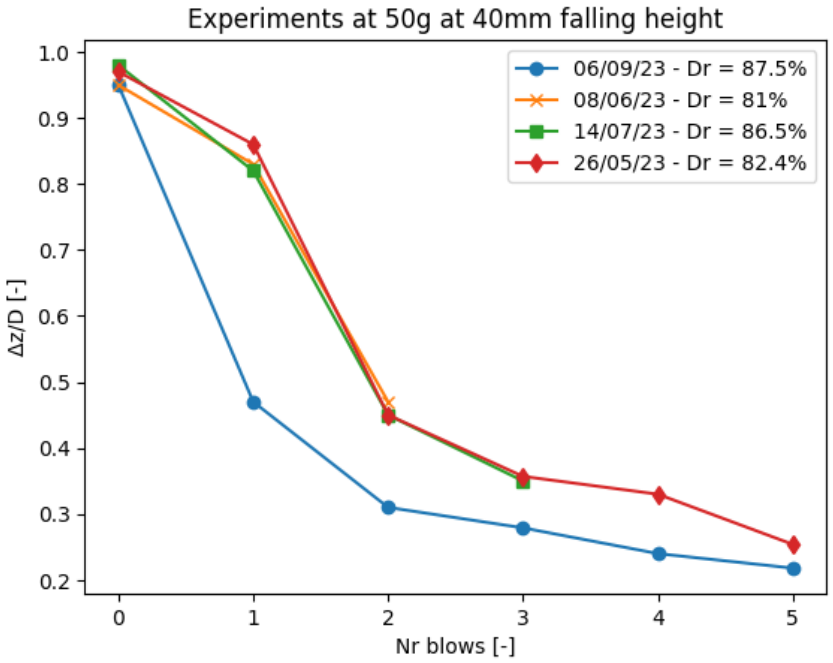

Figure 5.31: penetration against Nr of blows for dry sample at 50g for 40mm falling height

From the comparison of the Figure 5.31 and Figure 5.33 above, it is evident that during the first spin, where the pile penetrates under its own weight, both the saturated and dry samples exhibit similar penetration behavior. However, starting with the first blow, the incremental penetration of the saturated pile is significantly smaller than that of the dry sample. Although the experiment with the saturated sample required fewer blows, this is due to early termination of both trials caused by equipment malfunctions. Despite the reduced number of blows, it is clear that the saturated sample presented greater resistance to penetration compared to the dry sample, even though all other parameters, such as the acceleration level and the falling height of the mass, were kept constant. This observation is also in compliance with Hypothesis 3.
Additionally, the Figure 5.32 below represents the first blow of the initial experiment with the viscous

fluid. This preliminary test was conducted to ensure that all equipment was functioning correctly. During this test, the g-level was gradually increased until it reached the desired value, but the mass was not released. The primary objective was to verify that the pore fluid pressure sensors were responsive and accurately recording data at different acceleration levels.

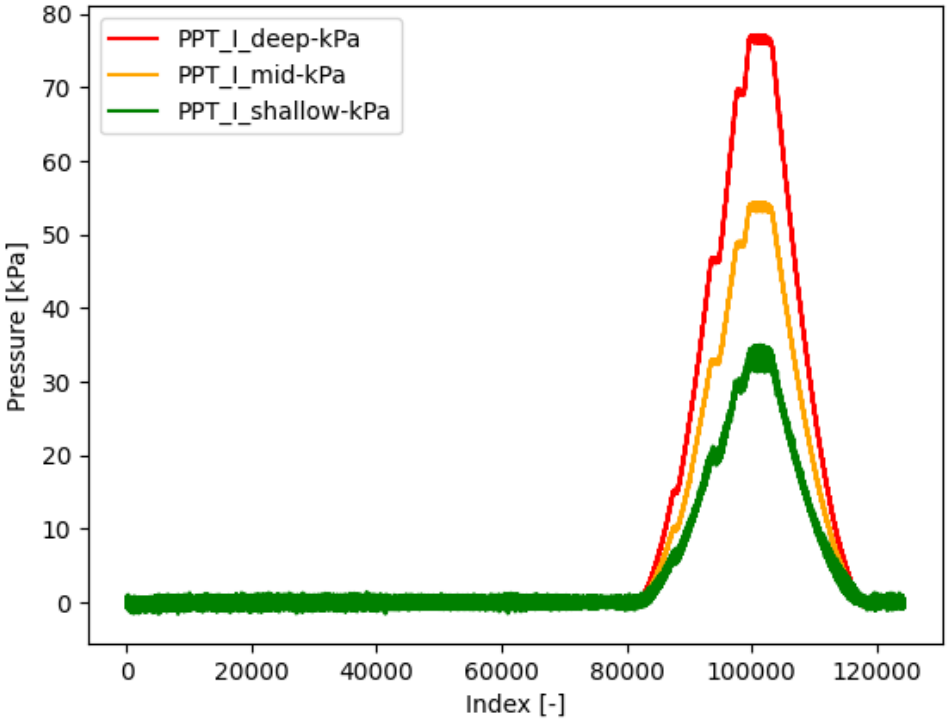

Figure 5.32: Pore Fluid Pressure against time for the first blow of a saturated experiment at 50g

5.7.3. High frequency measurements

In this section, the data acquired from the high frequency system are presented. The Figure 5.33 and Figure 5.34 below focus on the impact duration, depicting the force, pile displacement. As shown, the pile displacement (blue line) begins the moment the mass strikes the pile. The key observation here is that although the impact duration is nearly identical for both the dry and saturated experiments at 50g and with the same mass falling height, the pile displacement in the dry sample is greater than in the saturated sample. This is expected, as the presence of fluid in the saturated soil increases resistance, making it more challenging for the pile to penetrate compared to its installation in dry soil. Additionally, the force signal shows slight variation, likely due to differences in strain measurements when the pile was installed in saturated rather than dry conditions. The force signal is derived from the strain that develops within the pile. It is reasonable to expect that in a saturated sample, the forces generated in the soil during pile penetration differ from those in a dry sample. Consequently, it is anticipated that the force signals for the two cases will vary, despite all other parameters remaining constant, with the exception of the saturation of the sample.

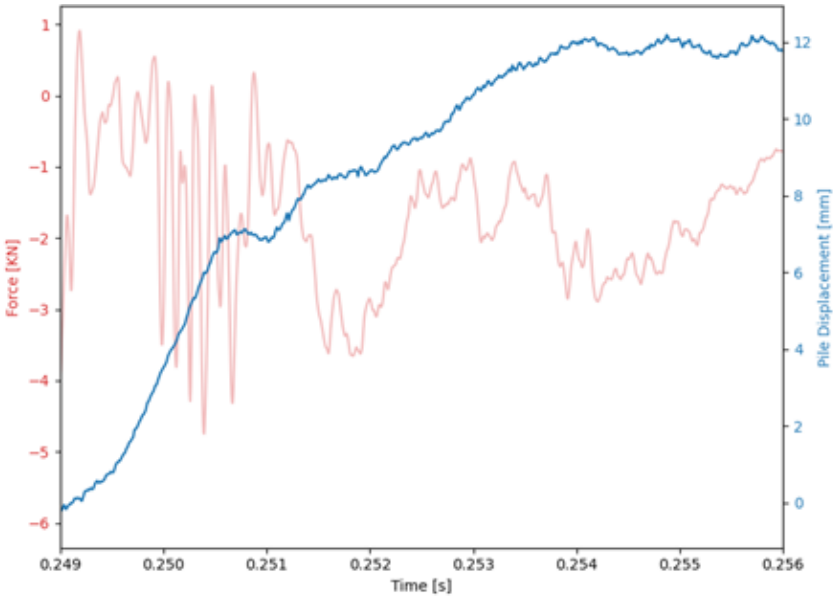

Figure 5.33: Force, Pile displacement over Time for the saturated sample at 50g for the third blow

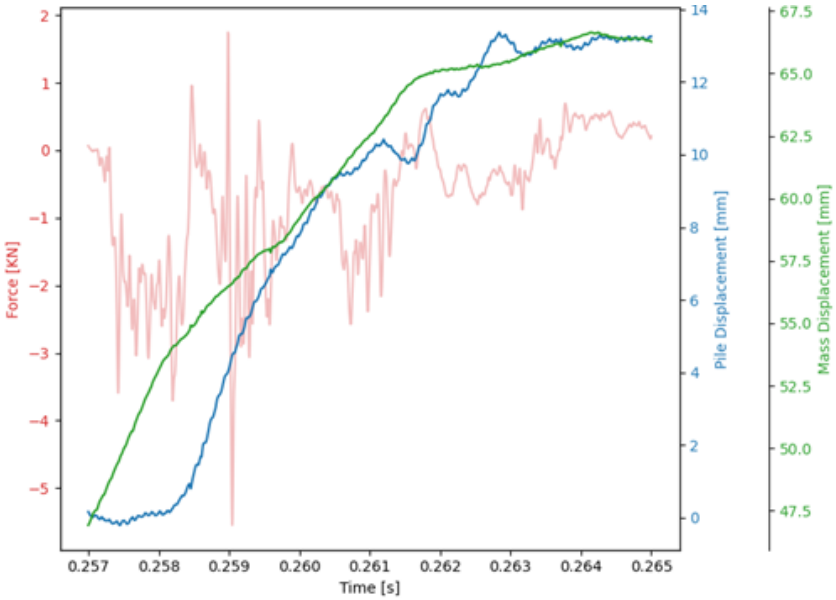

Figure 5.34: Force, Mass and Pile displacement over Time for the dry sample at 50g for the third blow

The Figure 5.35 below displays only the pore fluid pressure sensor data against time, clearly illustrating that pressure is generated upon impact and begins to dissipate after a brief period.
Specifically, the data presented below represents the pressure differential recorded by the sensor. To determine the actual pressure, the hydrostatic pressure corresponding to the g-level at which the centrifuge is operating must first be calculated (see Figure 5.32). Once this hydrostatic pressure is determined, the pressure differential resulting from the blow, as captured by the sensor, should be added to obtain the total pressure.

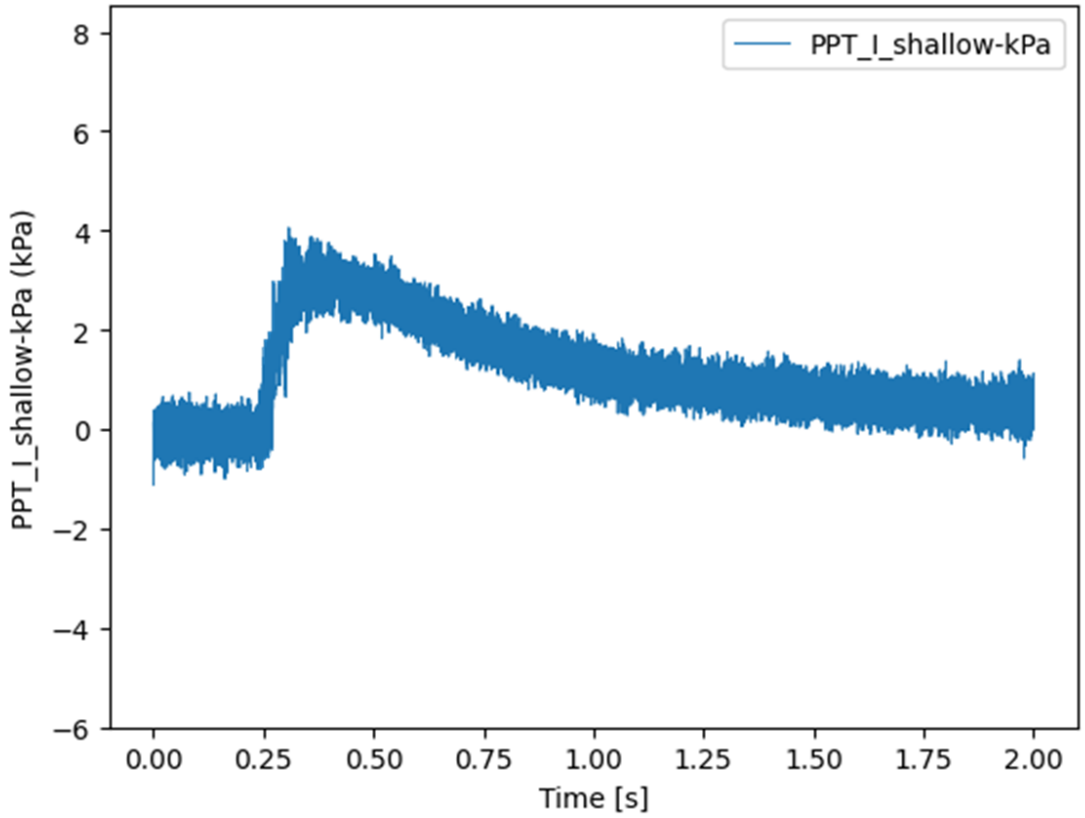

Figure 5.35: Pore Fluid Pressure against Time for the first blow of a saturated experimnet at 50g at 40mm falling height

The following describes how to calculate the actual pressure recorded by the sensor during a centrifuge test. The sensor captures the pressure difference, but to find the actual value of the pressure, it is first necessary to compute the hydrostatic pressure at the respective g-level of the centrifuge 5.32. After determining the hydrostatic pressure, the pressure difference caused by the event (e.g., a blow) captured by the sensor is added to find the total pressure.
The following describes how to calculate the actual pressure recorded by the sensor during a centrifuge test. The sensor captures the pressure difference, but to find the actual value of the pressure, it is first necessary to compute the hydrostatic pressure at the respective g-level of the centrifuge 5.32. After determining the hydrostatic pressure, the pressure difference caused by the blow captured by the sensor is added to find the total pressure. 1. Hydrostatic Pressure Calculation: The hydrostatic pressure at a specific g-level is calculated using the equation:

$$P_{\text{hydrostatic}} = \rho \cdot g \cdot h$$

where: - ρ is the density of the fluid, - g is the effective gravitational acceleration, which is the product of Earth's gravitational acceleration ($g_{\text{earth}} = 9.81\,\text{m/s}^2$) and the g-level at which the centrifuge is spinning ($g_{\text{centrifuge}}$), - h is the height or depth of the sensor from the surface or reference point. For example, if the centrifuge is spinning at 100g, the effective gravitational acceleration is:

$$g_{\text{centrifuge}} = 100 \times 9.81\,\text{m/s}^2$$

2. Pressure Difference: The sensor measures the pressure difference (ΔP) caused by external events such as a blow. This is the additional pressure that the sensor captures beyond the baseline hydrostatic pressure.
3. Total Pressure Calculation: To calculate the total pressure experienced by the sensor, the hydrostatic pressure and the pressure difference are added together:

$$P_{\text{total}} = P_{\text{hydrostatic}} + \Delta P$$

where P_{total} is the total pressure that combines the fluid pressure and the additional pressure from the external event. In summary, the total pressure at the sensor location is a combination of the hydrostatic pressure (due to the fluid and the g-level of the centrifuge) and the pressure difference from external events, providing a full understanding of the sensor's recorded pressure.

5.7.4. Overall Conclusions for Research Question 3

It was also evident in earlier graphs that, when comparing the dry and saturated samples under identical conditions, the pile displacement in the dry sample was greater. This difference could be attributed to the dilation of soil particles in the saturated sample, potentially leading to the development of negative change in water pressure, which would result in higher effective stresses during installation. However, due to the limited data and lack of comprehensive evidence on soil behavior during pile installation with prolonged blows, further investigation is required. What can be inferred from the current data is that, since a noticeable difference was observed between the dry and saturated samples, the condition of the saturated sample is either partially drained or undrained. This is inferred from the fact that under fully drained conditions, the effective stresses in the saturated sample are lower. Therefore, one would expect the penetration to be greater in the saturated test compared to the dry test. However, in this instance, the penetration of the saturated sample is indeed lower. This suggests that, despite the lower loading rate compared to conventional impact hammers, the sample does not have sufficient time to fully drain. Future research should prioritize saturated experiments, aiming to provide more comprehensive comparisons with dry samples and a deeper understanding of pore pressure generation and dissipation in saturated conditions.

6

Conclusions

In summary, this research provides a comprehensive examination of the factors affecting pile driving efficiency, addressing three distinct research questions. Starting with the first research question, all experimental conditions were held constant except for the falling height, which was tested at three different levels: 20 mm, 40 mm, and 50 mm. This investigation aimed to explore the effect of impact energy on installation efficiency. A notable observation was the relationship between the falling height and the number of blows required for the pile to achieve full penetration. It was found that as the falling height increased, the number of blows needed to acieve a given penetration depth, decreased, a trend that aligns logically with the higher impact energy resulting from greater falling heights.

Additionally, the research examined the proportion of the offered energy converted into piling energy during the driving process. Graphical analyses indicated that more energy was transformed into piling energy when the mass was released from a higher falling height. Given that gravitational acceleration remained constant, variations in falling height translate directly to differences in impact energy. Consequently, increased falling heights result in greater impact energy. However, it is important to note that not all of the piling energy was fully utilized. Further analysis of saturated samples, along with the examination of pore pressure generation and dissipation, will provide greater insight into the effective employment of piling energy.

Regardless of the falling height, energy losses occur when the mass strikes the pile. A portion of the impact energy is transmitted to the pile, while another portion is dissipated as energy loss. Although energy losses are associated with falling height, a fixed energy loss inherent to the system upon impact also exists. When the offered energy is greater, the fixed energy loss constitutes a smaller proportion of the total energy, resulting in more efficient conversion to piling energy. Thus, it can be concluded that with increased impact energy, a larger fraction of the energy is available for driving the pile.

The results also provide insights into cumulative work generated throughout the experiments. For the 50g experiment, less energy was sufficient to drive the pile, as the experiments at 20 mm and 50 mm falling heights exhibited significant differences in work produced for the same resistance, favoring the 20 mm falling height. Conversely, the observations were not the same for the 30g experiment, which demonstrated similar results between different falling heights at least up to a specific depth. This indicates that falling height alone cannot control the efficiency of the system. A combination of parameters—impact energy, pile dimensions, and intergranular forces—must be understood, and a balance among these factors must be established.

Moving to the second research question, the objective was to investigate the effect of pile diameter on installation efficiency. To achieve this, all experimental parameters were kept constant while only the acceleration level of the centrifuge was varied, with tests conducted at 10g, 30g, and 50g. It is crucial to recognize that energy is influenced by the g-level. As the g-level increases, both the pile diameter and the energy also increase. This distinction is essential to avoid the misconception that comparisons are made between cases with different pile diameters but the same energy. Even with a constant falling height, the actual energy increases with the g-level.

Comparisons were drawn between tests conducted at different acceleration levels, ensuring all other parameters remained unchanged. The study also examined whether plugging effects developed during the pile driving process. As anticipated, no plugging effects were observed up to the target depth of approximately three times the pile diameter for the tested dimensions. Notably, altering the g-level also modifies the dimensions of the prototype pile. Another aspect investigated was the impact duration. As expected, the impact duration for experiments conducted at lower g-levels was longer, given that the time required for the mass to free fall is inherently time-dependent. A significant observation was that

when the g-level increased while the mass was released from the same falling height, a larger proportion of the offered energy was converted into piling energy. This finding suggests that, under prototype conditions, piles with larger diameters are more efficient than those with smaller diameters. Additionally, it was noted that smaller pile diameters correspond to higher internal horizontal stresses at the pile toe. While no plugging was observed, the increase in lateral stresses could help explain why larger diameter piles penetrate more easily and demonstrate greater efficiency.

A particularly interesting observation is that the cumulative work for the two cases with the same falling height at different energy levels is very similar up to a certain depth. Beyond this point, the experiment with the higher g-level appears to be more efficient, as it requires less work to achieve a similar penetration depth. This finding could suggest that piles with larger diameters are more efficient. However, the underlying reasons for this observation remain unclear. One explanation could be that piles with smaller diameters are more susceptible to plugging effects and increased horizontal stresses within the pile. Therefore, it can be concluded that, even though plugging effects may not be visibly apparent, stresses within the pile begin to accumulate after a certain depth. This accumulation likely accounts for the observed differences between the two cases at varying g-levels when measuring cumulative work against resistance.

Moreover, as with the previous research question, the impact energy is also dictated by the g-level. Thus, higher g-levels result in increased energy. Considering the fixed energy losses, the efficiency of experiments conducted at higher g-levels is enhanced due to the greater energy involved. Overall, these results highlight the critical relationship between pile diameter, g-level, and installation efficiency.

Finally, in addressing the third and final research question, this study investigates the effect of saturation on driving efficiency. To address this question, experiments were conducted using a viscous fluid to saturate the soil, with tests performed in the centrifuge under 50g acceleration and the mass released from a height of 40 mm. Unfortunately, due to equipment malfunctions, only limited data were obtained from the saturated experiments.

The most significant finding was that pile penetration was noticeably reduced when driving through saturated soil. Under fully drained conditions, the total stresses in the saturated sample are not affected by the pore pressures therefore the penetration of the pile should be the same. However, the observed reduction in penetration indicates that the conditions may be partially drained or undrained, suggesting that pore pressures likely do not have sufficient time to dissipate completely.

According to the principles of installation with prolonged blows, energy is dissipated over a longer duration compared to the instantaneous shockwave generated by conventional impact hammering. However, in this context, the soil still lacks adequate time to drain, which further complicates the driving efficiency. Consequently, the experiments revealed that the driveability of the pile was negatively impacted when the soil was saturated.

In conclusion, this research emphasizes the critical importance of various factors—including falling height, pile diameter, g-level, and soil saturation—on the efficiency of pile driving. These insights contribute significantly to the understanding and improvement of pile installation practices in engineering applications.

7

Recommendations

This research has provided valuable insights into the dynamics of pile driving. However, several enhancements can be implemented to yield more accurate and robust results in future studies. Firstly, it would be beneficial to repeat the experiments using saturated samples. Analyzing pore fluid pressures in these scenarios would enable researchers to quantify the energy transmitted to the soil more precisely, thereby enhancing the understanding of energy distribution within the system.

Secondly, to gain a deeper understanding of plugging behavior, it is essential to measure horizontal stresses both inside and outside the pile. As indicated in Henke and Grabe, 2013 research on the influence of pile cross-section on driving resistance through centrifuge tests, the tendency for pile plugging was evaluated based on stress state development during penetration, recorded using total pressure sensors mounted on both the internal and external faces of the pile shaft. The fact that the height of the soil column inside the pile matches that outside does not necessarily confirm the absence of plugging.

Moreover, the stiffness of the anvil utilized in this research plays a significant role in energy transmission during impact. Investigating how variations in anvil stiffness affect system response could lead to a more nuanced understanding of energy dynamics within the context of pile driving. The anvil controls the stiffness of the system, impacting energy transmission through the pile. Utilizing a different anvil could enhance or reduce system efficiency. In this research, a consistent stiffness was maintained throughout the experiments. Another important factor to consider is the mass of the system. Given that energy transmission is influenced by both falling height and mass, exploring how changes in mass affect energy dynamics would be a valuable avenue for further research. A larger mass would result in greater forces, making it interesting to investigate the role of mass in the efficiency and drivability of the pile.

Finally, as the pile penetrates deeper, shaft friction at a given horizon typically decreases, a phenomenon known as friction fatigue. The use of lateral stress sensors could facilitate a detailed investigation into the friction fatigue experienced by the pile, providing critical insights into its performance under varying conditions, as demonstrated in D. J. White and Lehane, 2004 research assessing friction fatigue in displacement piles in sand. Overall, these suggested enhancements aim not only to refine the experimental methodology but also to deepen the understanding of the complex interactions involved in pile driving, contributing to the advancement of this important field of study.

Bibliography

Athanasopoulos, G. A., Pelekis, P. C., & Anagnostopoulos, G. A. (2000). Effect of soil stiffness in the attenuation of rayleigh-wave motions from field measurements. *Soil Dynamics and Earthquake Engineering*, *19*, 277–288. https://doi.org/10.1016/S0267-7261(00)00009-9

Bilgili, M., Yasar, A., & Simsek, E. (2011). *Offshore wind power development in europe and its comparison with onshore counterpart*. https://doi.org/10.1016/j.rser.2010.11.006

B.V., H. E. (2024). Fistuca's blue piling technology draws major investment from the huisman group.

Cheshomi, A. .-., Sadeghi, A., & Zadeh, N. G. (2021). New criterion for shutter designing by dry pluviation method. https://doi.org/10.21203/rs.3.rs-169218/v1

Desalegn, B., Gebeyehu, D., Tamrat, B., Tadiwose, T., & Lata, A. (2023). Onshore versus offshore wind power trends and recent study practices in modeling of wind turbines' life-cycle impact assessments. *Cleaner Engineering and Technology*, *17*. https://doi.org/10.1016/j.clet.2023.100691

Galparsoro, I., Menchaca, I., Garmendia, J. M., Borja, Á., Maldonado, A. D., Iglesias, G., & Bald, J. (2022). Reviewing the ecological impacts of offshore wind farms. *npj Ocean Sustainability*, *1*. https://doi.org/10.1038/s44183-022-00003-5

Gómez, S. S., Tsetas, A., & Metrikine, A. V. (2022). Energy flux analysis for quantification of vibratory pile driving efficiency. *Journal of Sound and Vibration*, *541*. https://doi.org/10.1016/j.jsv.2022.117299

Gourvenec, S., White, D. (J., & of Western Australia. Centre for Offshore Foundation Systems., U. (2011). *Frontiers in offshore geotechnics ii : Proceedings of the 2nd international symposium on frontiers in offshore geotechnics, perth, australia, 8-10 november 2010*. CRC Press/Balkema.

Han, F., Ganju, E., Salgado, R., & Prezzi, M. (2019). Comparison of the load response of closed-ended and open-ended pipe piles driven in gravelly sand. *Acta Geotechnica*, *14*, 1785–1803. https://doi.org/10.1007/s11440-019-00863-1

Henke, S., & Grabe, J. (2008). Numerical investigation of soil plugging inside open-ended piles with respect to the installation method. *Acta Geotechnica*, *3*, 215–223. https://doi.org/10.1007/s11440-008-0079-7

Henke, S., & Grabe, J. (2013). Field measurements regarding the influence of the installation method on soil plugging in tubular piles. *Acta Geotechnica*, *8*, 335–352. https://doi.org/10.1007/s11440-012-0191-6

Jeong, S., Ko, J., Won, J., & Lee, K. (2015). Bearing capacity analysis of open-ended piles considering the degree of soil plugging. *Soils and Foundations*, *55*, 1001–1014. https://doi.org/10.1016/j.sandf.2015.06.007

Leunissen, E. M., & Dawson, S. M. (2018). Underwater noise levels of pile-driving in a new zealand harbour, and the potential impacts on endangered hector's dolphins. *Marine Pollution Bulletin*, *135*, 195–204. https://doi.org/10.1016/j.marpolbul.2018.07.024

Li, Y., Huang, X., Tee, K. F., Li, Q., & Wu, X. P. (2020). Comparative study of onshore and offshore wind characteristics and wind energy potentials: A case study for southeast coastal region of china. *Sustainable Energy Technologies and Assessments*, *39*. https://doi.org/10.1016/j.seta.2020.100711

Maatouk, S., Blanc, M., & Thorel, L. (n.d.). *Isbn (print*.

Morgano, M. (1990). Effectsofporewaterpressurevariationunderdynamicloads.

of Environmental Effects Research, U. O. W. S. (n.d.). *Underwater noise effects on marine life associated with offshore wind farms main takeaways*.

The paris agreement. (2017). United Nations Framework Convention on Climate Change (UNFCCC). https://unfccc.int/process-and-meetings/the-paris-agreement

Puller, M. (2003). *Deep excavations : A practical manual*. Thomas Telford.

Summerfield-Ryan, O., & Park, S. (2023). The power of wind: The global wind energy industry's successes and failures. *Ecological Economics*, *210*. https://doi.org/10.1016/j.ecolecon.2023.107841

Taylor, R. N. (n.d.). *2 centrifuges in modelling: Principles and scale effects*. http://ebookcentral.proquest.com/lib/delft/detail.action?docID=181351.

Thompson, T. (2016). Renewable energy sources benefit health, climate, and the economy [Originally published as "Benefits of Renewable Energy Use" on ucsusa.org, 2012]. In T. Thompson (Ed.), *What is the impact of green practices?* Greenhaven Press. https://www.gale.com

Thomsen, K. E. (2014). *What is an offshore wind farm?*

Tsouvalas, A. (2020, June). *Underwater noise emission due to offshore pile installation: A review*. https://doi.org/10.3390/en13123037

Wang, Y., Liu, X., Zhang, M., Bai, X., & Mou, B. (2020). Fiber bragg grating sensors for pile jacking monitoring in clay soil. *Sensors (Switzerland)*, *20*, 1–14. https://doi.org/10.3390/s20185239

White, D. J., & Lehane, B. M. (2004). Friction fatigue on displacement piles in sand. *Geotechnique*, *54*, 645–658. https://doi.org/10.1680/geot.2004.54.10.645

White, D. S., Johnston, K. L., & Rice, G. T. (2007). The center for reservoir research over its first twenty years with special reference to the long-term monitoring program. *Journal of the Kentucky Academy of Science*, *68*, 3. https://doi.org/10.3101/1098-7096(2007)68[3:tcfrro]2.0.co;2

WindEurope. (2023). *Wind energy in europe 2023: Statistics and the outlook for 2024-2030*. https://windeurope.org/intelligence-platform/product/wind-energy-in-europe-2023-statistics-and-the-outlook-for-2024-2030/

Zeben, V. (2017). *Physical modelling of pore pressure development during impact pile driving using geocentrifuge*. http://repository.tudelft.nl/

8

Appendix

8.1. Work and Pile Capacity

The work is calculated by this formula:

$$\text{Work (KNmm)} = \text{Force (KN)} \times \Delta z\,\text{(mm)} \tag{8.1}$$

Where the force is the force of the system, as it is translated from the strain that the strain gauges record at full bridge configuration. The Δz is the incremental penetration of the pile for every blow.

The ultimate pile capacity consists of two parts, the base resistance and the skin friction resistance:

$$Q_t = Q_f + Q_s\,[\text{(KN)}] \tag{8.2}$$

The base resistance term is derived from Terzaghi's equation for bearing capacity:

$$q_f = 1.3cN_c + q_oN_q + 0.4\gamma BN_\gamma \tag{8.3}$$

The term $0.4\gamma BN_\gamma$ can be ignored because the pile diameter B is significantly smaller than the pile depth. Additionally, the term $1.3cN_c$ becomes zero as the soil is non-cohesive.

Thus, the net unit base resistance is:

$$q_{nf} = q_f - q_o = q_o(N_q - 1) \tag{8.4}$$

The net total base resistance can be expressed as:

$$Q_b = q_o(N_q - 1)A_b \tag{8.5}$$

For the shaft resistance, the ultimate unit skin friction is given by:

$$q_s = K_s\sigma_v' \tan\delta \tag{8.6}$$

where:

- σ_v' = average vertical effective stress in a given layer,
- δ = angle of wall friction, which depends on the pile material and ϕ',
- K_s = earth pressure coefficient.

The total skin friction resistance is obtained by summing the resistances of each layer:

$$Q_s = \sum (K_s\sigma_v' \tan\delta \cdot A_s) \tag{8.7}$$

The self-weight of the pile is ignored, as the weight of the concrete is approximately equal to the weight of the displaced soil.

Thus, the ultimate pile capacity is:

$$Q_f = A_bq_oN_q + \sum (K_s\sigma_v' \tan\delta \cdot A_s) \tag{8.8}$$

In the context of pile capacity calculations, typical values for the angle of wall friction δ and the internal friction angle ϕ' are dependent on the soil type and pile material. Below are typical values based on common conditions:

1. Internal Friction Angle ϕ' The internal friction angle ϕ' is related to the shear strength of the soil and is typically measured for granular or non-cohesive soils (e.g., sands and gravels). Typical ranges for ϕ' are:

- Loose sand: $\phi' \approx 28° - 32°$
- Medium dense sand: $\phi' \approx 30° - 35°$
- Dense sand or gravel: $\phi' \approx 35° - 40°$
- Silts may have lower values of ϕ', around $25° - 30°$.

For design purposes, ϕ' is often obtained from soil testing, such as direct shear tests, triaxial tests, or correlations with standard penetration tests (SPT) or cone penetration tests (CPT).

2. Angle of Wall Friction δ

The wall friction angle δ depends on the interaction between the pile material (e.g., steel, concrete, or timber) and the surrounding soil. Typically, δ is related to the internal friction angle ϕ', and for non-cohesive soils, it is often taken as a fraction of ϕ'. Common ranges for δ are:

- For steel piles, $\delta \approx 0.6\phi'$, so δ is typically in the range of $18° - 24°$ for loose to dense sands.
- For concrete piles, $\delta \approx 0.7\phi'$, so δ can range from $21° - 28°$.
- For timber piles, δ can be even higher, sometimes approaching $0.8\phi'$.

3. Earth Pressure Coefficient K_s The earth pressure coefficient K_s accounts for the lateral stress that the soil applies to the pile shaft. It varies based on the soil condition:

- For active conditions:

$$K_s \approx K_a = \frac{1 - \sin(\phi')}{1 + \sin(\phi')}$$

- For at-rest conditions:

$$K_s \approx K_0 = 1 - \sin(\phi')$$

- For passive conditions (rarely applicable in this context):

$$K_s \approx K_p = \frac{1 + \sin(\phi')}{1 - \sin(\phi')}$$

In most design cases, the values for K_s can range from 0.3 to 1.0 for typical soil conditions, with values closer to 0.3 for loose soils and higher values for dense soils or over-consolidated materials. Summary of Typical Values:

- ϕ' (Internal friction angle): - Loose sand: $28° - 32°$ - Dense sand: $35° - 40°$
- δ (Wall friction angle): - Steel piles: $0.6\phi'$ - Concrete piles: $0.7\phi'$ - Timber piles: $0.7 - 0.8\phi'$
- K_s (Earth pressure coefficient): - Loose sand: $0.3 - 0.5$ - Dense sand: $0.5 - 1.0$

For this research ϕ' was selected 35, δ was selected $0.6\phi'$ anK_s was selected 0.5.

8.2. Experiment with 10g and High Energy level

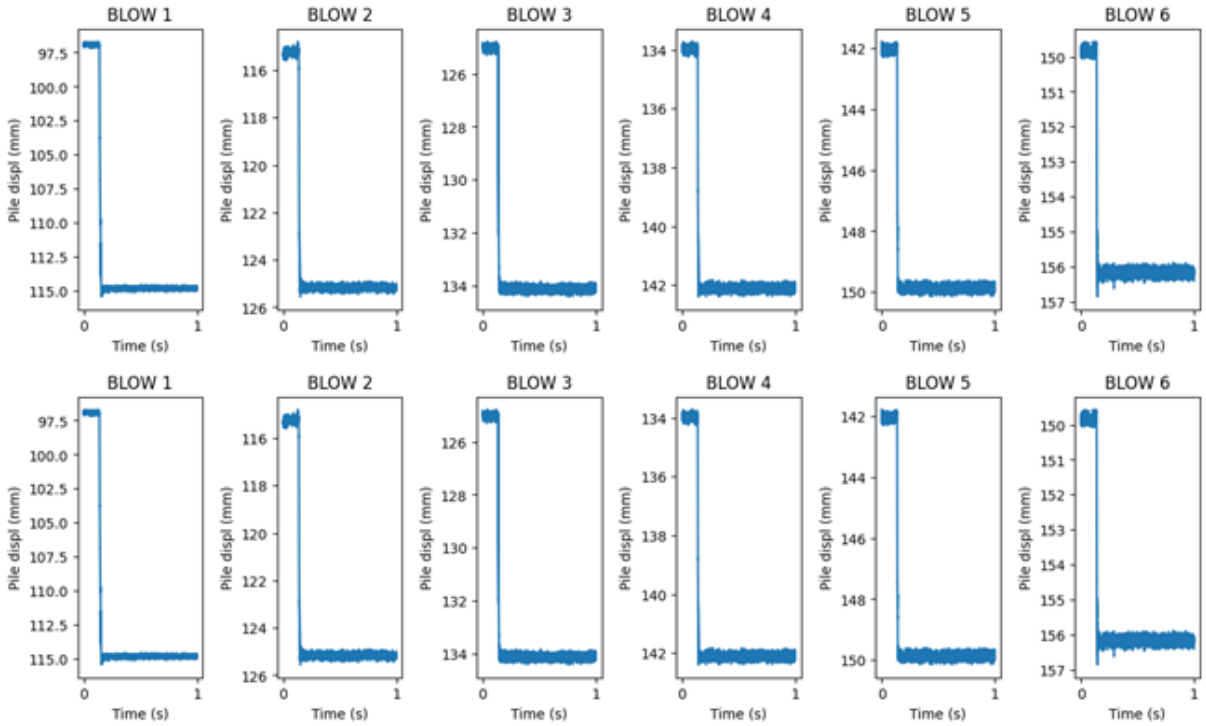

Figure 8.1: Top row Pile displ (mm) vs Time (s) and second row Mass displ (mm) vs Time (s)

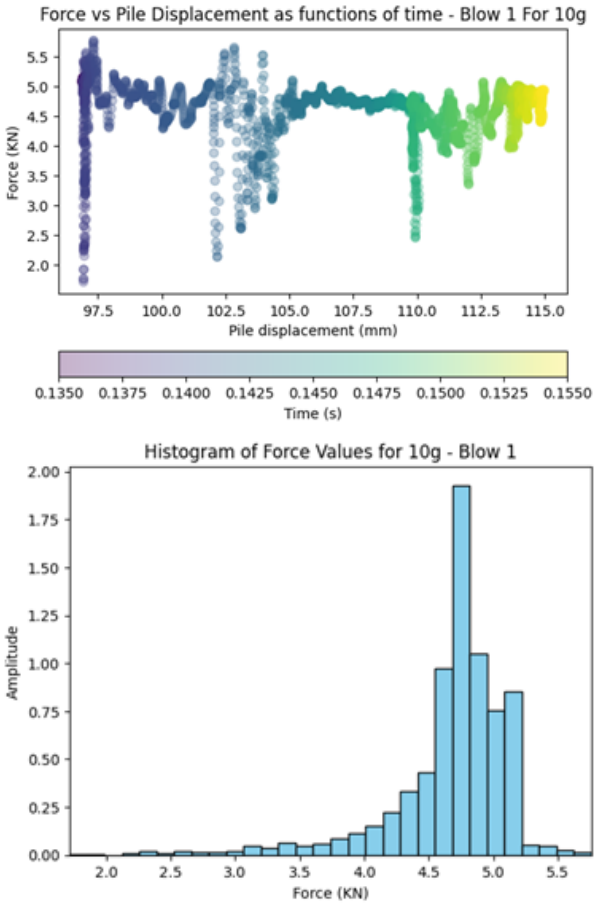

Figure 8.2: Top row Force (KN) vs Pile displ (mm) and second row Histogram of Force

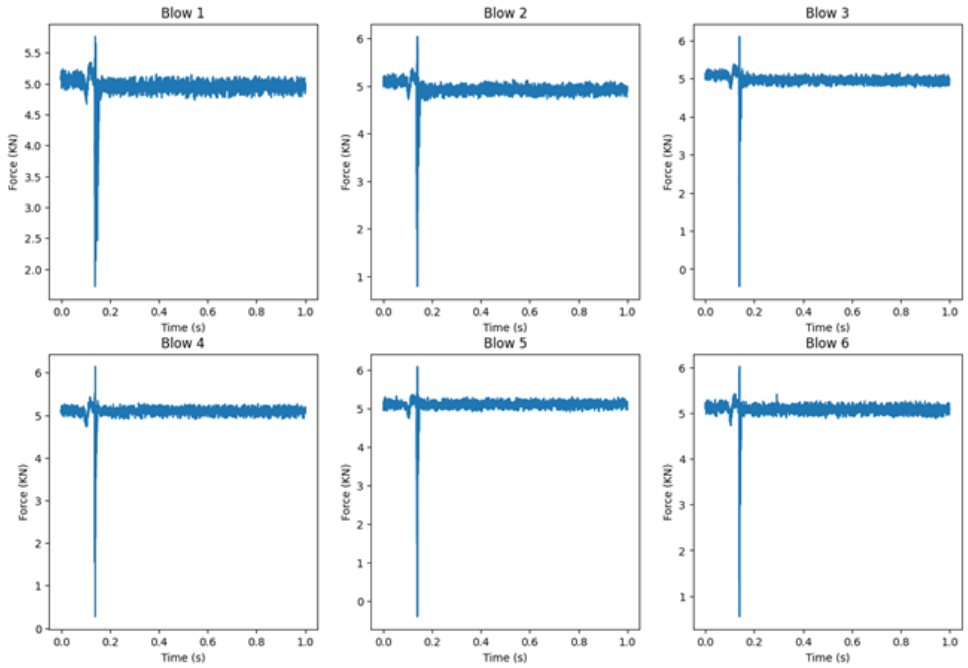

Figure 8.3: Load (KN) vs Time (s)

8.3. Experiment with 10g and Middle Energy level

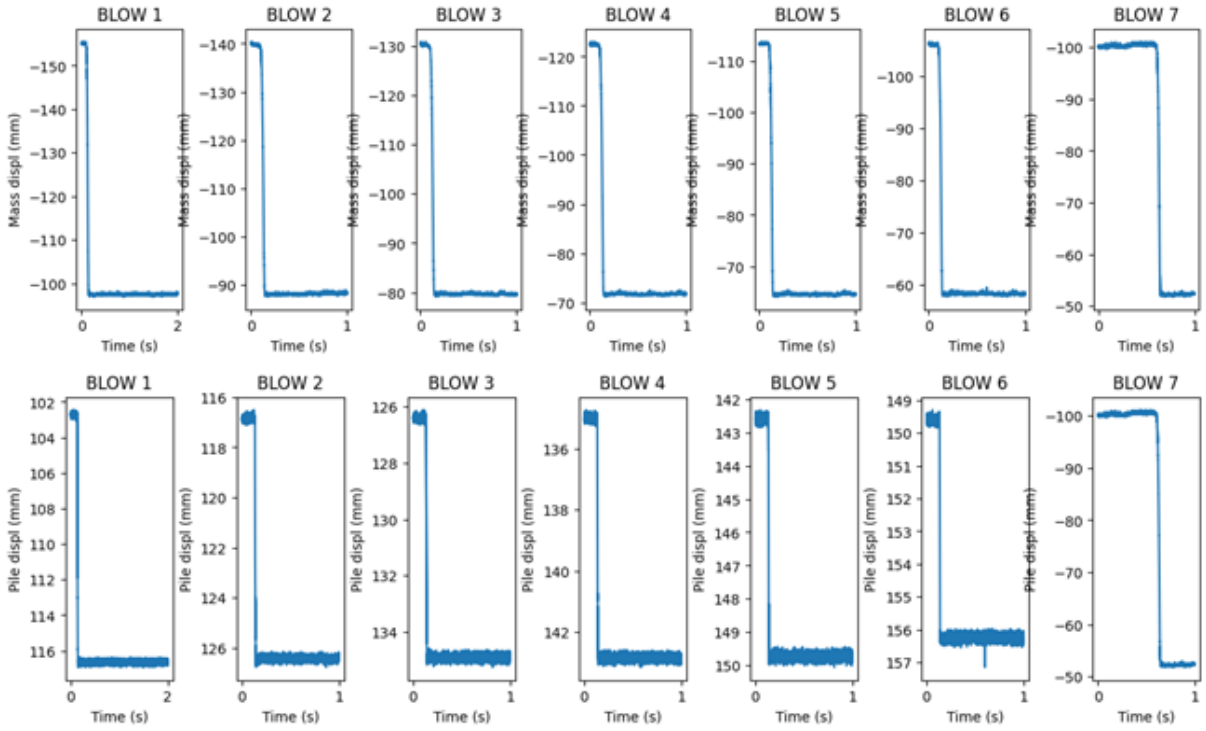

Figure 8.4: Top row Pile displ (mm) vs Time (s) and second row Mass displ (mm) vs Time (s)

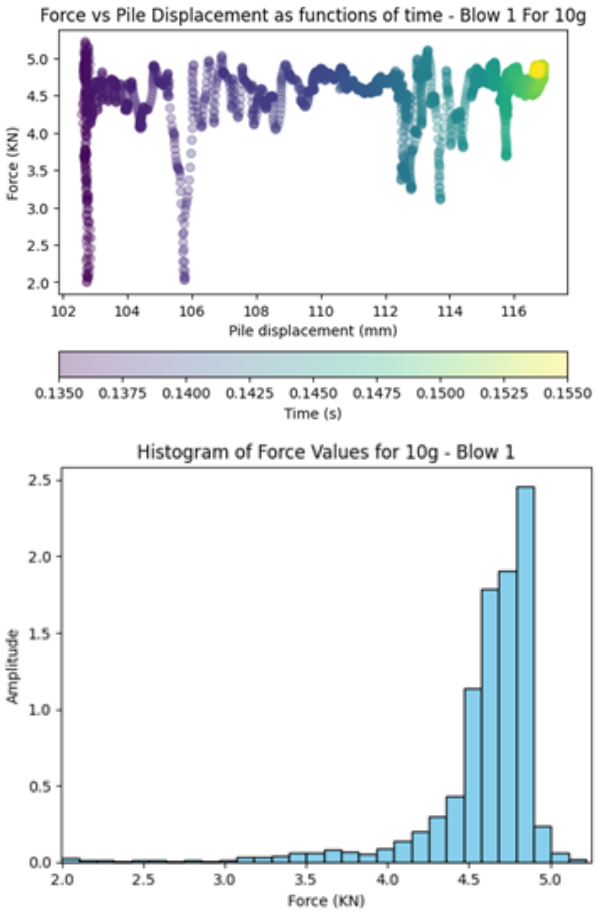

Figure 8.5: Top row Force (KN) vs Pile displ (mm) and second row Histogram of Force

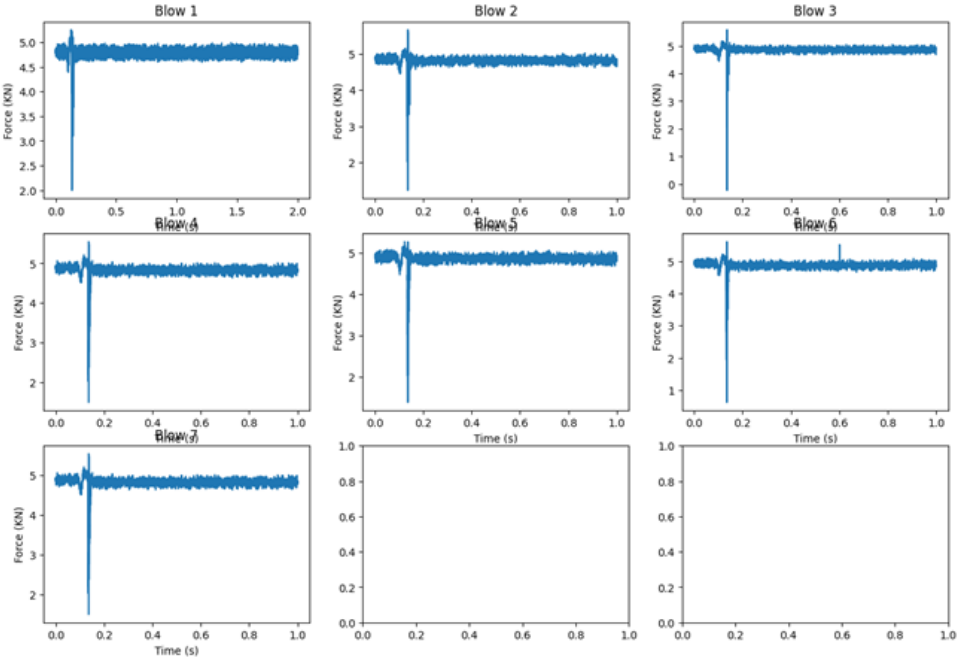

Figure 8.6: Load (KN) vs Time (s)

8.4. Experiment with 10g and Low Energy level

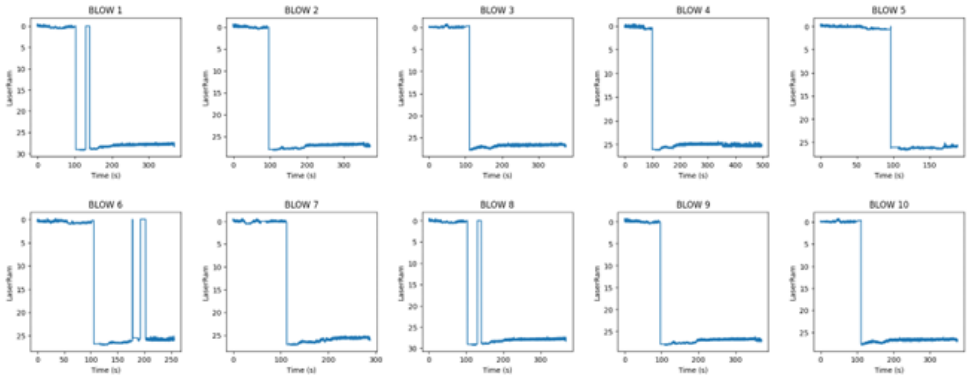

Figure 8.7: Mass displ (mm) vs Time (s)

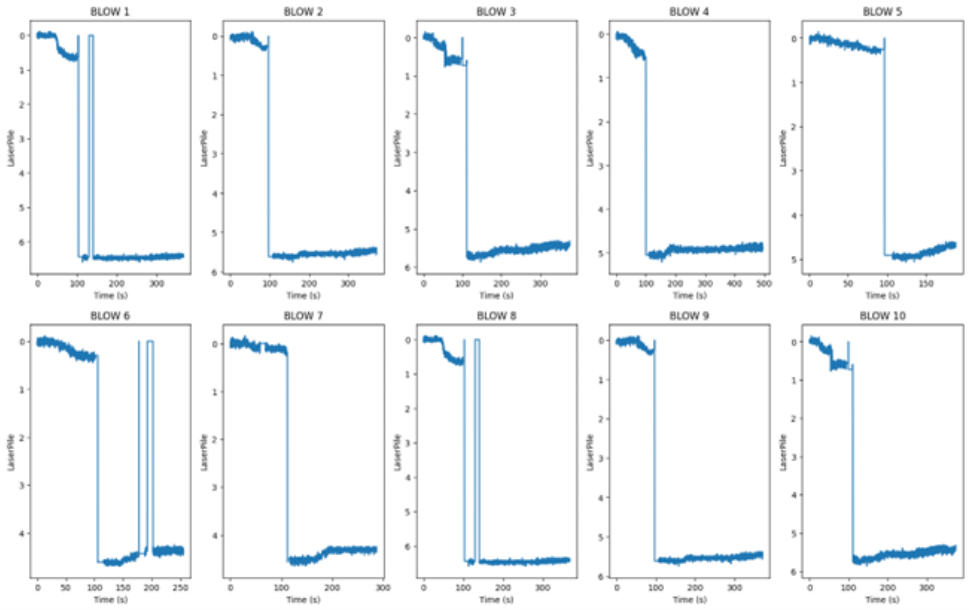

Figure 8.8: Load (KN) vs Time (s)

8.5. Experiment with 20g and Middle Energy level

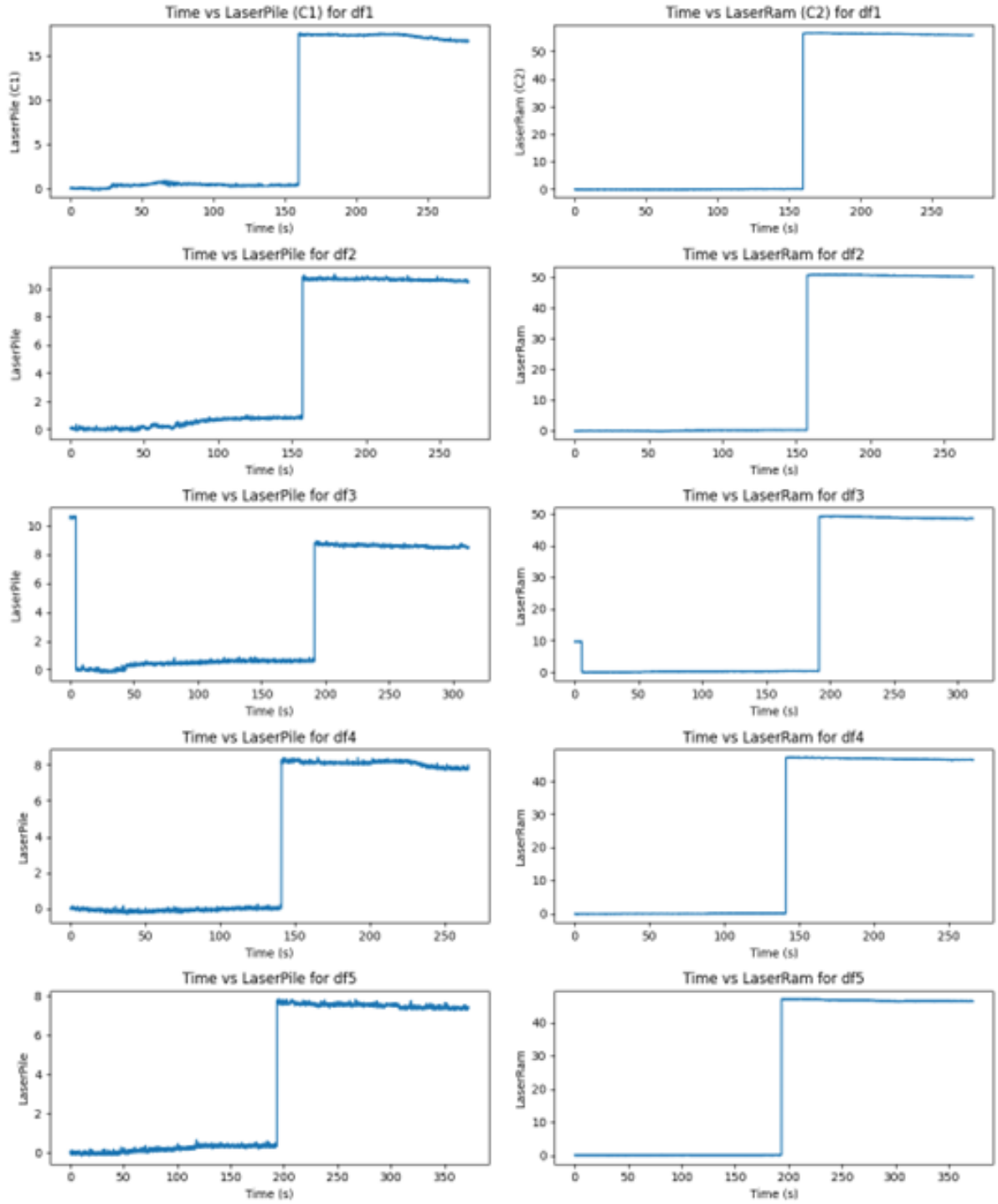

Figure 8.9: On the left Pile displ (mm) vs Time (s) and on the right Mass displ (mm) vs Time (s)

8.6. Experiment with 30g and High Energy level

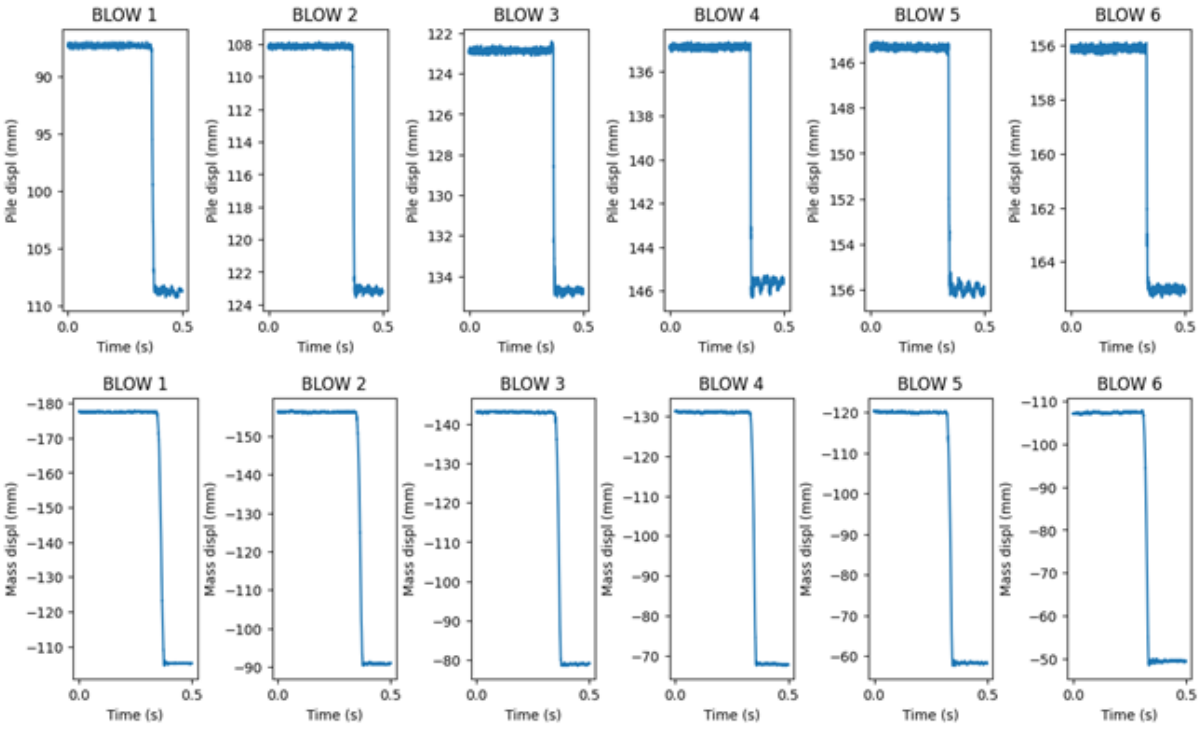

Figure 8.10: Top row Pile displ (mm) vs Time (s) and second row Mass displ (mm) vs Time (s)

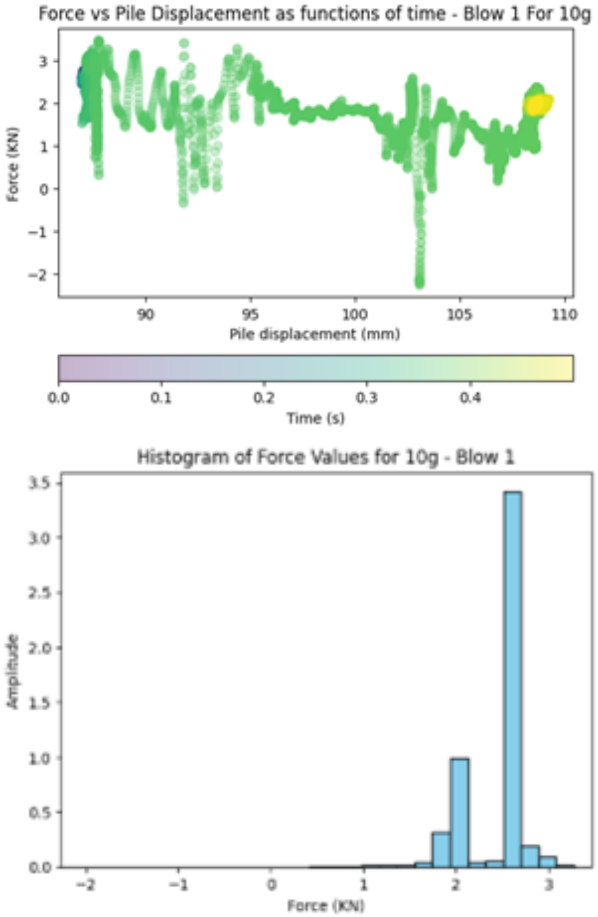

Figure 8.11: Top row Force (KN) vs Pile displ (mm) and second row Histogram of Force

8.7. Experiment with 30g and Middle Energy level

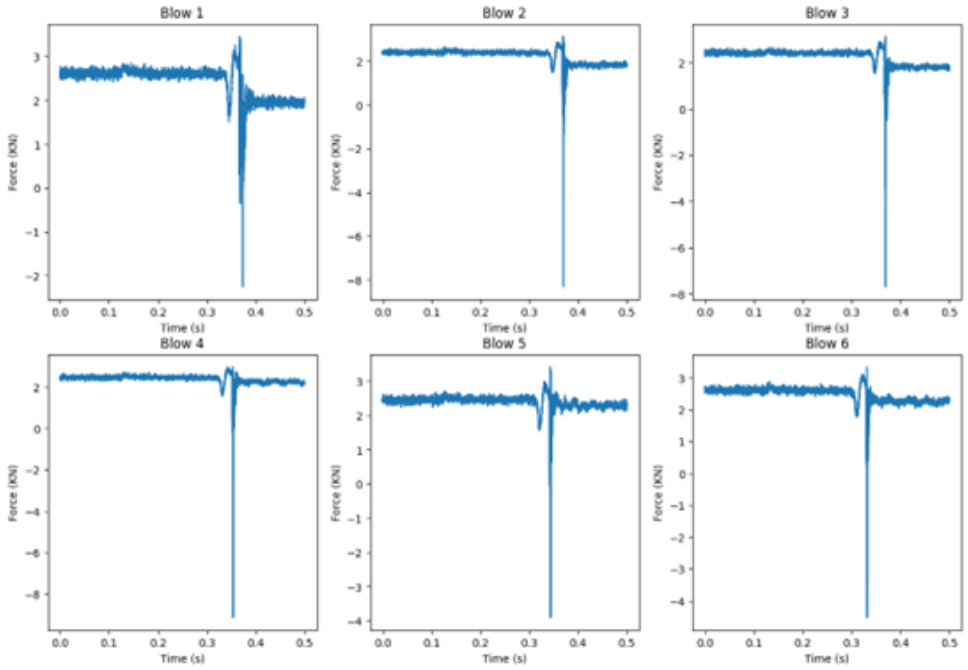

Figure 8.12: Load (KN) vs Time (s)

8.8. Experiment with 30g and Low Energy level

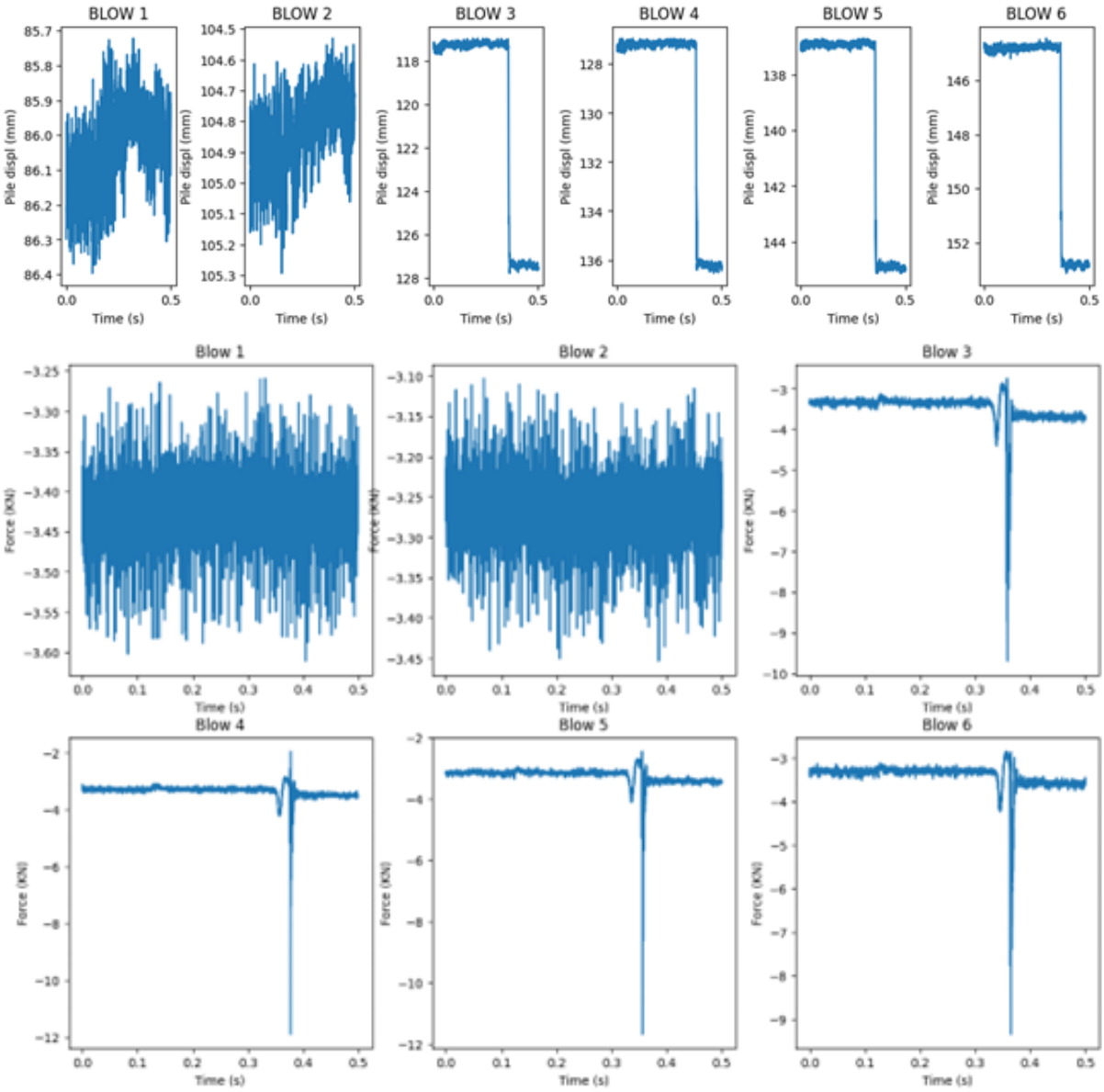

Figure 8.13: Top row Pile displ (mm) vs Time (s) and second row Force (KN) vs Time (s)

8.9. Experiment with 50g and High Energy level

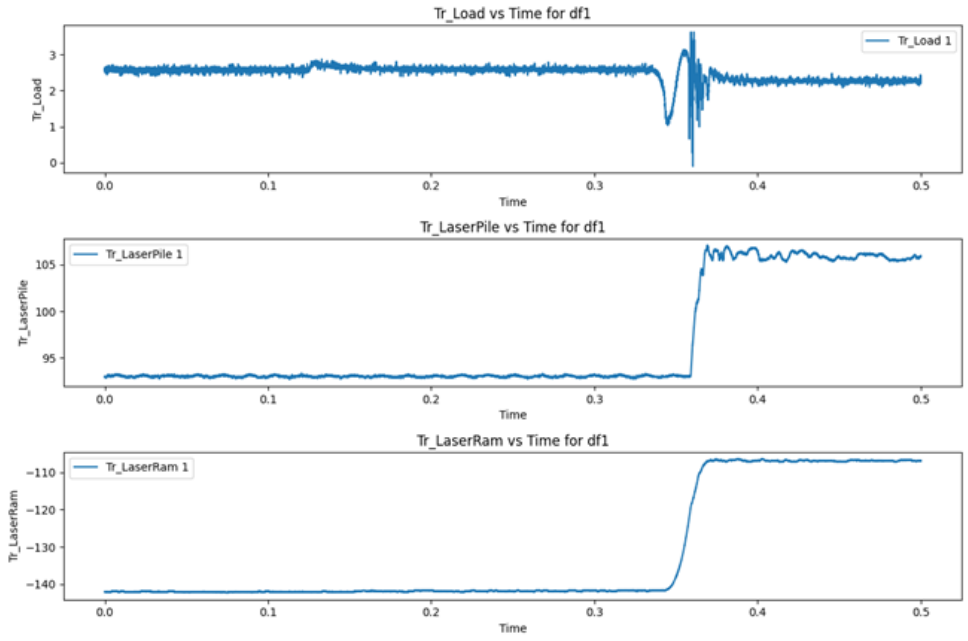

Figure 8.14: Blow1

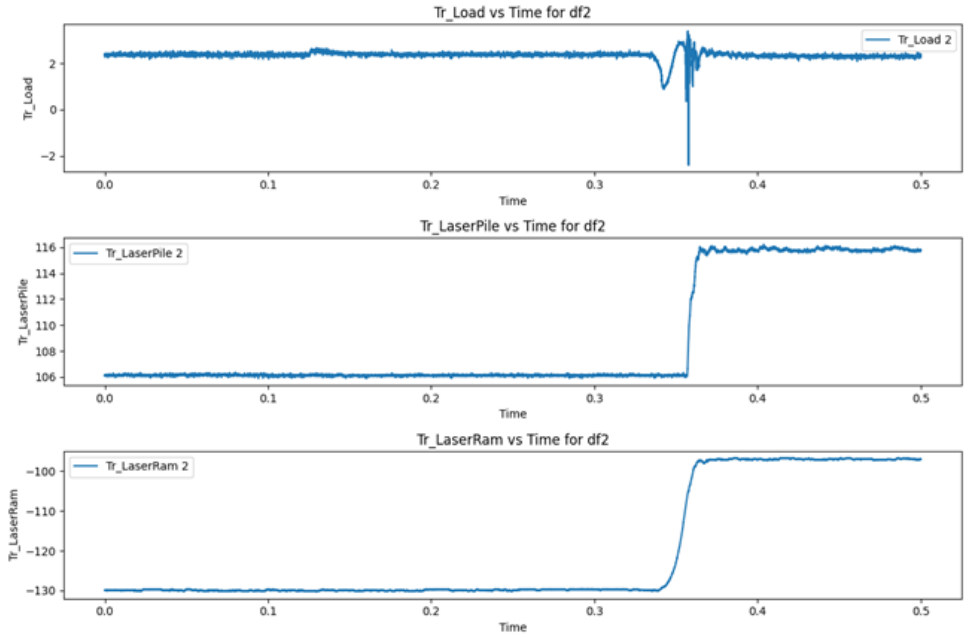

Figure 8.15: Blow2

8.10. Experiment with 50g and Middle Energy level

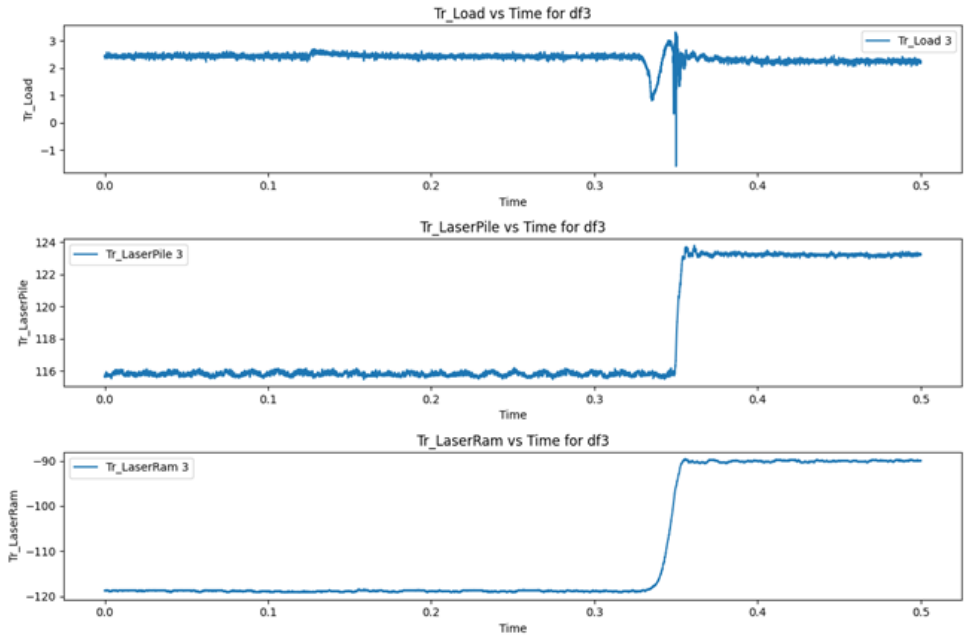

Figure 8.16: Blow3

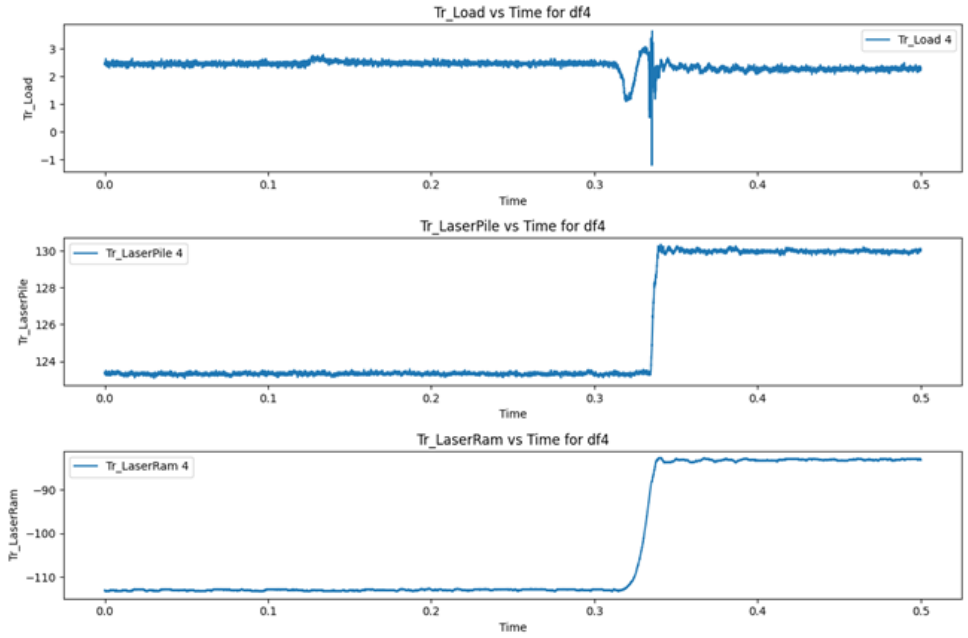

Figure 8.17: Blow4

8.11. Experiment with 50g and Low Energy level

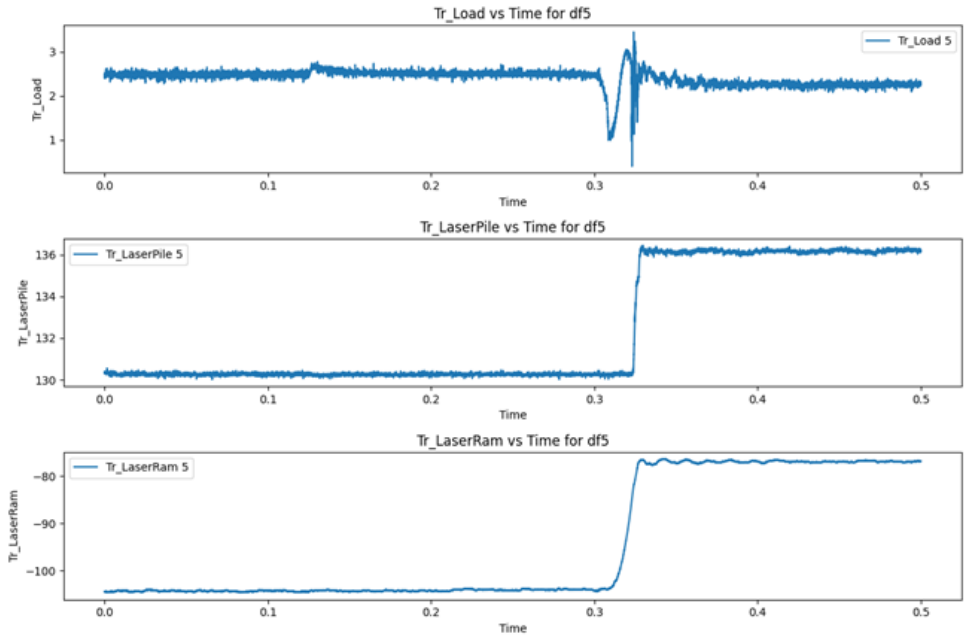

Figure 8.18: Blow5

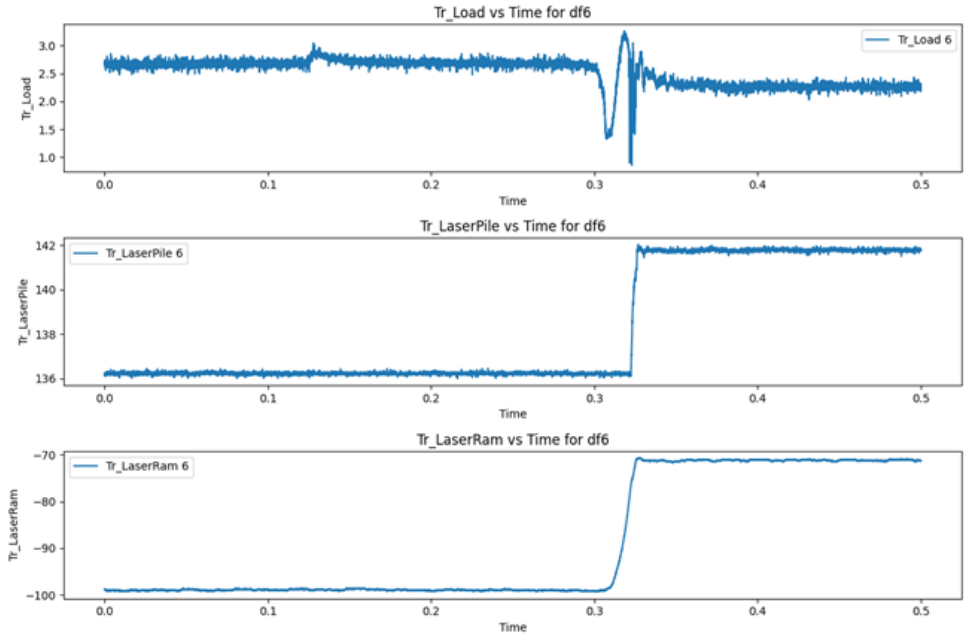

Figure 8.19: Blow6

8.12. Experiment with 50g at non constant falling height

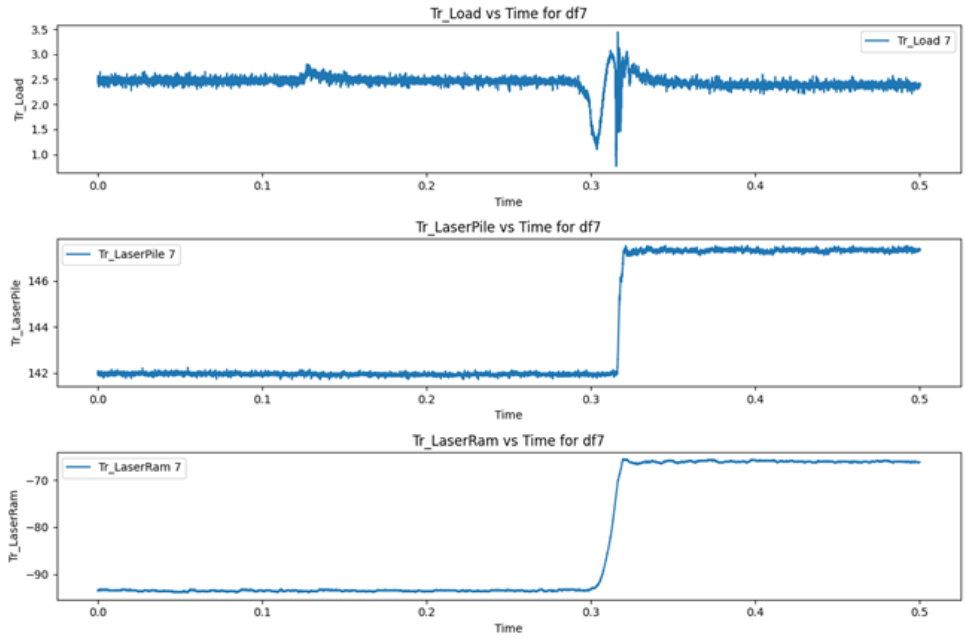

Figure 8.20: Blow7

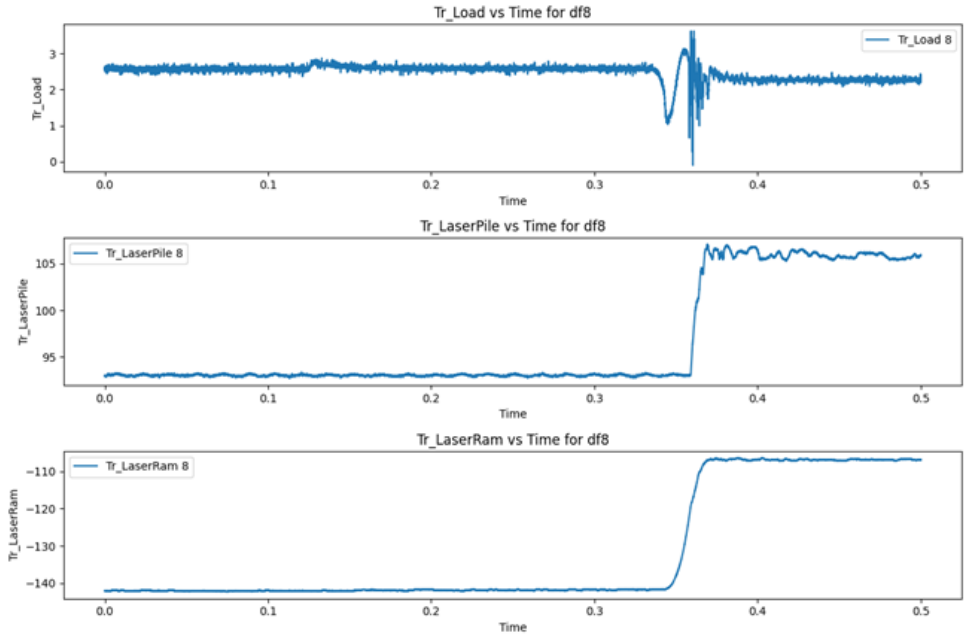

Figure 8.21: Blow8

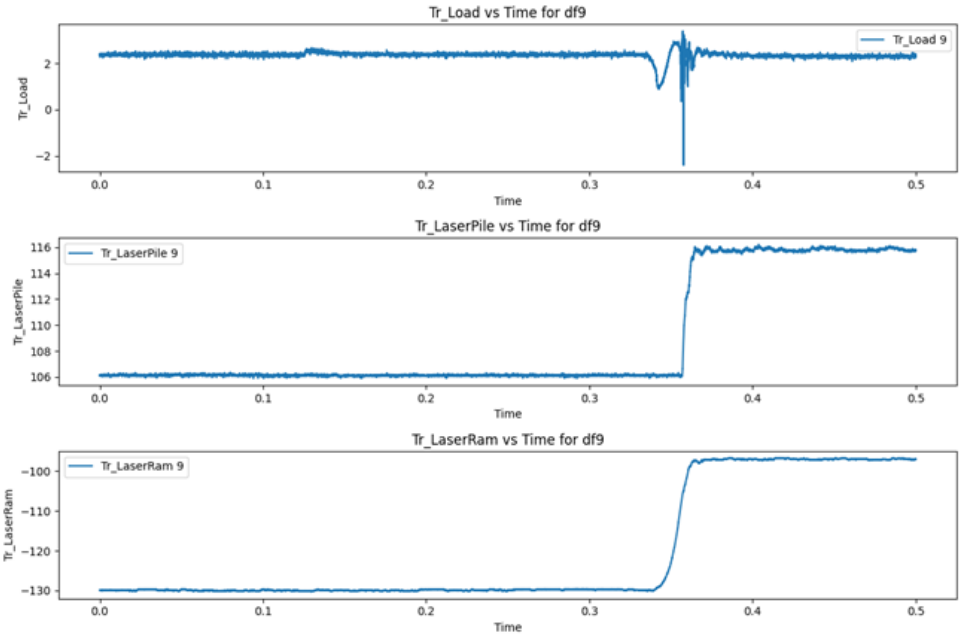

Figure 8.22: Blow9

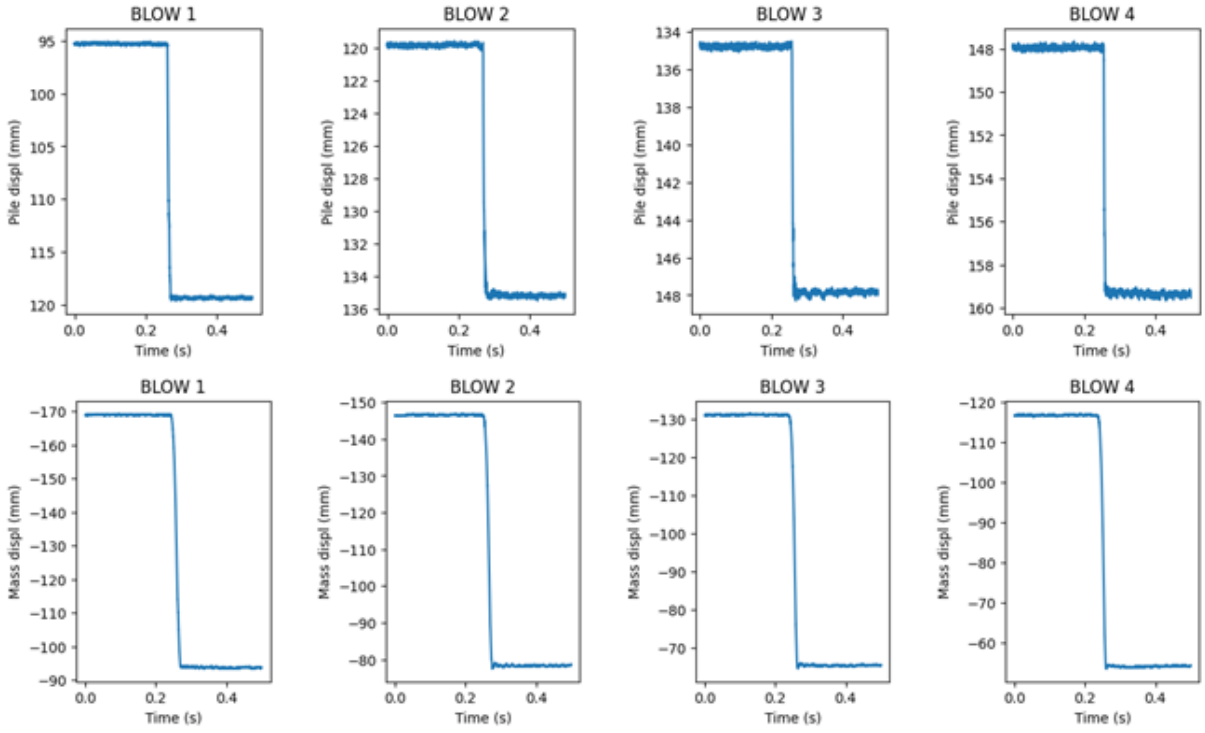

Figure 8.23: Top row Pile displ (mm) vs Time (s) and second row Mass displ (mm) vs Time (s)

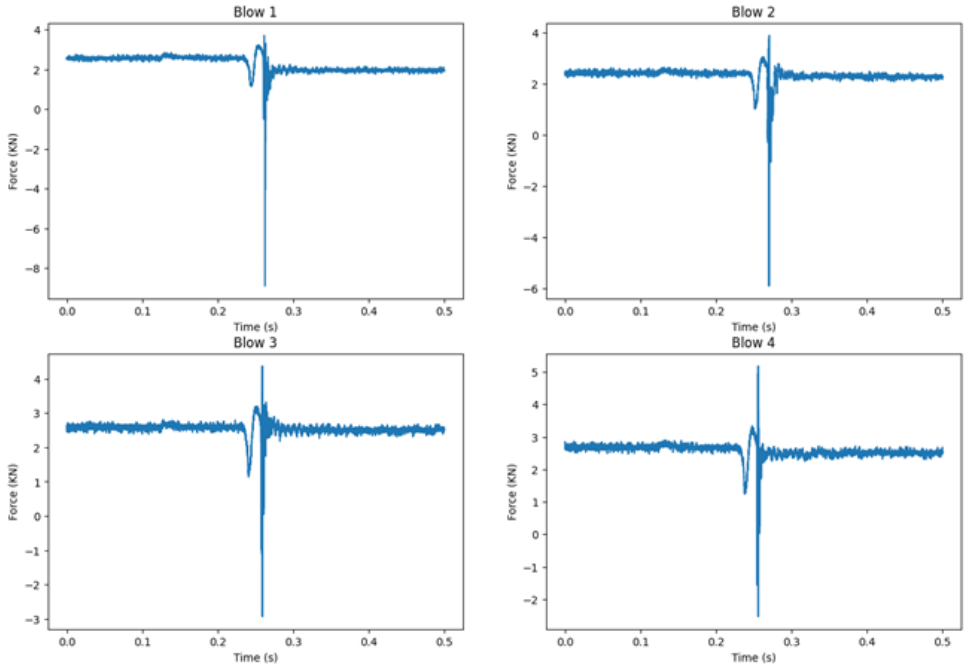

Figure 8.24: Load (KN) vs Time (s)

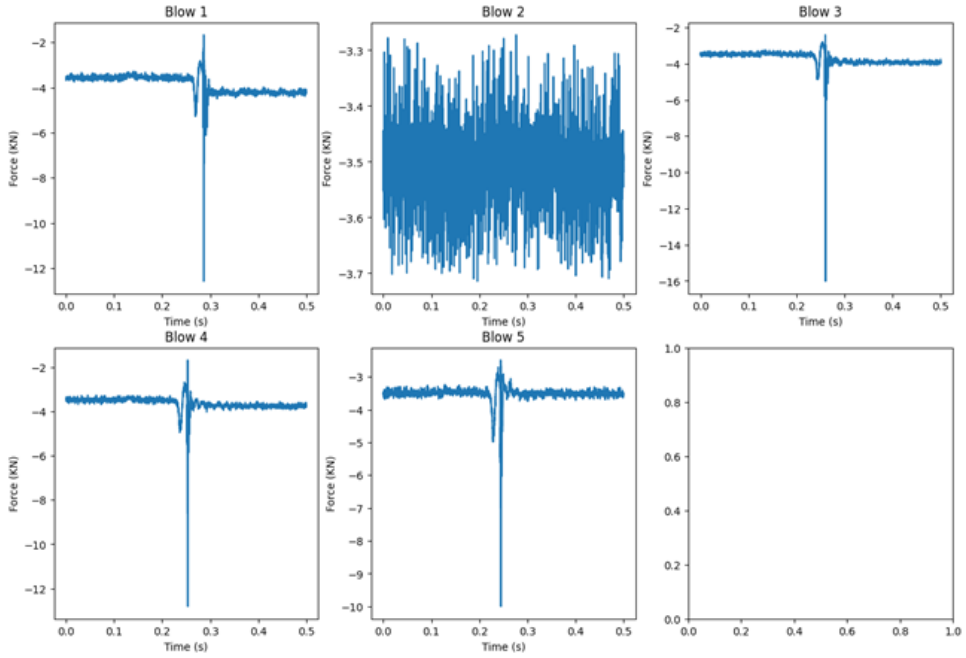

Figure 8.25: Load (KN) vs Time (s)

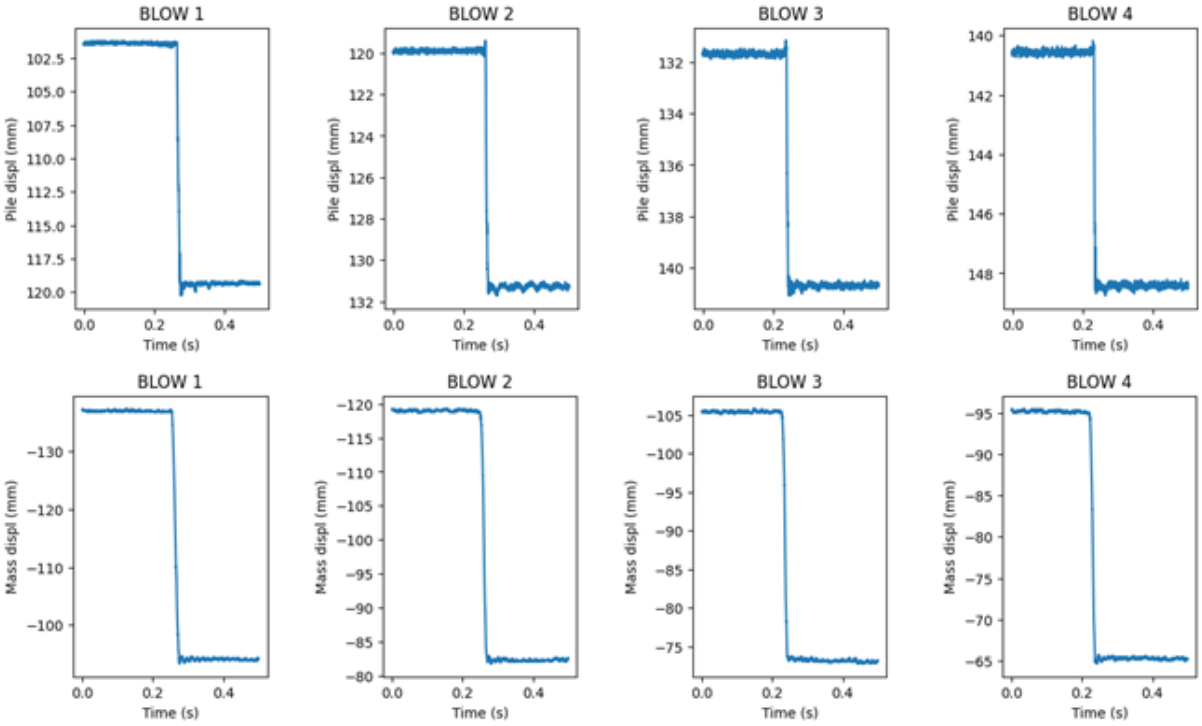

Figure 8.26: Top row Pile displ (mm) vs Time (s) and second row Mass displ (mm) vs Time (s)

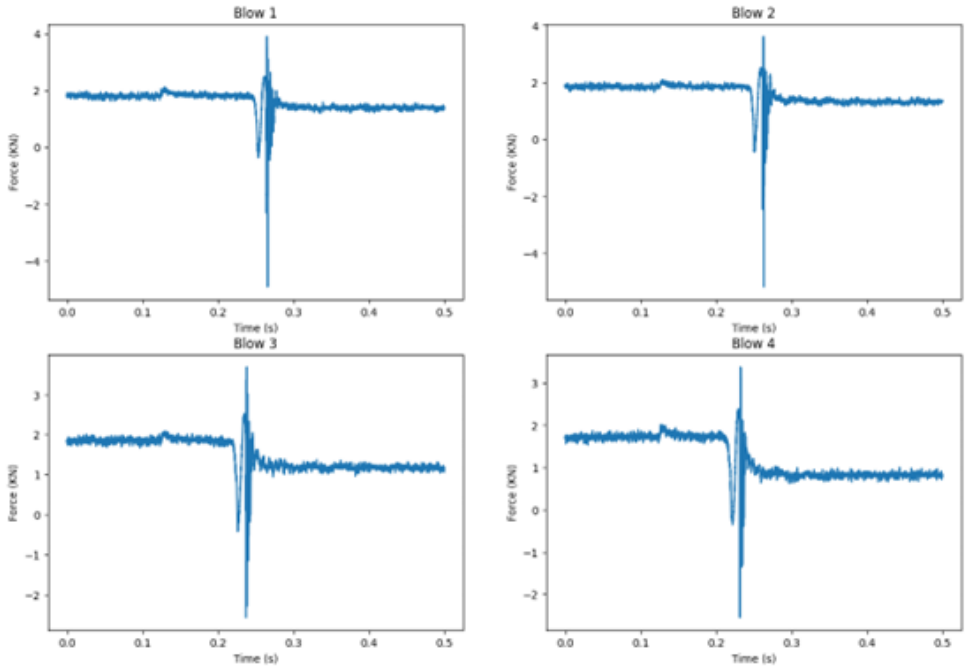

Figure 8.27: Load (KN) vs Time (s)

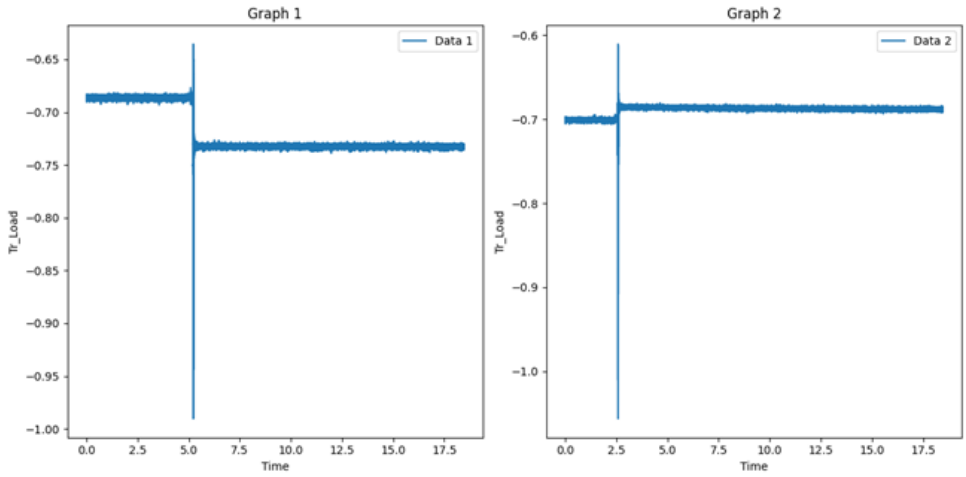

Figure 8.28: Load (KN) vs Time (s)